

This is to certify that the

thesis entitled

A Simplified Discrete-Tow Model for Modeling Stiffness and Failure within Woven Composites

presented by

Craig Ryan Carrier

has been accepted towards fulfillment of the requirements for

Master's degree in Engineering Mechanics

Ronald a Averile

Date 10/31/00

MSU is an Affirmative Action/Equal Opportunity Institution

0-7639



PLACE IN RETURN BOX to remove this checkout from your record.

TO AVOID FINES return on or before date due.

MAY BE RECALLED with earlier due date if requested.

DATE DUE	DATE DUE	DATE DUE
-		
		·

11/00 c:/CIRC/DateDue.p65-p.14

A SIMPLIFIED DISCRETE-TOW MODEL FOR MODELING STIFFNESS AND FAILURE WITHIN WOVEN COMPOSITES

Ву

Craig Ryan Carrier

A Thesis

Submitted to
Michigan State University
in partial fulfillment of the requirements
for the degree of

MASTER'S OF SCIENCE

Materials Science and Mechanics

2000

possi

and .

of th

pred in a

mod

red

rep

ABSTRACT

A SIMPLIIFIED DISCRETE-TOW MODEL FOR MODELING STIFFNESS AND FAILURE WITHIN WOVEN COMPOSITES

By

Craig Ryan Carrier

Using a simplified discrete-tow model of a woven composite structure, it is possible to accurately predict the stiffness of a woven composite. The simplified discrete-tow model is based on the idea of discretely representing the fiber tows and resin independently as beam and shell finite elements respectively. The use of the discrete-tow model in progressive failure allows for the ability to better predict the behavior and physical orientation of the tows throughout the analysis in a manner that is more computationally efficient than a fully three-dimensional model. In the present study progressive failure is conducted using stiffness reduction in both the beam and shell elements of the discrete-tow model to represent fiber and matrix damage respectively.

Copyright by

Craig Ryan Carrier 2000

To my loving parents

ACKNOWLEDGMENTS

This work was sponsored by the Department of Energy and the Automotive Composites Consortium under USAMP/DOE Co-operative agreement DE - FC05 - 95OR22363. I wish to express my gratitude for the financial support as well as the many helpful comments that have molded this work. I would also like to thank Dr. Averill for his thoughtful guidance and depth of knowledge that he provided for me.

LIST O

LIST C

CHAPT

CHAPT

CHAF

СНА

TABLE OF CONTENTS

LIST OF TABLES	VIII
LIST OF FIGURES	. IX
CHAPTER 1 INTRODUCTION	1
1.1 Introduction	2
CHAPTER 2 THREE-DIMENSIONAL ANALYSIS OF A WOVEN COMPOSITE	10
2.1 Introduction 2.2 Model Description 2.2.1 Loading	.11 .12 .12 .14 .15 .15 .16 .17 .18 .19 .20
CHAPTER 3 THE SIMPLIFIED DISCRETE-TOW MODEL	
3.1 Introduction 3.2 The Simplified Discrete-Tow Model	.42 .43 .44 .49 .52 .53 .53 .54
CHAPTER 4 MODELING PROGRESSIVE FAILURE USING THE SIMPLIFIED DISCRETE-TOW MODEL	
4.1 Introduction	73

CHAP

BIBLIO

4.2 Progressive Failure Model	73
4.2.1 finite element mesh	74
4.2.2 Modelling progressive failure	74
4.2.3 Progressive Failure Algorithm	
4.3 Numerical Results	
4.4 Conclusions	77
CHAPTER 5 CONCLUSIONS	91
5.1 Conclusions	91
5.2 Future Work	
BIBLIOGRAPHY	93

Table 2
Table 2
Table 2
Table 3
Table 4
Table 4

LIST OF TABLES

Table 2.1 Load	case summary	22
Table 2.2 Tow	geometrical properties	22
Table 2.3 Mate	erial properties of the constituent materials of the woven	
composite	beam	22
Table 2.4 Mid-s	span deflection data of points A and B for each load case	23
Table 3.1 Mate	rial properties for comparison of predicted stiffness	57
Table 3.2 Com	parison of results for a plain weave	57
Table 3.3 Geom	netric data for the three waviness ratios studied	58
Table 3.4 Mater	rial properties for all waviness ratios studied	58
Table 3.5 Com	parison of predicted effective properties for a plain weave	
composite.		59
Table 3.6 Geor	metric and braid data for triaxial weaves	60
Table 3.7 Prop	erties for the constituent materials of the triaxial weaves	60
Table 3.8 Com	parison of effective properties for a triaxial weave with num	erical
and experi	mental methods	61
Table 4.1 Failu	re criteria used in the resin and tow	79
Table 4.2 Appli	ied boundary for the linear and failure cases studied	79

Figure Fi

LIST OF FIGURES

Figure 2.2 Refined brick and plate model	Figure 2.1 (Geometry of the cantilever beam with a single undulating fiber	24
Figure 2.4 Fully three-dimensional finite element model	Figure 2.2 F	Refined brick and beam model	25
Figure 2.5 Arrangement of the brick elements in the brick and beam and brick and plate models	Figure 2.3 F	Refined brick and plate model	26
Figure 2.5 Arrangement of the brick elements in the brick and beam and brick and plate models	Figure 2.4 F	Fully three-dimensional finite element model	27
and plate models			
Figure 2.7 Normal (X-Y bending) loading condition applied to each model	_		28
Figure 2.7 Normal (X-Y bending) loading condition applied to each model	Figure 2.6 A	Axial loading condition applied to each model	29
Figure 2.8 Transverse (X-Z bending) loading condition applied to each model. 30 Figure 2.9 Torsional load case applied to each model. 30 Figure 2.10 Piece-wise linear approximation of the fiber tow path-line using beam and shell elements (a) coarse model, (b) refined model. 31 Figure 2.11 Axial displacement (u) along the tow centerline of the coarse brick & beam and brick & plate models due to an axial load. 32 Figure 2.12 Axial displacement (u) along the tow centerline of the refined brick & beam and brick & plate models due to an axial load. 32 Figure 2.13 Normal displacement (v) along the tow centerline of the coarse brick & beam and brick & plate models due to an axial load. 33 Figure 2.14 Normal displacement (v) along the tow centerline of the refined brick & beam and brick & plate models due to an axial load. 33 Figure 2.15 Axial displacement (u) along the tow centerline of the coarse brick & beam and brick & plate models due to a normal (y) load. 34 Figure 2.16 Axial displacement (u) along the tow centerline of the refined brick & beam and brick & plate models due to a normal (y) load. 34 Figure 2.17 Normal displacement (v) along the tow centerline of the coarse brick & beam and brick & plate models due to a normal (y) load. 35 Figure 2.18 Normal displacement (v) along the tow centerline of the refined brick & beam and brick & plate models due to a normal (y) load. 35 Figure 2.19 Axial displacement along the tow centerline of the refined brick & beam and brick & plate models due to a transverse (z) load. 36 Figure 2.20 Axial displacement along the tow centerline of the refined brick & beam and brick & plate models due to a transverse (z) load. 36 Figure 2.21 Normal displacement (v) along the tow centerline of the refined brick & beam and brick & plate models due to a transverse (z) load. 37 Figure 2.22 Normal displacement (v) along the tow centerline of the refined brick & beam and brick & plate models due to a transverse (z) load. 37 Figure 2.23 Transverse displacement (w) along the tow centerline of th			
Figure 2.9 Torsional load case applied to each model			
Figure 2.10 Piece-wise linear approximation of the fiber tow path-line using beam and shell elements (a) coarse model, (b) refined model			
beam and shell elements (a) coarse model, (b) refined model	•	· ·	
Figure 2.11 Axial displacement (u) along the tow centerline of the coarse brick & beam and brick & plate models due to an axial load	beam a	nd shell elements (a) coarse model, (b) refined model	31
beam and brick & plate models due to an axial load	Figure 2.11	Axial displacement (u) along the tow centerline of the coarse brick	&
Figure 2.12 Axial displacement (u) along the tow centerline of the refined brick & beam and brick & plate models due to an axial load			
beam and brick & plate models due to an axial load			
Figure 2.13 Normal displacement (v) along the tow centerline of the coarse brick & beam and brick & plate models due to an axial load	•	· · · · · · · · · · · · · · · · · · ·	
& beam and brick & plate models due to an axial load		ullet	
Figure 2.14 Normal displacement (v) along the tow centerline of the refined brick & beam and brick & plate models due to an axial load	•	· · · · · · · · · · · · · · · · · · ·	
& beam and brick & plate models due to an axial load		•	
Figure 2.15 Axial displacement (u) along the tow centerline of the coarse brick & beam and brick & plate models due to a normal (y) load	_	· · · · · · · · · · · · · · · · · · ·	
beam and brick & plate models due to a normal (y) load		•	
Figure 2.16 Axial displacement (u) along the tow centerline of the refined brick & beam and brick & plate models due to a normal (y) load	_	· · · · · · · · · · · · · · · · · · ·	
beam and brick & plate models due to a normal (y) load			
Figure 2.17 Normal displacement (v) along the tow centerline of the coarse brick & beam and brick & plate models due to a normal (y) load	-	· · · · · · · · · · · · · · · · · · ·	
& beam and brick & plate models due to a normal (y) load		•	
Figure 2.18 Normal displacement (v) along the tow centerline of the refined brick & beam and brick & plate models due to a normal (y) load	_	· · · · · · · · · · · · · · · · · · ·	
& beam and brick & plate models due to a normal (y) load			
Figure 2.19 Axial displacement along the tow centerline of the coarse brick & beam and brick & plate models due to a transverse (z) load	_	· · · · · · · · · · · · · · · · · · ·	
beam and brick & plate models due to a transverse (z) load			
Figure 2.20 Axial displacement along the tow centerline of the refined brick & beam and brick & plate models due to a transverse (z) load			36
beam and brick & plate models due to a transverse (z) load			
Figure 2.21 Normal displacement (v) along the tow centerline of the coarse brick & beam and brick & plate models due to a transverse (z) load37 Figure 2.22 Normal displacement (v) along the tow centerline of the refined brick & beam and brick & plate models due to a transverse (z) load37 Figure 2.23 Transverse displacement (w) along the tow centerline of the coarse	•	•	36
brick & beam and brick & plate models due to a transverse (z) load37 Figure 2.22 Normal displacement (v) along the tow centerline of the refined brick & beam and brick & plate models due to a transverse (z) load37 Figure 2.23 Transverse displacement (w) along the tow centerline of the coarse			
Figure 2.22 Normal displacement (v) along the tow centerline of the refined brick & beam and brick & plate models due to a transverse (z) load37 Figure 2.23 Transverse displacement (w) along the tow centerline of the coarse			37
brick & beam and brick & plate models due to a transverse (z) load37 Figure 2.23 Transverse displacement (w) along the tow centerline of the coarse			
Figure 2.23 Transverse displacement (w) along the tow centerline of the coarse			37
brick & beam and brick & plate models due to a transverse (z) load38		beam and brick & plate models due to a transverse (z) load	
Figure 2.24 Transverse displacement (w) along the tow centerline of the refined			
brick & beam and brick & plate models due to a transverse (z) load38			
Figure 2.25 Axial displacement (u) along the tow centerline of the coarse brick			
& beam and brick & plate models due to a torsional load			

Figure

Figure Figure
Figure
Figure
Figure
(v
Figure
Figure

Figure 2.26 Axial displacement (u) along the tow centerline of the refined brick
& beam and brick & plate models due to a torsional load39
Figure 2.27 Normal displacement (v) along the tow centerline of the coarse
brick & beam and brick & plate models due to a torsional load40
Figure 2.28 Normal displacement (v) along the tow centerline of the refined
brick & beam and brick & plate models due to a torsional load40
Figure 2.29 Transverse displacement (w) along the tow centerline of the coarse
brick & beam and brick & plate models due to a torsional load41
Figure 2.30 Transverse displacement (w) along the tow centerline of the refined
brick & beam and brick & plate models due to a torsional load41
Figure 3.1. (a) Plain weave and (b) one possible repeating volume element of a
plain weave62
Figure 3.2 (a) Geometry of a triaxial braid (b) cross section of the triaxial braid
made perpendicular to the axial tows (c) cross section of the triaxial braid
made alone the direction of the braider tows63
Figure 3.3 The area enclosed by A,B,C,D represents one possible RVE for a
[0/±0] triaxial braided composite64
Figure 3.4 (a) Assembled finite element model of the unit cell and (b) exploded
view of the finite element model for a plain weave material system65
Figure 3.5 (a) Discretized representation of a RVE in a triaxial braid. (b)
Assembled and (c) exploded views of the finite element model for a triaxial
braid66
Figure 3.6 Division of the RVE of a triaxial braid into two regions for calculation of
the effective properties (a) plan view (b) side view67
Figure 3.7 (a) Curved fiber tow. (b) Straight fiber tow68
Figure 3.8 Curved beam on an elastic foundation (a) geometry of the undulating
region and (b) applied load69
Figure 3.9 Geometry defining the waviness ratio ($\lambda = L_{ub} / LI$)
Figure 3.10 Plot of the effective stiffness E_{11} as the waviness ratio (λ) is
increased
Figure 3.11 Plot of the effective Poisson's ratio v_{12} as the waviness ratio (λ) is
increased
Figure 3.12 Plot of the effective shear modulus G_{12} as the waviness ratio (λ) is
increased72
Figure 4.1 Implementation of the progressive failure algorithm80
Figure 4.2 Stress strain curve illustrating progressive damage (not immediate).
81
Figure 4.3 Stress strain curve illustrating immediate material failure81
Figure 4.4 Illustration of applied boudary conditions to (a) a plain weave and (b)
a triaxial braid
Figure 4.5 Force deflection curve for a plain weave under tensile loading
(without failure)83
Figure 4.6 Force deflection curve for a plain weave under compressive loading
(without failure)83
Figure 4.7 Linear validation of one RVE of a plain weave under a tensile load. 84
Carrier and the commence of th

Figure 4.8 Linear validation of one RVE of a plain weave under a compressive load	e 84
Figure 4.9 Force deflection curve for a plain weave under tensile loading (with failure)	า 85
Figure 4.10 Force deflection curve for a plain weave under compressive loadi (with failure).	ing .85
Figure 4.11 Failure validation of one RVE of a plain weave under a tensile loa	ad. .86
Figure 4.13 Failure validation of one RVE of a plain weave under a compress load	ive .86
Figure 4.14 Force deflection curve for a triaxial weave under tensile loading (without failure).	.87
Figure 4.14 Force deflection curve for a triaxial weave under compressive loading (without failure)	.87
Figure 4.15 Linear validation of one RVE of a triaxial weave under a tensile lo (without failure)	ad .88
Figure 4.16 Linear validation of one RVE of a triaxial weave under a compressive load (without failure).	.88
Figure 4.18 Force deflection curve for a triaxial weave under tensile loading (v	with
Figure 4.19 Force deflection curve for a triaxial weave under compressive loading (with failure)	.89
Figure 4.19 Failure validation of one RVE of a triaxial weave under a tensile load	.90
Figure 4.21 Failure validation of one RVE of a triaxial weave under a	.90
compressive load	. y U

1.1 Intr

recent

stronge compos

plane c

been re

tradition

direction

stiffness

WFC's r

structure

T

for the .

Predictio

use in a

was ther

failure of

models a

Chapter 1

INTRODUCTION

1.1 Introduction

The popularity and interest in composites has grown considerably in recent years. Today laminated composite structures are engineered lighter, stronger and stiffer than their traditional counterparts. Typically, laminated composites are ideal for situations where the majority of the load is applied in the plane of the composite. The use of composites in structural applications has been revolutionized by the introduction of woven textiles composites. While traditional unidirectional composites have great strength and stiffness in the direction of the fibers, woven fabric composites (WFC's) have high strength and stiffness in both the warp and fill directions. Additionally, the woven nature of WFC's makes them less likely to fail due to delamination while increasing a structure's ability to carry large transverse loads.

The goal of the present research is to develop efficient methods and tools for the analysis of woven composite structures. First, an efficient stiffness prediction model is developed using traditional beam and shell finite elements for use in analyzing two-dimensional woven fabrics. This stiffness prediction model was then combined with a progressive failure algorithm to model the progressive failure of large-scale woven composite structures.

A brief review of literature concerning the various stiffness prediction models and modeling techniques is presented below.

that cre

tows. T

unit c

structi

compa

explic

homo

stiffn

many

[1] ar

1.2 Literature Review of Stiffness Prediction Models

Due in large part to integrated multi-directional fiber reinforcement, textile composite materials have many advantageous mechanical properties, including excellent out-of-plane strength and impact resistance. The ability of textile composites to conform to irregular shapes (i.e., to drape) and to integrate several parts into one piece makes them especially appealing for many applications. However, the same features that give rise to these sought-after mechanical properties also make it very difficult to analytically predict the mechanical response of these materials, thus complicating the design process.

Textile composite materials contain a very complex microstructure, where here the term microstructure is used to refer to the geometry and path of tows that create the fiber network and the resin regions that lie within and between the tows. The standard definition of the term microstructure does not always apply to textile composite materials, since often the tow size and the size of a repeating unit cell of the tow network are of the same order as the size of important structural features. Therein lies the primary difficulty in analyzing many textile composite materials: the microstructure is too complicated to be represented explicitly throughout the structure yet extremely large tows may be too large to homogenize.

Numerous analytical models have been developed to predict overall stiffness and strength of textile composite materials. Excellent reviews of the many classes of models and their assumptions are given by Cox and Flanagan [1] and by Tan, et al. [2].

develot mode: cross-a two on

continu

series

strain)

continu

matrice

tow.

hexaç cell is lamir

the b

conti load

ha

caus

in th

Early research conducted by Ishikawa and Chou [3-5] led to the development of three homogenization techniques. The first was the mosaic model [3], which idealized a textile composite as an assembly of asymmetric cross-ply laminates. The mosaic model divided the two-dimensional problem into two one-dimensional models, the series (iso-stress) model and the parallel (iso-strain) model. The mosaic model however did not account for the undulation or continuity of the fibers.

The Fiber Undulation Model (FUM) [4] was developed to consider the continuity and undulation of the fibers in one direction. The FUM is essentially a series model, however, the extension, bending-extension, and bending stiffness matrices of CLT are a function of the coordinate along the axis of the undulating tow.

Ishikawa and Chou [5] also developed the bridging model for predicting the behavior of satin weave composites. The bridging model idealizes the hexagonal shape of the unit cell as a square to simplify calculations. The unit cell is then divided into five regions, four of which are simply treated as cross-ply laminates, while the remaining region contains the interlaced fibers. The continuity and undulation of the warp fibers is ignored due to the fact that the load is applied in the fill direction and the effect of the warp fibers is expected to be small. The lower stiffness of the warp fibers in the direction of the loading causes the fill fibers to carry more of the applied load and act as a "bridge" to aid in the load distribution throughout the structure.

Mode!

the fib

stiffnes

the gid

stiffnes

averag

[8] to p

method

incline

accou

develo

assun

the b

accol

continue Effec

into t

[10]

SAN

Pastore and Gowayed [6] proposed a self-consistent Fabric Geometry Model (FGM). This model was a modification to the original FGM [7] that treated the fibers and matrix as composite rods with its correct orientation and local stiffness tensor. The local stiffness tensor of each rod is then transformed into the global coordinate system and assembled to obtain the global composite stiffness tensor based on each rod's relative volume fraction (stiffness averaging). The FGM was also used with an energy-based analysis by Ma, et al [8] to predict the effective properties of three-dimensional braided textiles.

The Fiber Inclination Model (FIM) introduced by Yang, et al. [9] is another method based on laminate theory. In the FIM the fiber tows are represented as inclined unidirectional lamina. Because of this idealization the FIM does not account for fiber interlock and bending.

Naik and Ganesh [10], Raju and Wang [11], and Aitharaju and Averill [12] developed improved laminate theories that did not make the simplifying assumptions associated with the mosaic model, the fiber undulation model, or the bridging model. Without these simplifications these new theories could account for undulation in both the warp and fill directions along with fiber continuity. Each method divided the unit cell of a textile into subregions. Effective properties for each subregion were calculated and then reassembled into the global model.

Two new modeling techniques that were introduced by Naik and Ganesh [10] were the slice array model (SAM) and the element array model (EAM). The SAM discretized the unit cell into slices along the direction of loading. The

effect separa

second

could t

were

assemi

then as

cell.

bridging assum

Effectiv

and re

was m

constitution system

eleme

mat.

was s

Howe

avera

effective properties of the unit cell were obtained by analyzing each slice separately and then reassembled the slices using the isostrain formulation. The second method, the EAM, also discretized the unit cell by slicing it, but the slices could be made either parallel or transverse to the direction of loading. The slices were again subdivided into elements, and the individual elements were assembled in parallel or series to obtain the slice properties. The slices were then assembled in series or parallel to obtain the effective properties of the unit cell.

Raju and Wang [11] developed improvements to the fiber undulation and bridging models, while retaining their simplicity without making any simplifying assumptions. The unit cells of a textile composite were divided into subregions. Effective properties for these subregions were calculated through laminate theory and reassembled using stress averaging.

Aitharaju and Averill [12] also subdivided the unit cell. Each subregion was modeled as an eight noded brick element. The material properties of the constituent material in each element were transformed into a local coordinate system and combined through the use of an effective modulus. The finite element method was then utilized to perform the analysis of a textile composite mat.

Sankar and Marrey [13] used the selective averaging model (SAM) which was similar to the slice array and element array models of Naik and Ganesh [10]. However, the SAM allowed the stiffness or compliance coefficients to be averaged selectively based on either an isostress or isostrain assumption.

construction conduction

param:

are hyt

repres∈

that full

model.

structure

٧

wavines

0.167, 0

a [0/90],

analysis

۷

subregio

approxir

rather th

within ea

very poo

single fi

Finite element models of the explicit textile structure are tedious to construct and computationally very expensive to solve. Some research has been conducted on the fully three-dimensional geometry to study the effect of various parameters on the effective moduli [14, 15]. Several other techniques exist that are hybrids of homogenization and the finite element method. This is achieved by homogenizing the material properties on the microscale level and representing them with finite elements on the macro scale.

Dasgupta et al. [14] developed a two-scale homogenization method that fully discretized the unit cell of a plain weave in the form of a finite element model. The macroscale stress and strain fields were volume averaged over the structure yielding the homogenized composite properties.

Whitcomb [15] applied the finite element method to the study of the effect waviness ratio on the effective moduli. Predicted moduli for waviness ratios of 0.167, 0.25, and 0.5 were studied and quantitative comparisons were made with a [0/90]_s tape laminate.

Whitcomb et al [16] also introduced the use of macro finite element analysis to study woven composites. The macro element was subdivided into subregions or subelements that modeled the fiber tows explicitly. A single approximation for the displacement field was used throughout the macro element rather than a multiple field approximation that would assume a different field within each subelement. In some instances the single field approximation gave very poor results compared to a multiple field approximation. However, the single field method was computationally much cheaper than the multiple field

approx

be use

great of a te

local/g

time it

finite e

with a

of inter

the lar

dimen

compu

materi

repres

three-

individ

dimen

repres

approximation. Despite the single field approximation's shortcomings, it can still be used with good success on a wide range of problems.

Woo and Whitcomb [17] also used the macro element combined with a local/global finite element analysis. The scale of textile composites contributes a great deal to the difficulties that arise in their analysis. Often, the microstructure of a textile composite is far too complex to model explicitly, while at the same time it is too large to model as a single homogenized material. A local/global finite element analysis can be used to obtain the overall response of the structure with a coarse global mesh, then refined meshes are used to capture local effects of interest.

Finite element analysis was used by Marrey and Sankar [18] to determine the laminate A, B, and D matrices along with the thermal expansion coefficients of a textile composite. The unit cell of a textile composite is modeled with three-dimensional finite elements. The effective properties of the unit cell are computed by assuming a uniform state of strain at the macroscale level.

Blackketter et al. [19] used the finite element method to model nonlinear material behavior. This was combined with a progressive failure algorithm to represent the effects of damage through the use of stiffness reduction. The three-dimensional model of the unit cell represented the fiber tows and resin individually for examining tensile and shear loading.

The Binary Model developed by Xu et al. [20] idealizes a three dimensional weave using finite elements. Two-noded line elements are used to represent the axial properties of the fiber tows while the transverse stiffness,

shear dimen

along compc: space s

was the

behavio from tov

features modelin

develop

such as

tow cros

basic fo

demons

a variet

1.3 Org

1

use in a modeling

needed

shear stiffness and Poisson's ratio of the composite are model with threedimensional "effective medium" elements.

Lei et al. [21] combined computer aided geometric modeling (CAGM) along with finite element procedures to represent three-dimensional braided composites. The identified unit cells of a braided composite were modeled as space structures and discretized using finite elements. A finite element analysis was then performed to predict the elastic behavior of the composite structure.

In the present study, a model is developed for simulating the structural behavior of textile composite materials throughout a wide range of scale sizes – from tow level to structural level. The model attempts to capture the essential features of the material behavior in the simplest possible form in order to allow modeling of large sections of a textile composite structure. The main objective in developing such a model is to allow the investigation of geometrical irregularities such as uneven tow spreading or compacting, tow waviness, spatial variations in tow cross-section due to tow pinching, spatially varying tow twist, etc. Here, the basic formulation of the discrete tow model is discussed in detail and its utility is demonstrated for the prediction of effective properties and progressive failure for a variety of plain weave and triaxial braid materials.

1.3 Organization of the Thesis

The goal of the present research is to develop fast and efficient tools for use in analyzing woven fabric composites. Chapter 2 describes a simplified modeling technique for a woven composite which is faster in terms of man hours needed to build the model and computational solution time required. Rather than

explic

eleme

tow.

hexah:

represe

represe

tow wa

of a cur

of com

model

structu

from

prese

each (

explicitly model the fiber tow and resin matrix as fully three-dimensional elements, traditional beam and shell elements are used to represent the fiber tow. These tow elements are then 'woven' through a repeating array of hexahedral brick elements that represent the resin matrix.

Chapter 3 extends the idea of using a simplified model by again representing the fiber tow with beam elements. However, the resin matrix is represented using traditional plane stress shell elements. While this simplified discrete-tow model is two-dimensional, it captures the three-dimensional effect of tow waviness through a stiffness reduction factor that is derived using the theory of a curved beam on an elastic foundation.

Using the simplified discrete-tow model, Chapter 4 introduces the concept of combining this modeling technique with a progressive failure algorithm to model damage and failure propagation within a large-scale woven composite structure.

The final chapter, Chapter 6, presents the conclusions that can be drawn from the present research. Recommendations for future study are also presented in this chapter.

In an effort to facilitate ease of reading this thesis, tables and figures of each chapter can be found immediately following the corresponding chapter.

size of

behavio

homoge

microlev

fraction

structure

C

woven o

models

these m

computa

use sor

these m

make si

limit thei

Chapter 2

Three-dimensional analysis of a woven composite

2.1 Introduction

The problem of analyzing woven composites is an issue of two conflicting scales. The micro-level represents the scale of the weave. Tow shape, spacing and waviness ratio are examples of dimensions on the order of the microlevel. The overall shape and geometry of the global structure is considered macrolevel. However, the size at the microlevel is such that it is small compared to the overall size of the structure itself, but often it is not small enough that the microstructural behavior and effects can simply be smeared together and represented as one homogenized material. This means that small changes or variations at the microlevel such as a change in tow spacing or a variation of the fiber volume fraction can have a significant impact on the overall behavior of the global structure.

Currently there are two dominant approaches used in the analysis of woven composites. The first method has been to create fully three-dimensional models of the woven fabric and its underlying microstructure. However, building these models is extremely time consuming and requires a prohibitive amount of computational time and resources for everyday use. The second method is to use some form of homogenization scheme to simplify the analysis. Although these methods require significantly less computing resources, they in general make simplifying assumptions that either degrade the quality of the results or limit their robustness.

computa fully thre between modeling a woven represen the resin beam or through centerline through r rise to se dimensio visualizat

Cı

2.2 Mode

has occu

composite

study con an idealize

was assur

Currently there is a great need for a modeling technique that combines the computational benefits of homogenization approaches with the robustness of a fully three-dimensional analysis. Clearly some form of tradeoff is necessary between the two approaches. This chapter presents two novel methods for modeling a woven composite structure. The first method models the fiber tows of a woven composite as one-dimensional beam elements while the second method represents the fiber tows as two-dimensional shell elements. In both methods the resin matrix is modeled using hexahedral brick elements. The appropriate beam or shell element that is used to discretize the fiber tow is then woven through the three-dimensional grid of resin elements along the fiber tow centerline. The attachments of the tow and resin elements are maintained through nodal connectivity. The discrete modeling of the tows and resin gives rise to several advantages of both the traditional homogenization and fully threedimensional methods currently used. The discrete models allow for the easy visualization of the structure and the locations of the fiber tows after deformation has occurred. Additionally, these models can be easily expanded to model large composite structures in a computationally efficient manner.

2.2 Model Description

The general model that was the basis for assessing the models in this study consisted of a rectangular composite cantilever beam, that is intended as an idealized section from a woven composite. The composite cantilever beam was assumed to be a strip of resin with a single fiber tow woven along the axis of

the beam (Figure 2.1). Three models were derived from the base model. The first of these was a brick and beam model (Figure 2.2), which represented the fiber tows and resin as beam and hexahedral brick elements respectively. The second model was the brick and plate model (Figure 2.3), which used the same hexahedral brick elements to represent the resin as in the brick and beam model. However, in this case, the fiber tows were modeled using two-dimensional shell elements. The final model was a fully three-dimensional model (Figure 2.4), which used tetrahedral elements to discretize both the resin and the fiber tow as fully three-dimensional model was to serve as a means of validating the previously discussed models.

2.2.1 LOADING

Four load cases were used to study the proposed finite element models. Each case was intended to analyze a specific characteristic of the proposed model and its ability to predict the fully three-dimensional equivalent behavior. The four load cases are summarized in Table 2.1 and graphical illustrations of each respective load case can be seen in Figure 2.6 – Figure 2.9.

2.2.2 GEOMETRY

The geometrical description of the model is found in Figure 2.1. The same exterior dimensions were used for each of the three models. Parameters specific to the geometry of the fiber tow were dependent on the type of model used.

The undulation of the fiber tow was assumed to be sinusoidal along the axis of the beam. The cross-sectional shape of the tow was assumed to be lenticular and to have the same sinusoidal shape as the tow centerline. The equations for the tow shape and other pertinent data are summarized in Table 2.2. In each of the models the path line of the beam or shell elements followed the centerline of the fiber tow.

In the case of the brick and beam model it was only necessary to assign a cross-sectional area and moments of inertia to the beam elements.

Consequently, the tow cross sectional area and moments of inertia were directly assigned to the beam elements.

Modeling the fiber tow with shell elements in the brick & plate model involves more consideration. It is desirable for the shell elements to have both the correct axial stiffness along with the bending stiffness. However, the cross-sectional shape of the fiber tow is assumed to be lenticular, while the cross-sectional shape of a shell element is rectangular. This mismatch in cross-sectional shapes makes it impossible to capture the correct axial and bending stiffness of a lenticular cross-section with a simple rectangle. Noting the previous argument, it is possible to make a sacrifice in the model's accuracy to help improve its ease of use. Therefore, the width and cross-sectional area of the shell element and the lenticular fiber tow were chosen to be identical. Knowing the width and area of the rectangular cross-section, the element thickness could then be easily found.

2.2.3 MATERIAL PROPERTIES

The goal of this study was not to compare with experiments, but rather to investigate the viability of the proposed models. To simplify the analysis process the material properties used in this analysis are approximate values that are typical of a glass/epoxy woven composite. Additionally, to aid in the simplification of the problem, the materials were assumed to be linearly isotropic. The properties used in the analysis can be found in Table 2.3.

2.3 Finite Element Models

In total, six finite element models were created for the purposes of this study, and their properties are summarized in Table 2.3. For the fully three-dimensional, brick and beam and brick and plate cases studied, two models were created of each case with different mesh refinements. Similar models with different levels of mesh refinement serve several purposes. At the most basic level, multiple models of the same problem help to eliminate possible user errors, which could be noticed if large discrepancies appeared between the solutions. Secondly, it is possible to conduct a convergence study with models of varying mesh refinement. This allows for the ability to see what level of refinement is needed when solving similar problems and to make sure that the solution is converging in the right manner.

Α

2.3.2 BR

beam. The block of composite simple state each other beam election center elements nodes. A rare that

centerline

nodes of

approxim

the path

2.3.1 FULLY THREE-DIMENSIONAL

A complete three-dimensional representation of the geometry was created using 10 noded tetrahedral elements (see Figure 2.4). The finite element mesh of the fiber tow and resin were created as separate objects. However, at the tow/resin interface mesh connectivity was maintained.

2.3.2 BRICK AND BEAM

The brick and beam concept is an idealized version of the composite beam. The first step in creating the model was to construct a three-dimensional block of 8-noded hexahedral elements with the same dimensions as the composite cantilever beam. The hexahedral brick elements were arranged in a simple stacked configuration that resembled boxes placed next to and on top of each other (see Figure 2.5). The fiber tow was then added by 'weaving' 2-noded beam elements through the block of hexahedral resin elements along the fiber tow centerline. The connectivity between the beam elements with the brick elements was accomplished by simply attaching the elements at coincident nodes. As a result of the stacked configuration of the brick elements, it was quite rare that the nodes of the brick elements coincided with the path of the tow centerline. Therefore, it was necessary to attach the beam elements to the nodes of the brick elements that were closest to the tow centerline. approximation, combined with the linear shape of the beam elements, resulted in the path of the actual fiber tow being represented as piece-wise linear (see

Figure 2 path con; were built

accurate

composit

2.3.3 BR

Sir

matrix (so

same ba

brick and

and plate

2.4 Num

models. between

T

reason t

deflectio

Point loc

Figure 2.10). Therefore, as the model is refined, the approximation of the tow path converges to the actual path of the fiber tow. Coarse and refined models were built in order to examine the necessary levels of refinement required for accurate results. The combination of the brick and beam elements to form the composite beam model is illustrated in Figure 2.2.

2.3.3 BRICK AND PLATE

Similar to the brick and beam model, the brick and plate model uses the same background mesh of hexahedral brick elements to represent the resin matrix (see Figure 2.5). However, the fiber tow is modeled with 4-noded shell elements (see Figure 2.3). As with the brick and beam model, the brick and plate model also represents the path of the fiber tow as piece-wise linear. The brick and plate model was conceived in order to overcome certain shortcomings of the brick and beam model. These shortcomings are discussed later in this chapter.

2.4 Numerical Results

The differences between the brick models and the fully three-dimensional models, such as the fiber volume fraction and the fundamental difference between the finite element models, made it difficult to compare results. For this reason two different forms of the results are presented. First, fiber tow path-line deflection results are compared and followed by deflection results of a single point located on the structure.

Path-line deflection results of the analyses for each of the models are shown in Figures 2.11 through 2.30. Each of the figures depicts a particular displacement component of the fiber tow centerline along the axis of the composite beam for a specified loading condition.

Table 2.4 contains deflection data from the top of the mid-span of the composite beam. This location was chosen because its distance from where the boundary conditions and loads were applied was great enough that their effect on the solution results would be minimized. It is also important to note that the three models were fundamentally different from each other and large variations in the analysis could occur. This was most evident where the loads were applied. In the models where the resin was represented with brick elements, extremely large displacements occurred because the resin is more compliant than the fiber tow and there was a considerably larger amount of resin in the brick models due to the resin volume fraction equaling one.

2.4.1 LOAD CASE A: AXIAL LOADING

Figures 2.11 through 2.14 illustrate the fiber tow path-line displacement along the beam axis under an axial load of 5 N. Table 2.4 contains displacement data of two fixed points A and B located on the top of the composite beam at its mid-span (see Figure 2.6)

As can be seen from the figures, both the brick and beam and the brick and plate models follow the same trends as the fully three-dimensional model. For this case the axial displacement, u(x), is predicted quite well by both the

coarse aldisplacer refined refined refined refined refined refined the normal finite elements.

of the dis

Re

2.4.2 LC

F

along the

trend as

attribut refined

model

both t

coarse and the refined models (Figure 2.11 and 2.12) However, the normal displacement, v(x), is not captured as well in the coarse model as in the more refined model (Figures 2.14 and 2.14), which agrees with the fully three-dimensional model quite well. Additionally, the trend in solution convergence of the normal displacement in the coarse and refined models demonstrates that the finite element solution is indeed converging in the correct manner from below.

Results for the transverse displacement, w(x), are meaningless as a result of the displacements being essentially zero in comparison to the displacements that occur in the other directions.

2.4.2 LOAD CASE B: BENDING ABOUT THE Y-AXIS

Figures 2.15 through 2.18 illustrate the fiber tow path-line displacement along the beam axis under a transverse (z) load of 5 N. Table 2.4 contains displacement data of two fixed points A and B.

The axial displacement of the brick and plate model follows the same trend as the fully three-dimensional model and agrees quite well except close to the end of the beam where the loads were applied. This most likely can be attributed to the boundary conditions affecting the results. The coarse and refined brick and beam models do not agree well with the fully three-dimensional model when x > 6 in.

The normal displacement (see Figure 2.17 and 2.18) is predicted well by both brick and plate models except near the location where the load was applied.

The

displa

the b

2.4.

(y) l

illus

2.4

ger 2.2

plat

pre

bric

aη

disp

The brick and beam models again do a poor job of predicting the correct displacements when v is greater than 6in.

The transverse displacements for both the coarse and refined versions of the brick and beam and brick and plate models agree well with the fully threedimensional model.

2.4.3 LOAD CASE C: BENDING ABOUT THE Z-AXIS

For the case of bending about the z-axis, Figures 2.19 through 2.24 illustrate the fiber tow path-line displacement along the beam axis under a normal (y) load of 5N. The displacement data for points A and B can be found in Table 2.4.

Both the brick and beam and the brick and plate models follow the same general trends as the fully three-dimensional model (see Figures 2.19 through 2.24). The axial displacement, u(x), of both the brick and beam and brick and plate models agree well with each other, however, the two models seriously over predict the axial displacement. This could be attributed to the fact that in the brick models the interaction of the tow thickness with the surrounding resin plays an important role in the overall behavior of the structure. However, the normal displacement, v(x), is captured well in both the coarse and refined models.

Ir

largest o

and bea

plate mo

The tran

beam or

notably,

elements

form of a

2.5 Conc

Th tow in th

process a

freedom.

^{brick} and

2.4.4 LOAD CASE D: TORSIONAL LOADING

Figures 2.25 through 2.30 depict the fiber tow path-line displacement along the beam axis under a torsional load of 5 N*cm and Table 2.4 contains displacement data of two fixed points A and B.

In the case of the axial displacements (Figures 2.24 and 2.25), the brick and beam and brick and plate models follow the same general trends, with the largest deviations occurring near the end of the composite beam where the load was applied. The normal displacements are closely predicted by the brick and plate model and most accurately in the refined model while the brick and beam model does not predict the displacement as accurately near the end of the beam. The transverse displacement, (z), is not captured very well by either the brick and beam or the brick and plate models, however, the basic trends are present. Most notably, the brick and beam model results are poor due to the fact that the beam elements have no length in the z direction and therefore respond poorly to any form of an applied torque.

2.5 Conclusions

The intent of this study was to show the validity of representing the fiber tow in the simplest yet most accurate form to expedite the model building process and to decrease solution time by decreasing the number of degrees of freedom. However, in the majority of the cases studied, it was evident that the brick and plate model outperformed the brick and beam model. Consequently,

the more

In

evident

suited.

technique

the more accurate brick and plate model contained more degrees of freedom within the problem.

In the cases where the brick and plate model performed poorly it was evident that a fully three-dimensional representation of the model was best suited. This of course is the paradox encountered with simplified modeling techniques. With each simplification some information is lost in the process.

Table Lo

1 1 1

Table 2.1 Load case summary.

Load Case	Description	Force (N)	Applied Direction
Α	Axial Loading	5	+x
В	Bending about y	5	-Z
С	Bending about z	5	-у
D	Torsion	2 2	-y +v

Table 2.2 Tow geometrical properties.

Property	Value	Location	
Centerline Equation:	$y = \frac{1}{4} \sin \frac{2\pi}{5} x + 0.5$	z=0	
Cross section top:	$y = \frac{1}{4} \sin \frac{2\pi}{5} z + 0.8$	x=0	
Cross section bottom:	$y = \frac{1}{4} \sin \frac{2\pi}{5} z + 0.7$	x=0	
Width:	21.7 mm		
Volume:	5463 mm ³	1	
Area:	54.6 mm ²		
lxx:	46.5 mm⁴		
lyy:	124.0 mm⁴		
lxy:	-4.014E-02 mm⁴		

Table 2.3 Material properties of the constituent materials of the woven composite beam.

	Young's Modulus (GPa)	Poisson's Ratio 0.34	
Resin	4.3		
Fiber Tow	72	0.2	

Table 2.4 Mid-span deflection data of points A and B for each load case.

Model Description	Mesh	Load Case	Displacement		
			Point A	Point B	% Error
Fully 3D model w/ lenticular fiber	7858 10-noded tetrahedrons	Α	9.35E-08	9.35E-08	N/A
		В	-3.96E-05	-3.96E-05	N/A
		С	-4.84E-06	-4.84E-06	N/A
		D	-1.88E-06	1.88E-06	N/A
Fully 2D model	23040 10- noded tetrahedrons	Α	8.14E-08	8.14E-08	N/A
Fully 3D model w/ lenticular		В	-3.56E-05	-3.56E-05	N/A
fiber		С			N/A
11501		D	-1.65E-06	1.65E-06	N/A
	1600 8-noded	Α	9.75E-08	9.75E-08	-4.29%
Brick and Beam	hexahedrons	В	-3.88E-05	-3.88E-05	2.02%
coarse	40 2-noded	С	-4.24E-06	-4.24E-06	12.53%
	beams	D	-8.86E-07	8.86E-07	52.94%
	12800 8-noded	Α	9.49E-08	9.49E-08	-1.47%
Brick and Beam	hexahedrons	В	-3.90E-05	-3.90E-05	1.67%
refined	80 2-noded	С	-4.28E-06	-4.28E-06	11.66%
	beams	D	-1.03E-06	1.03E-06	45.13%
	1600 8-noded	Α	9.58E-08	9.58E-08	-2.44%
Brick and Plate	hexahedrons	В	-3.91E-05	-3.91E-05	1.34%
coarse	160 4-noded	С	-4.10E-06	-4.10E-06	15.47%
	quad	D	-1.75E-06	1.75E-06	6.99%
Brick and Plate refined	12800 8-noded	Α	9.35E-08	9.35E-08	-0.03%
	hexahedrons	В	-4.01E-05	-4.01E-05	-1.23%
	80 4-noded	С	-3.76E-06	-3.76E-06	22.32%
	quad	D	-1.77E-06	1.77E-06	6.00%

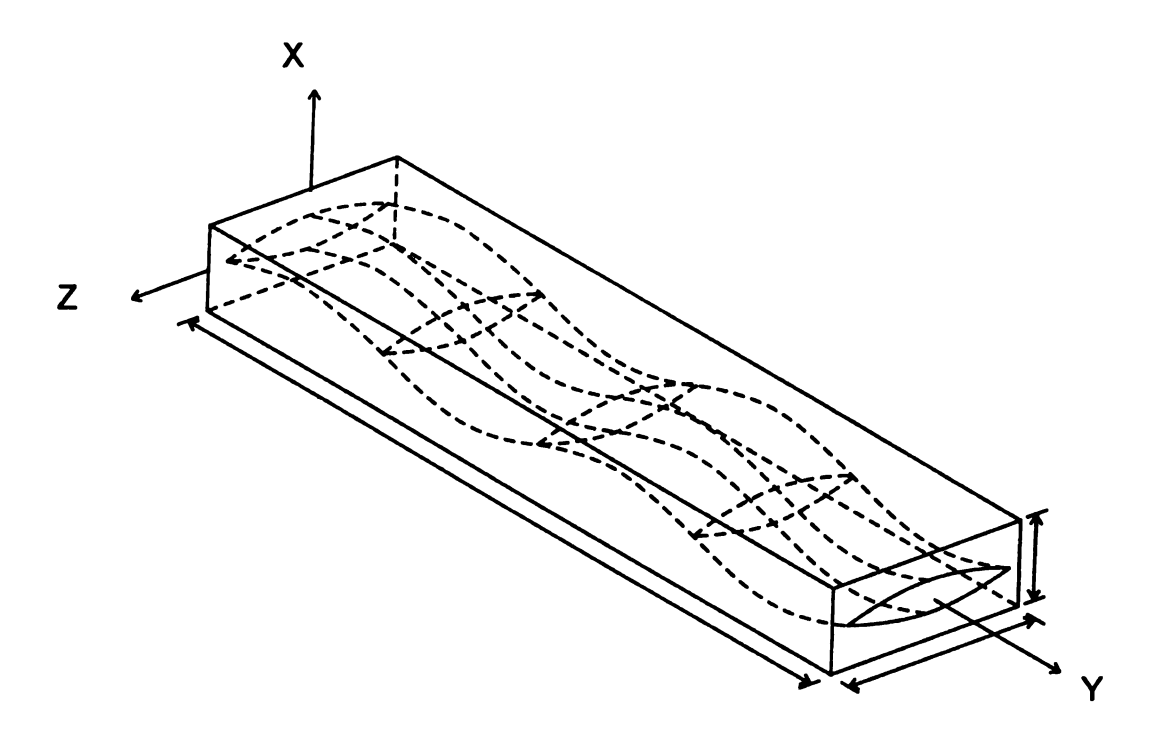


Figure 2.1 Geometry of the cantilever beam with a single undulating fiber.

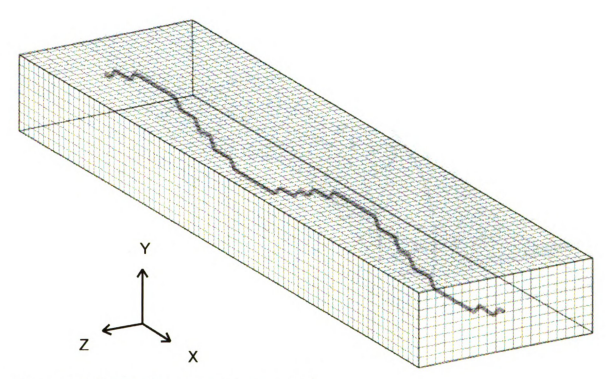


Figure 2.2 Refined brick and beam model.

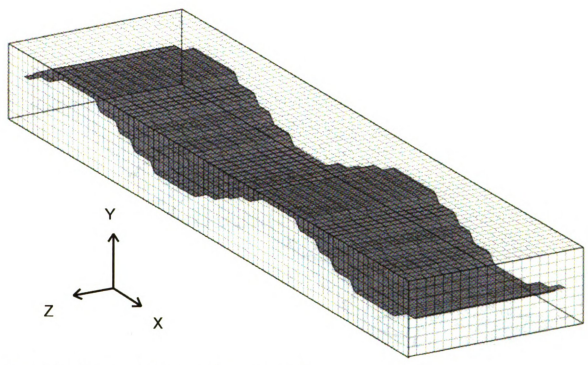
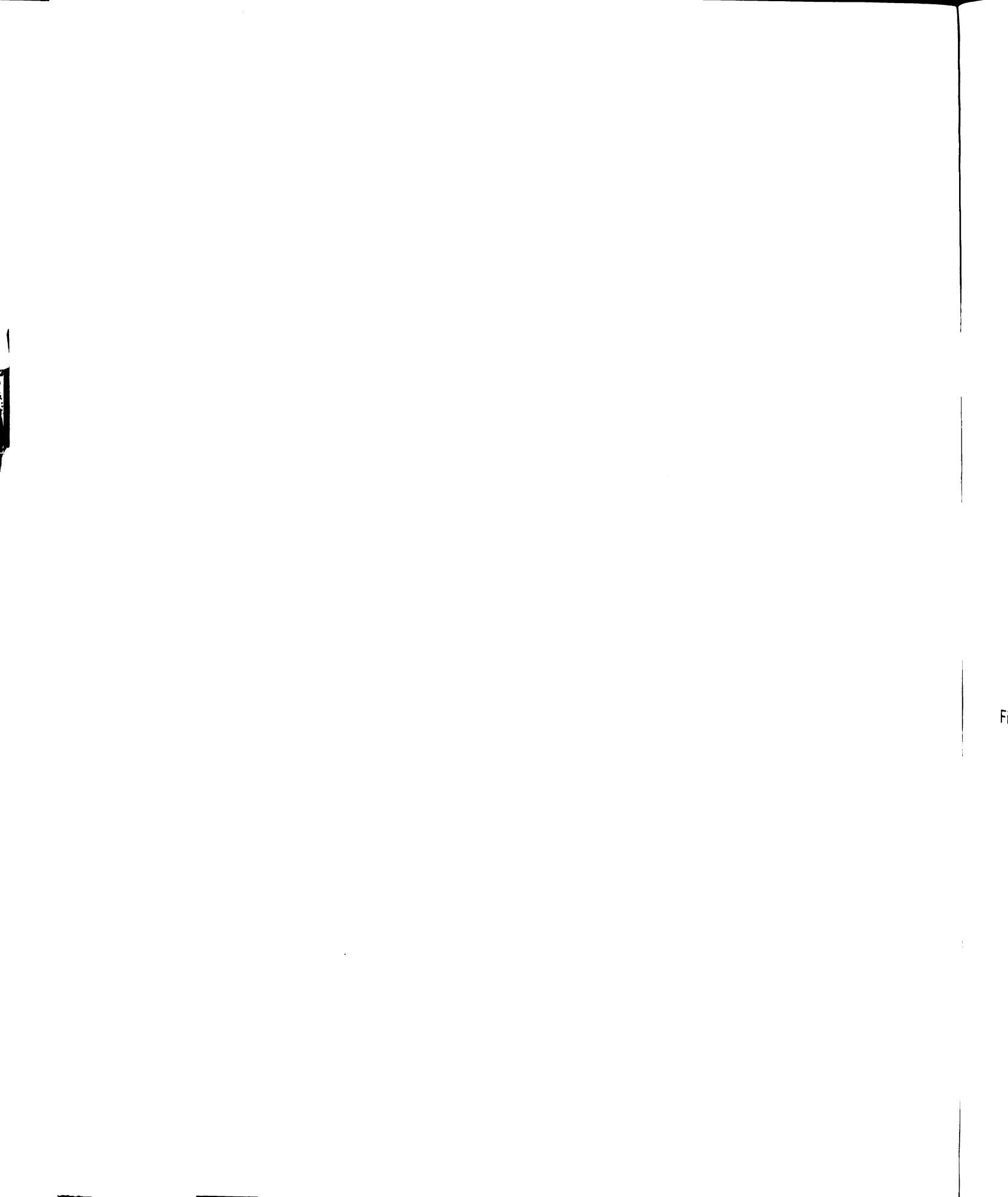


Figure 2.3 Refined brick and plate model.



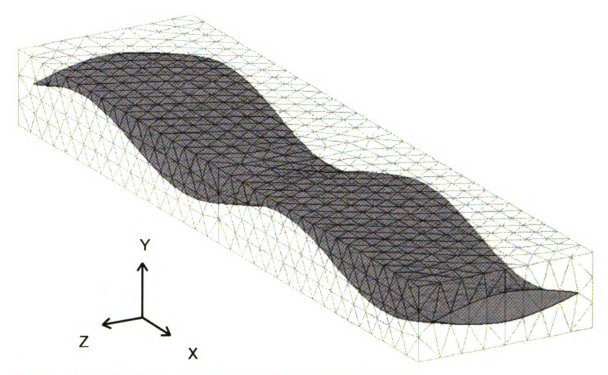


Figure 2.4 Fully three-dimensional finite element model.

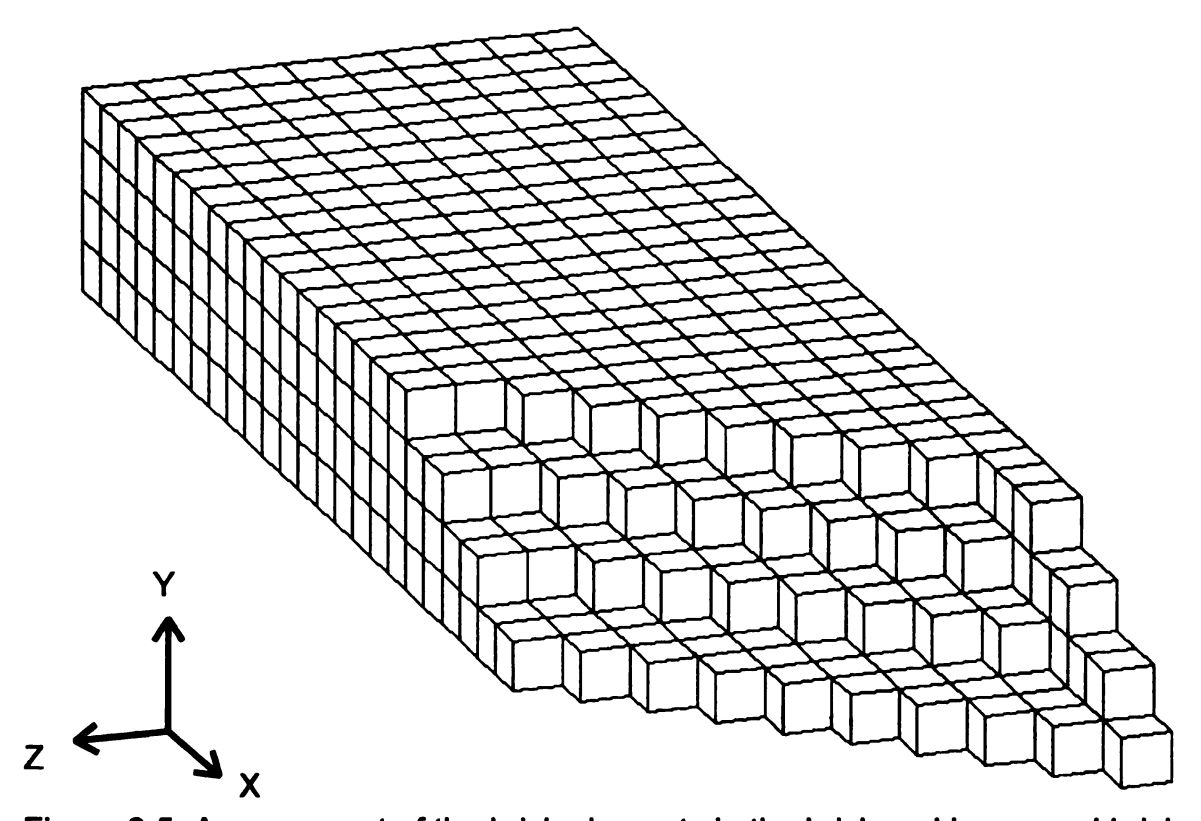


Figure 2.5 Arrangement of the brick elements in the brick and beam and brick and plate models.

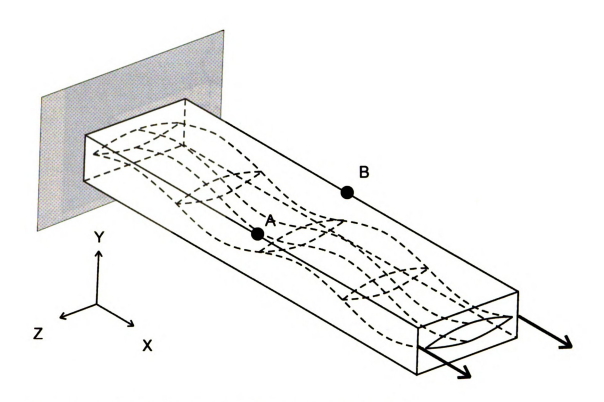


Figure 2.6 Axial loading condition applied to each model.

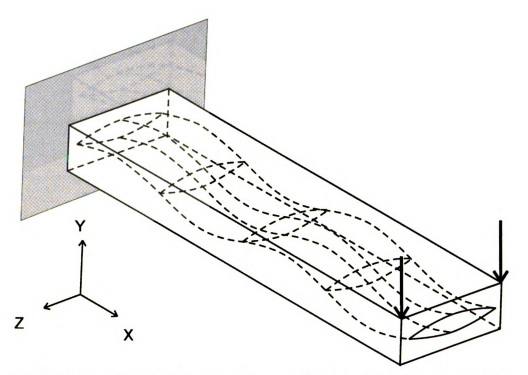


Figure 2.7 Normal (X-Y bending) loading condition applied to each model.

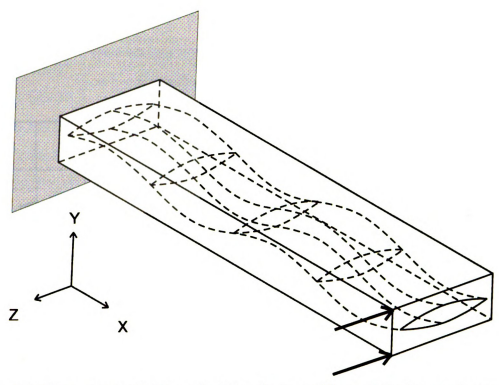


Figure 2.8 Transverse (X-Z bending) loading condition applied to each model.

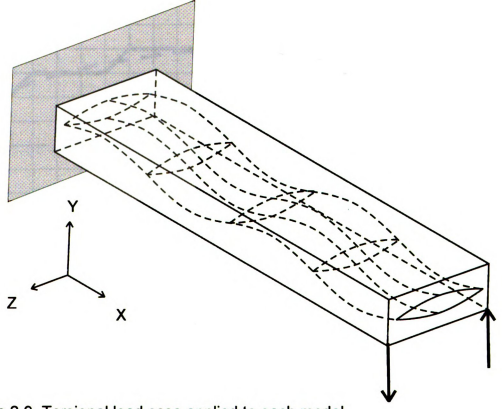
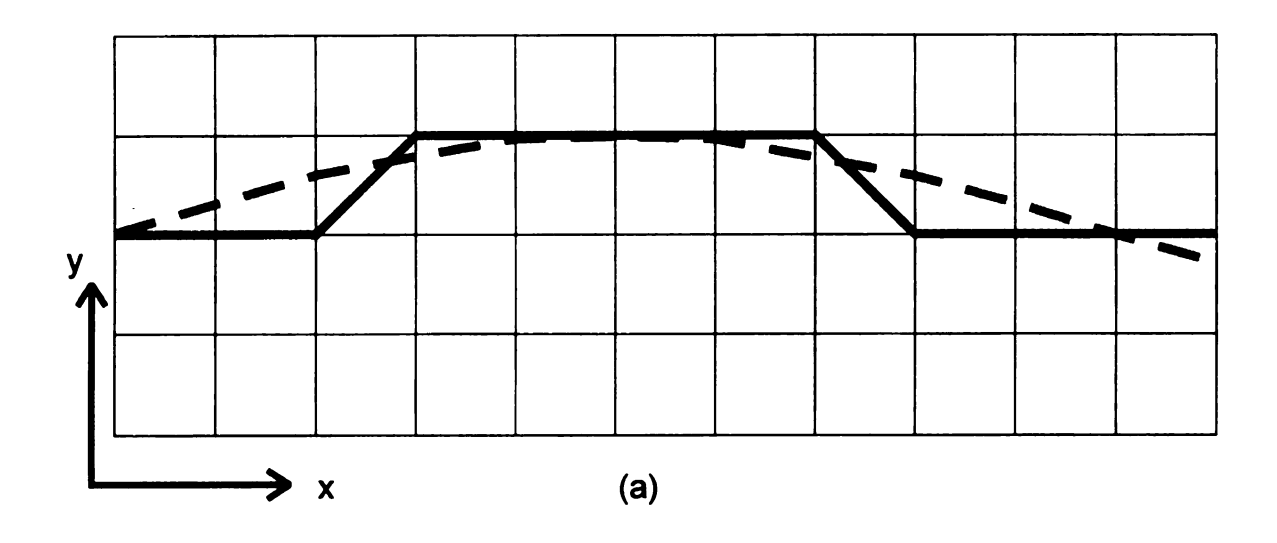
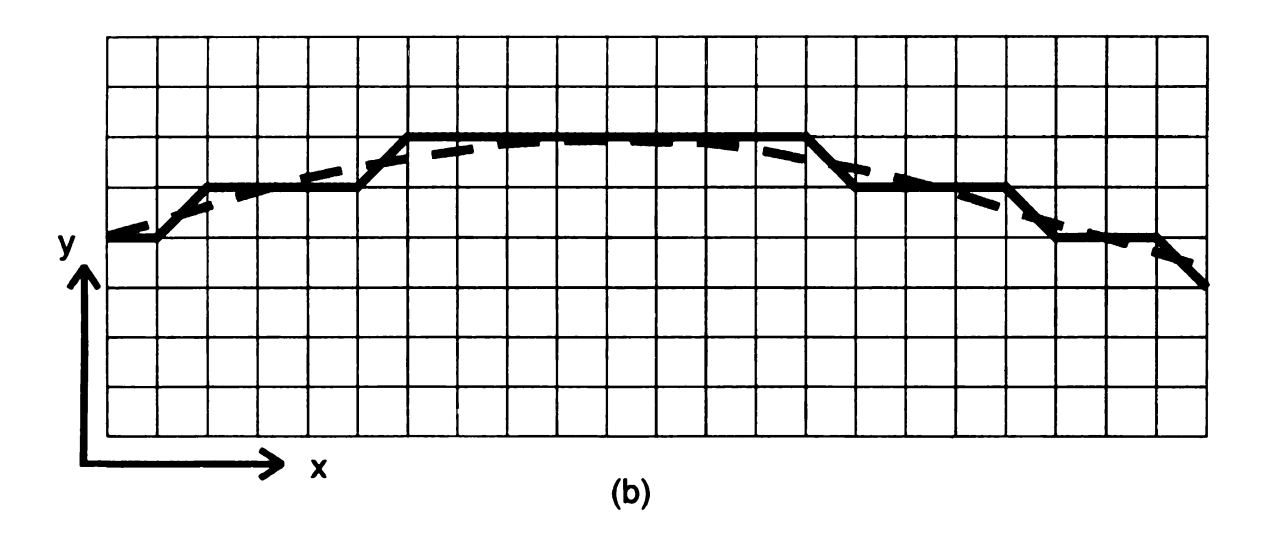


Figure 2.9 Torsional load case applied to each model.





— — True fiber pathline

----- Approximated pathline

Figure 2.10 Piece-wise linear approximation of the fiber tow path-line using beam and shell elements (a) coarse model, (b) refined model.

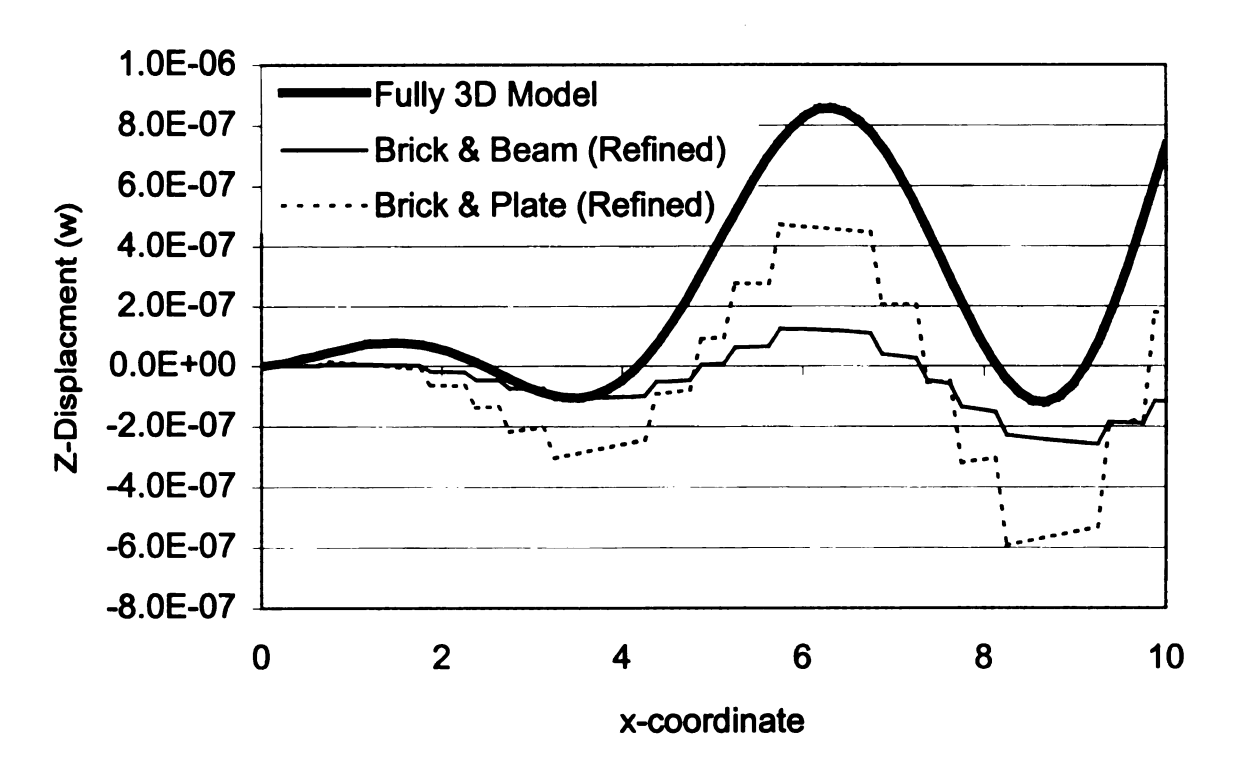


Figure 2.11 Axial displacement (u) along the tow centerline of the coarse brick & beam and brick & plate models due to an axial load.

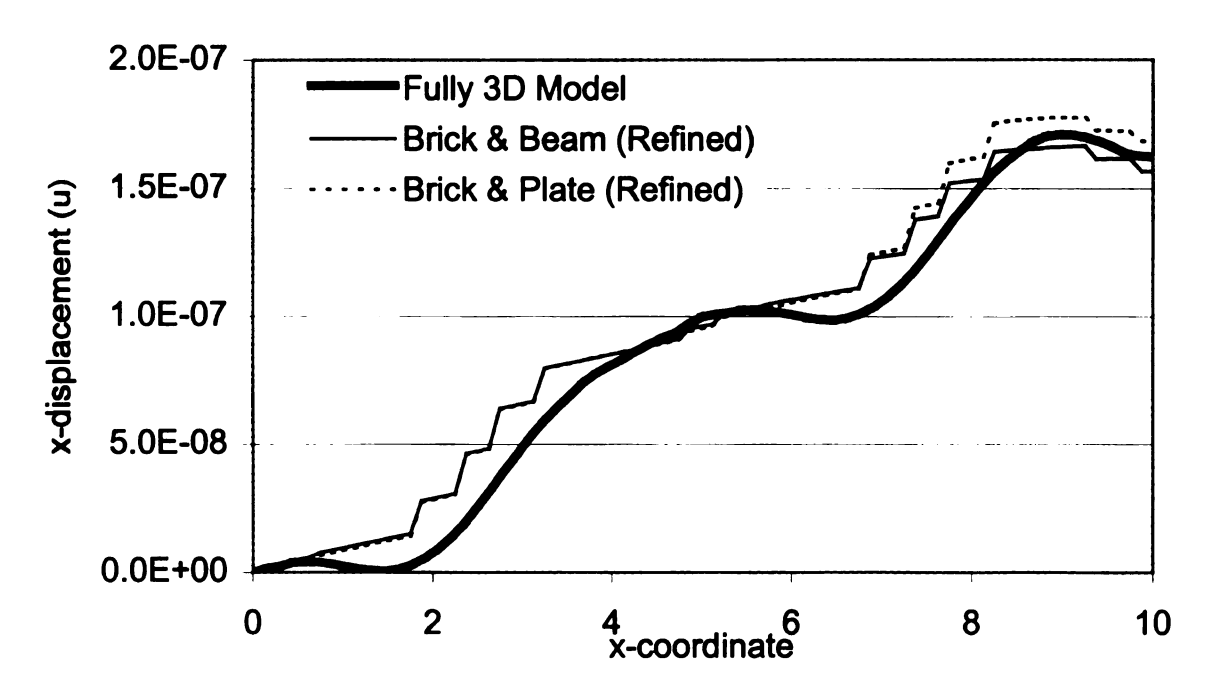


Figure 2.12 Axial displacement (u) along the tow centerline of the refined brick & beam and brick & plate models due to an axial load.

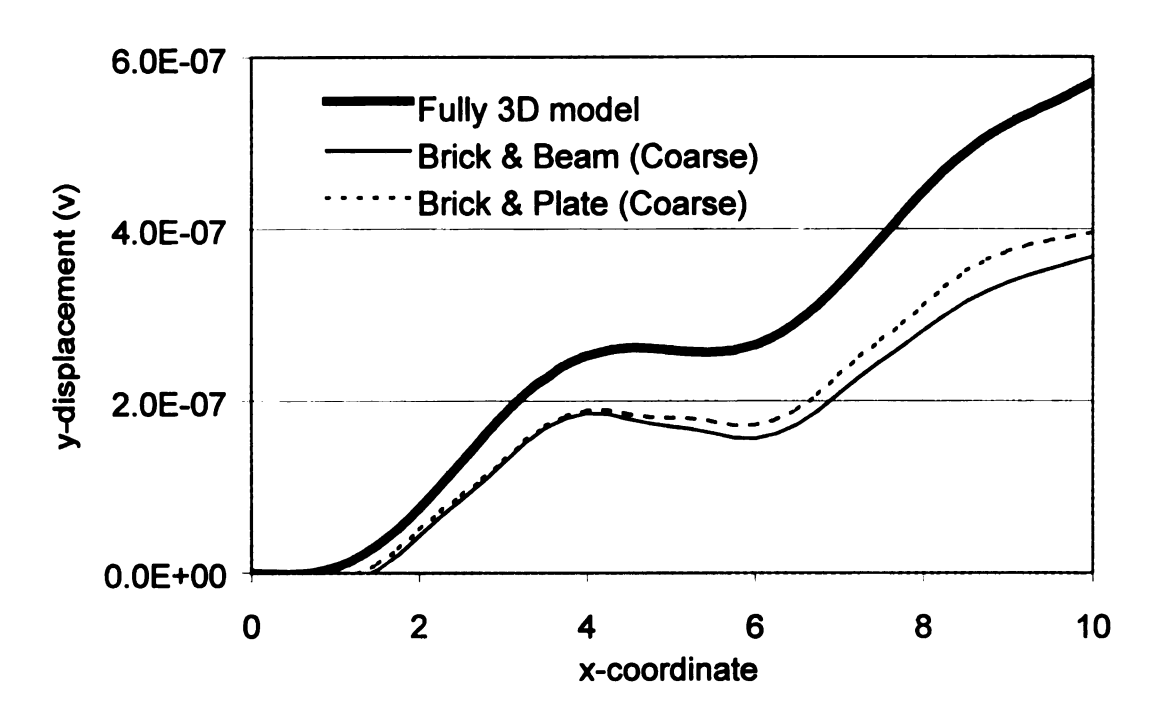


Figure 2.13 Normal displacement (v) along the tow centerline of the coarse brick & beam and brick & plate models due to an axial load.

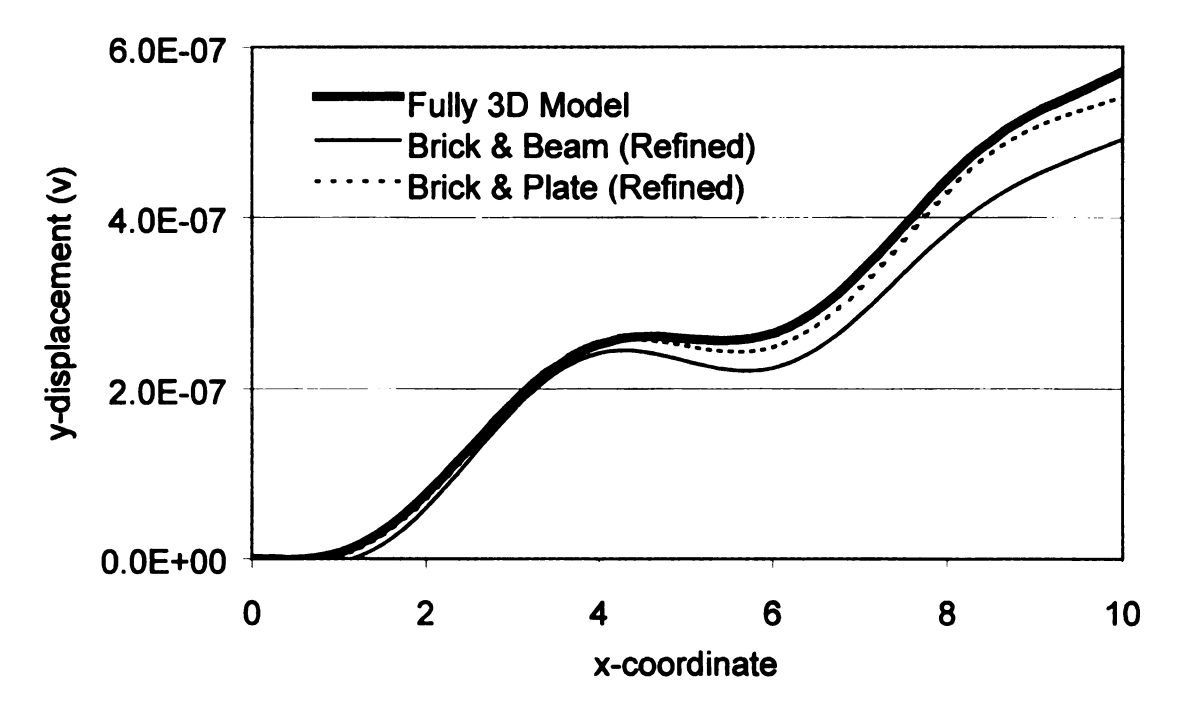


Figure 2.14 Normal displacement (v) along the tow centerline of the refined brick & beam and brick & plate models due to an axial load.

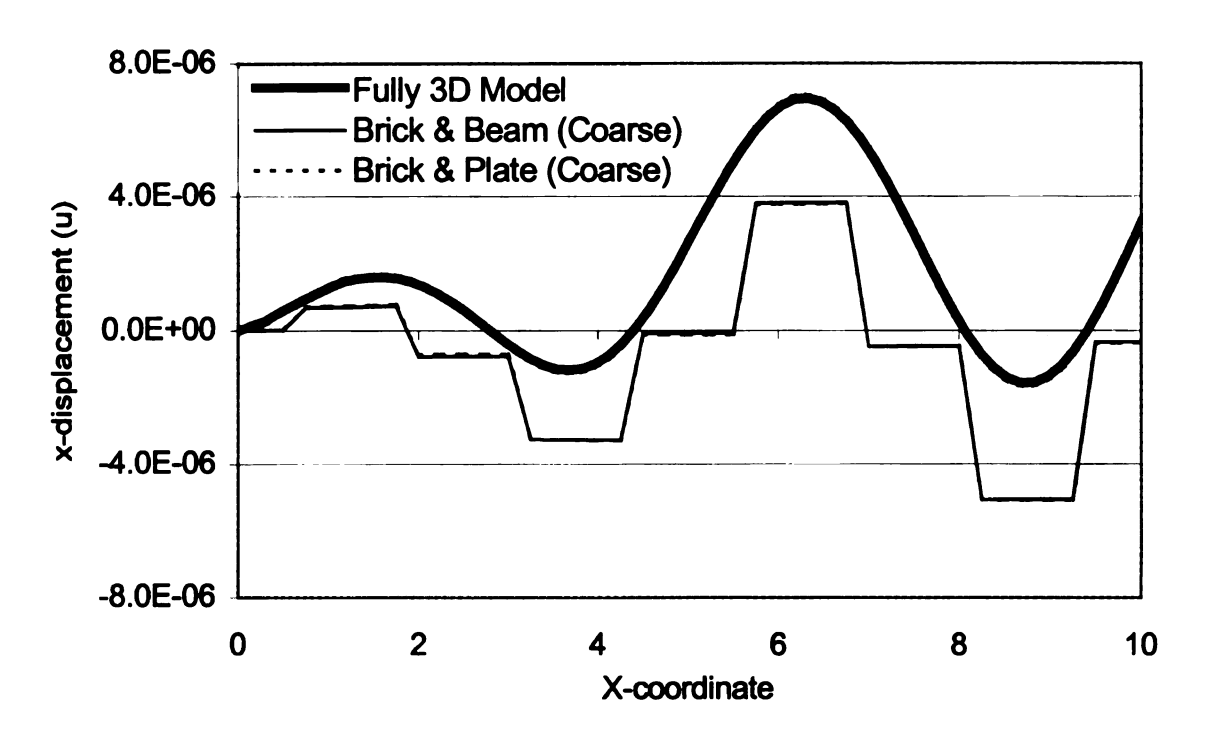


Figure 2.15 Axial displacement (u) along the tow centerline of the coarse brick & beam and brick & plate models due to a normal (y) load.

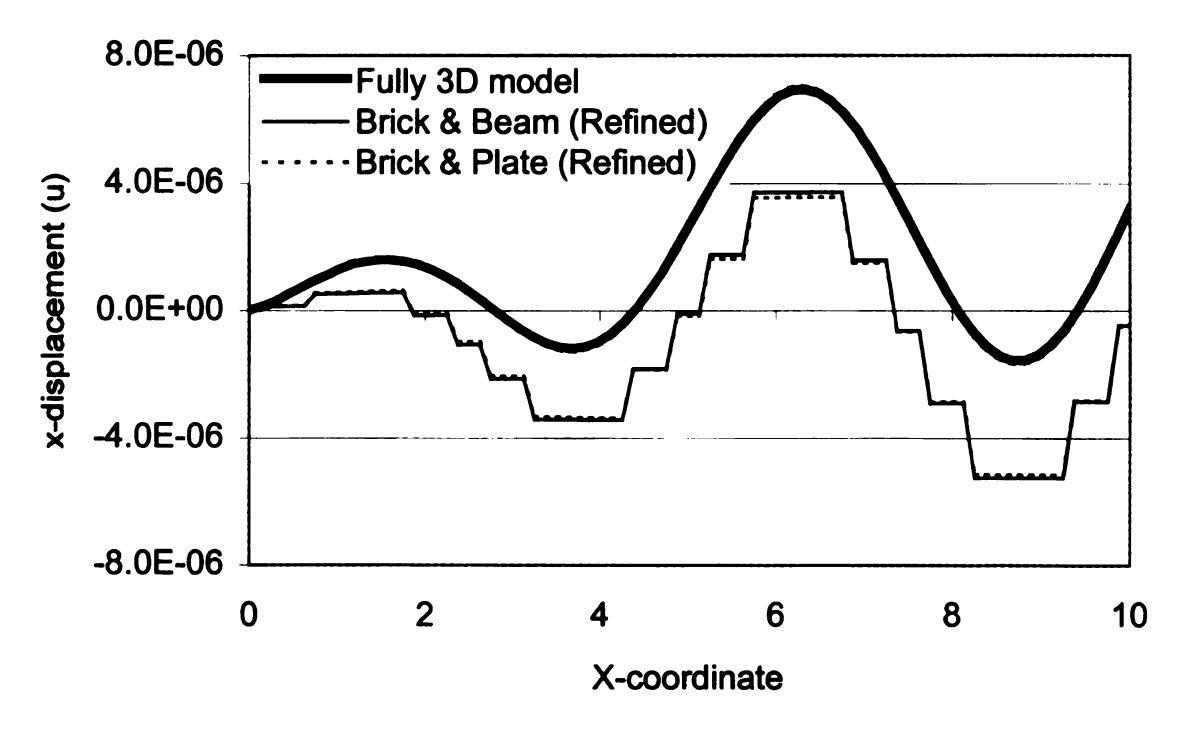


Figure 2.16 Axial displacement (u) along the tow centerline of the refined brick & beam and brick & plate models due to a normal (y) load.

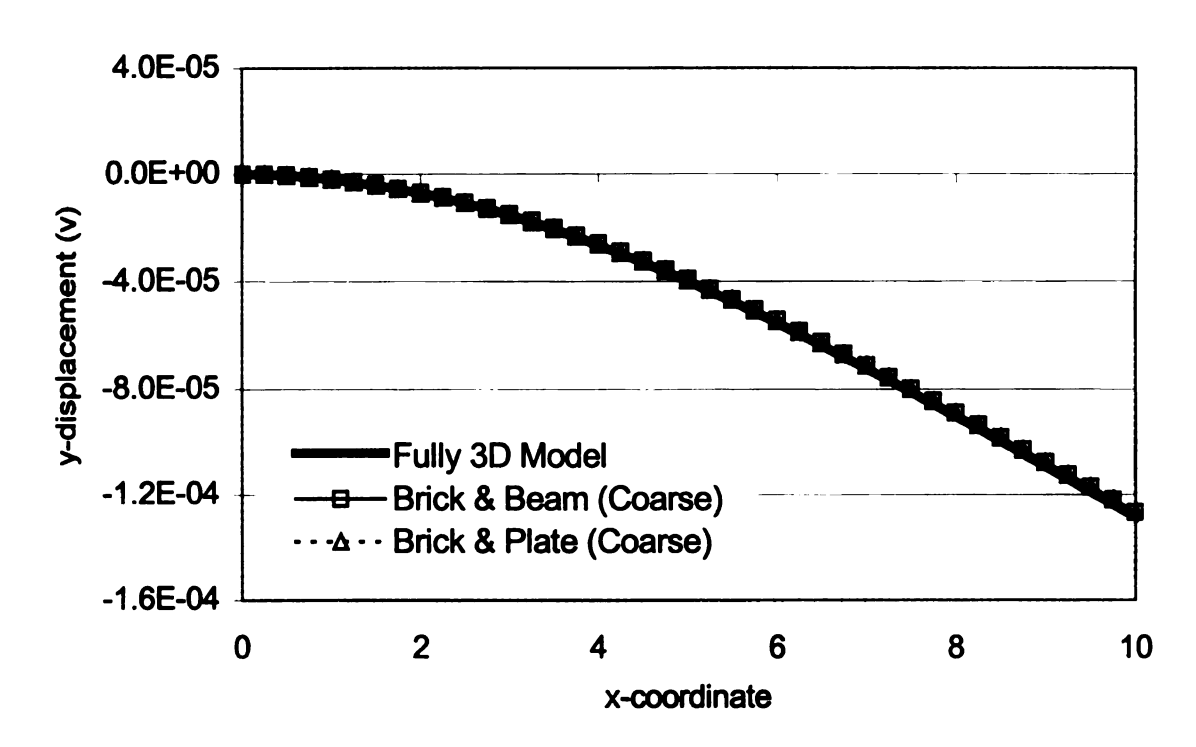


Figure 2.17 Normal displacement (v) along the tow centerline of the coarse brick & beam and brick & plate models due to a normal (y) load.

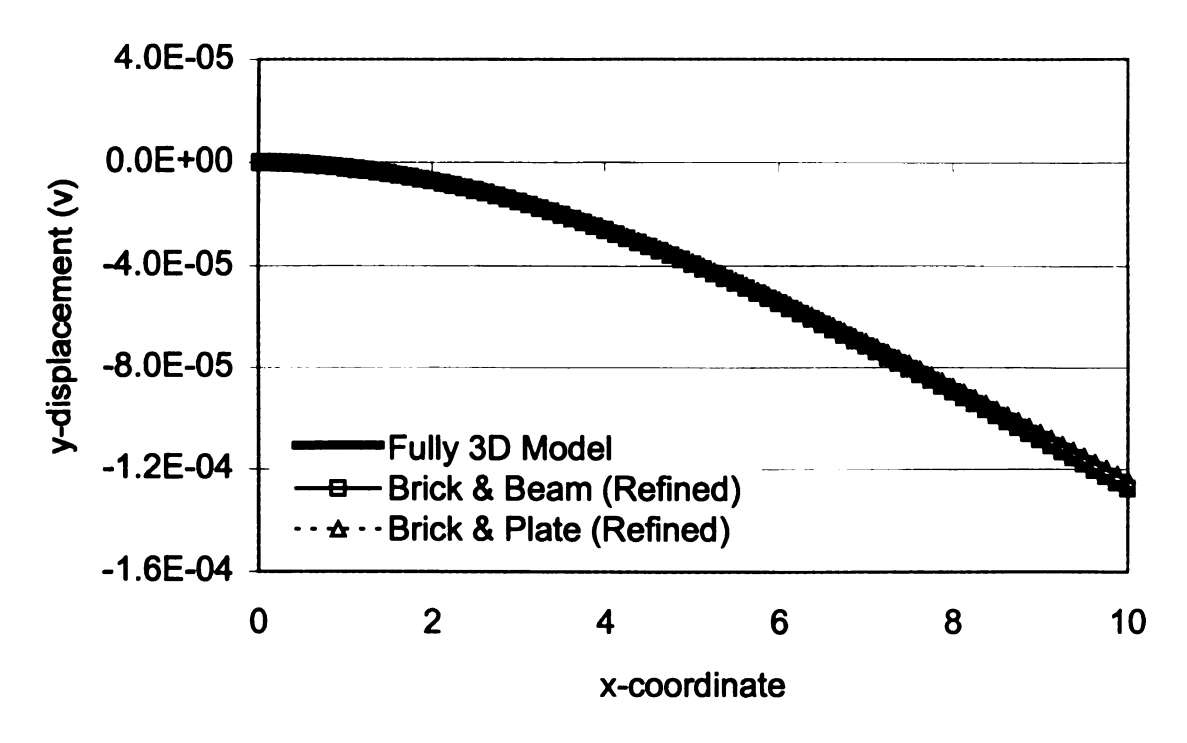


Figure 2.18 Normal displacement (v) along the tow centerline of the refined brick & beam and brick & plate models due to a normal (y) load.

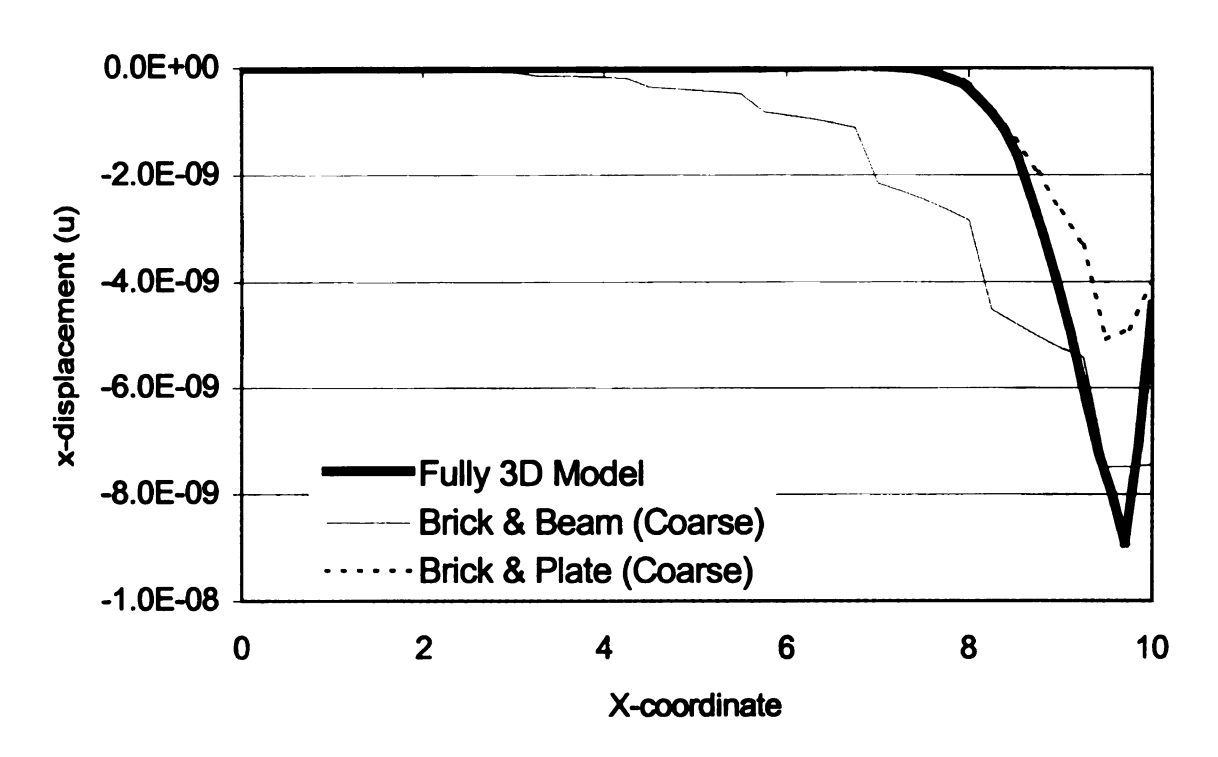


Figure 2.19 Axial displacement along the tow centerline of the coarse brick & beam and brick & plate models due to a transverse (z) load.

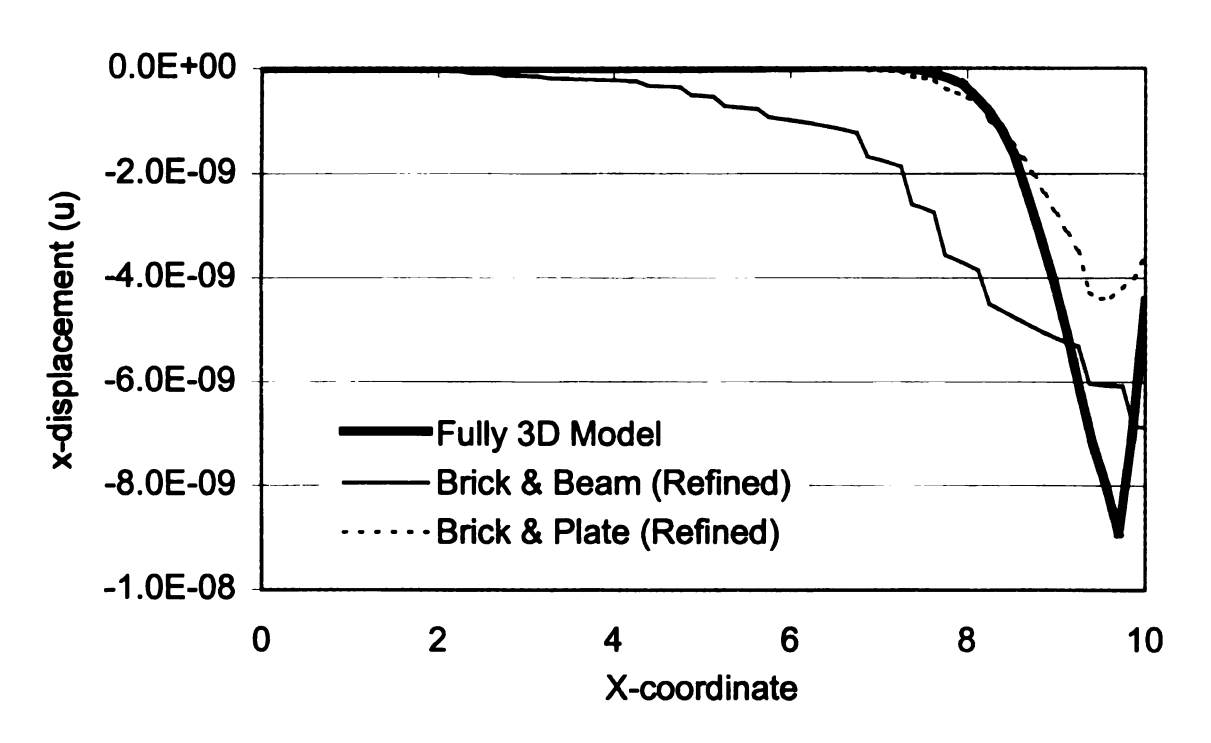


Figure 2.20 Axial displacement along the tow centerline of the refined brick & beam and brick & plate models due to a transverse (z) load.

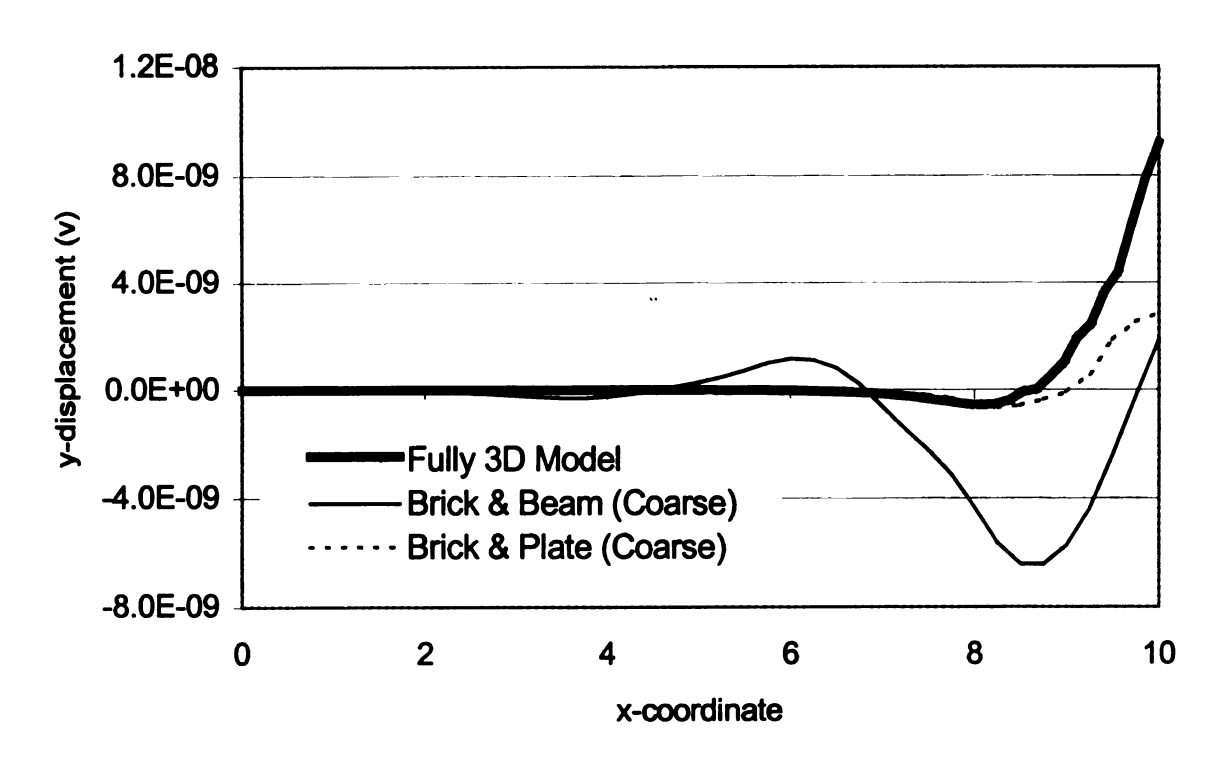


Figure 2.21 Normal displacement (v) along the tow centerline of the coarse brick & beam and brick & plate models due to a transverse (z) load.

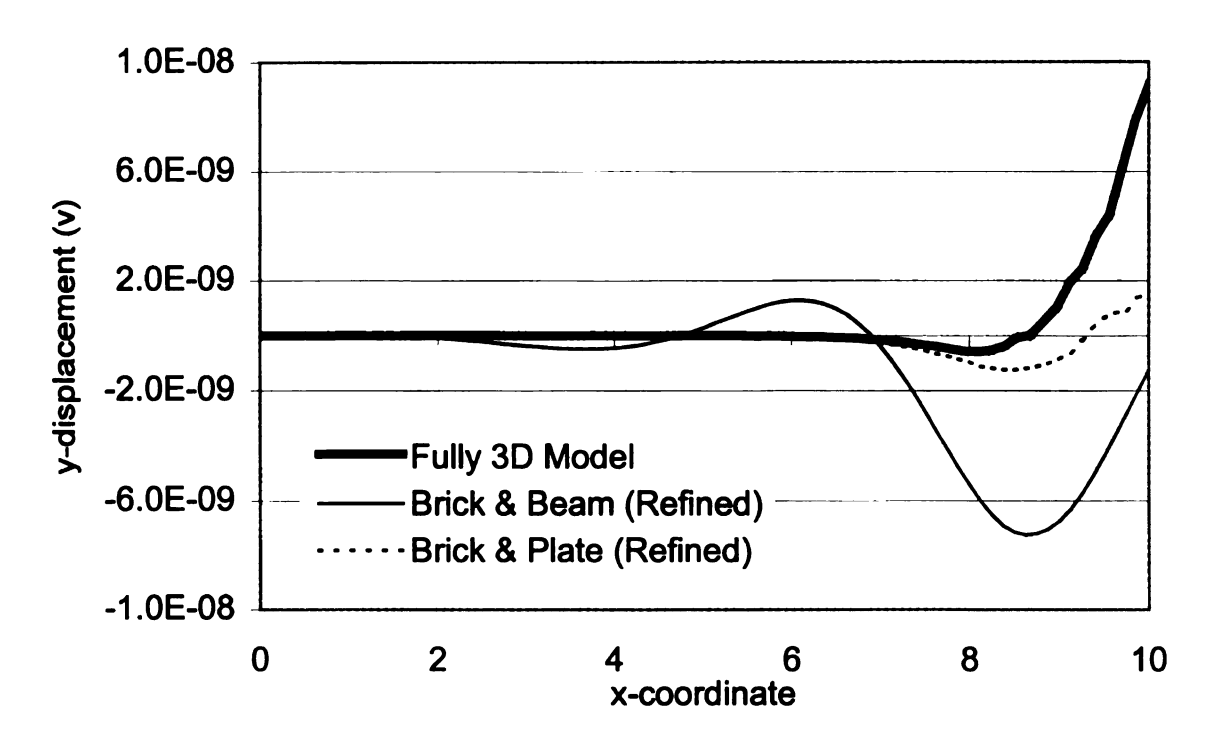


Figure 2.22 Normal displacement (v) along the tow centerline of the refined brick & beam and brick & plate models due to a transverse (z) load.

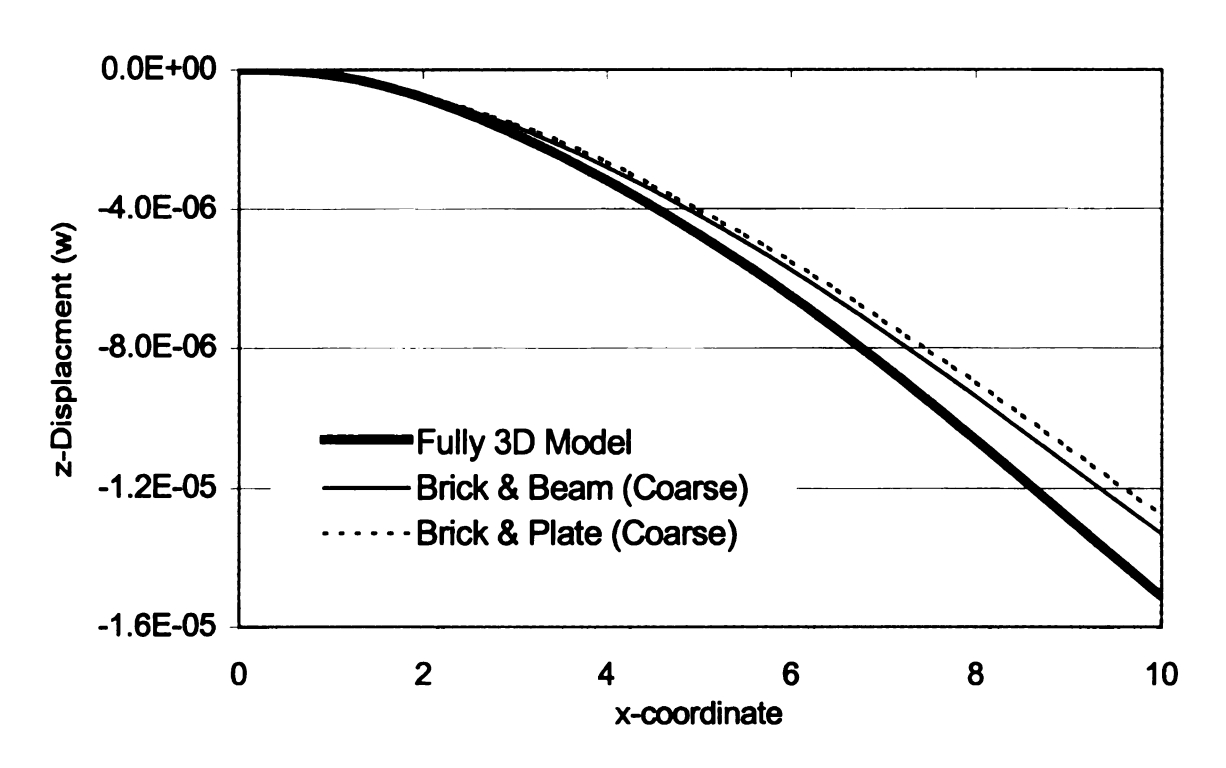


Figure 2.23 Transverse displacement (w) along the tow centerline of the coarse brick & beam and brick & plate models due to a transverse (z) load.

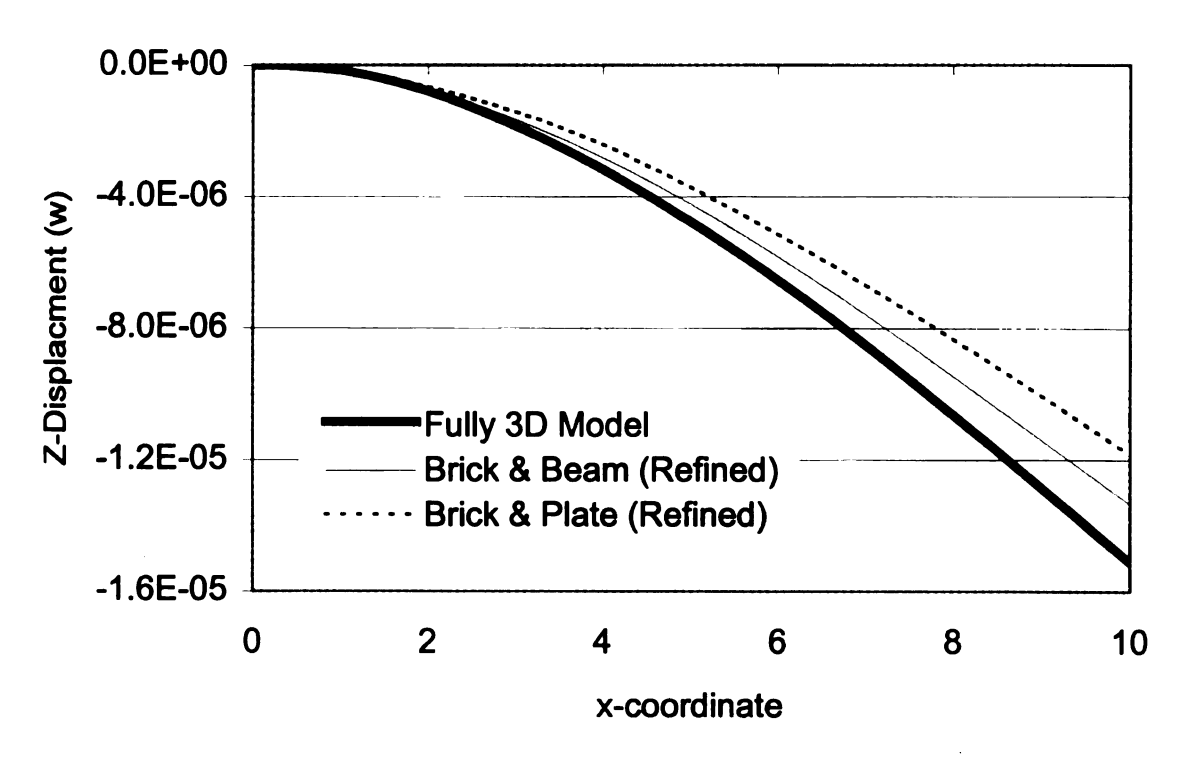


Figure 2.24 Transverse displacement (w) along the tow centerline of the refined brick & beam and brick & plate models due to a transverse (z) load.

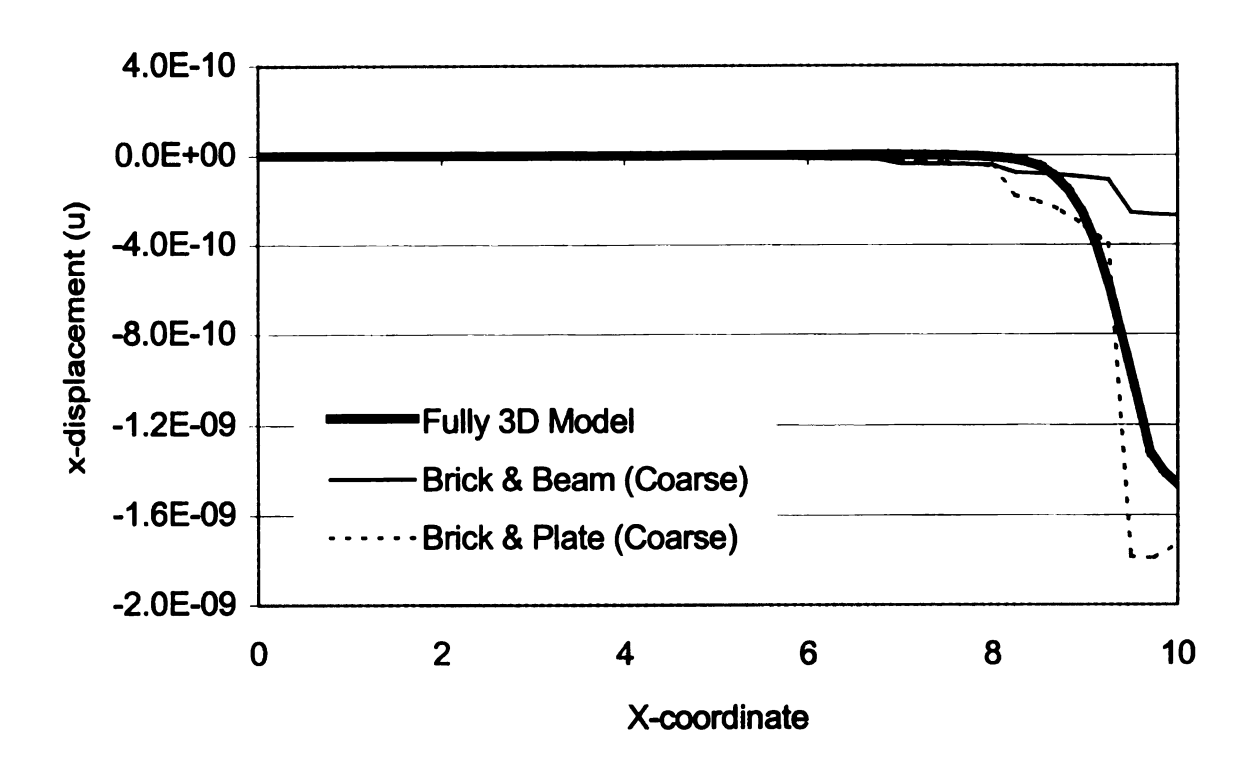


Figure 2.25 Axial displacement (u) along the tow centerline of the coarse brick & beam and brick & plate models due to a torsional load.

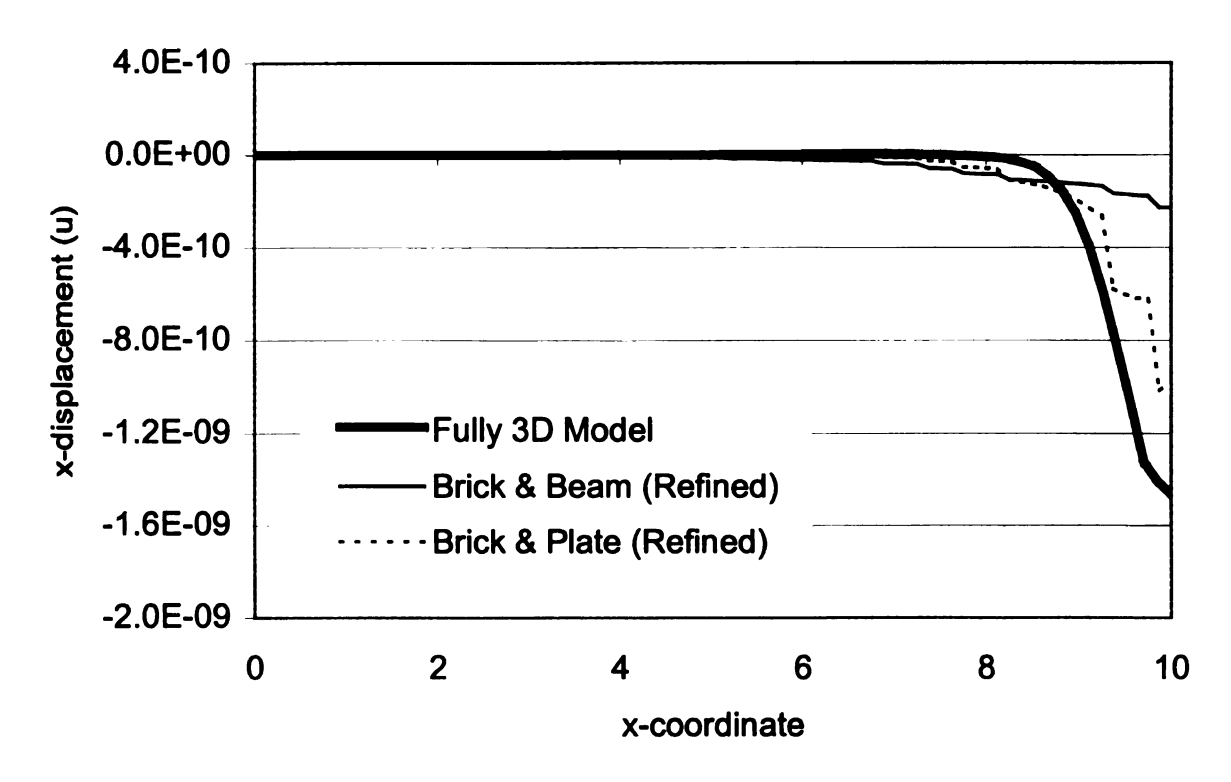


Figure 2.26 Axial displacement (u) along the tow centerline of the refined brick & beam and brick & plate models due to a torsional load.

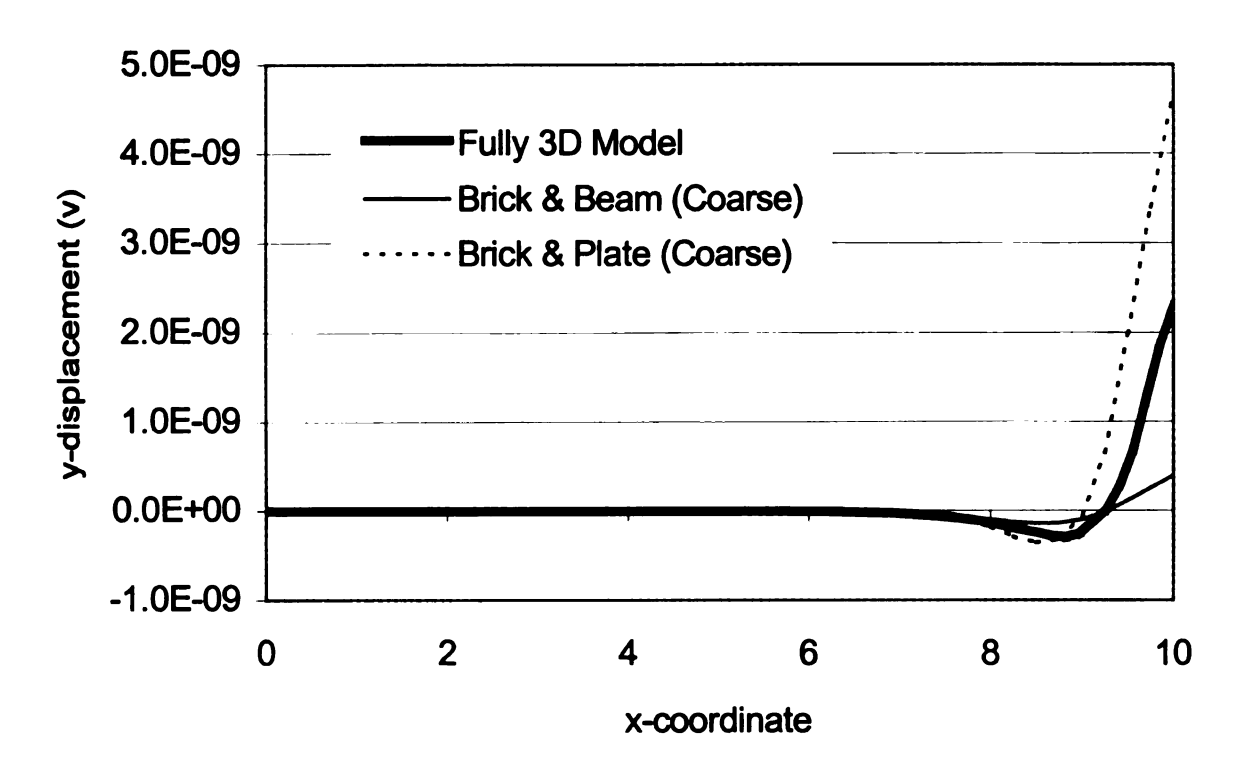


Figure 2.27 Normal displacement (v) along the tow centerline of the coarse brick & beam and brick & plate models due to a torsional load.

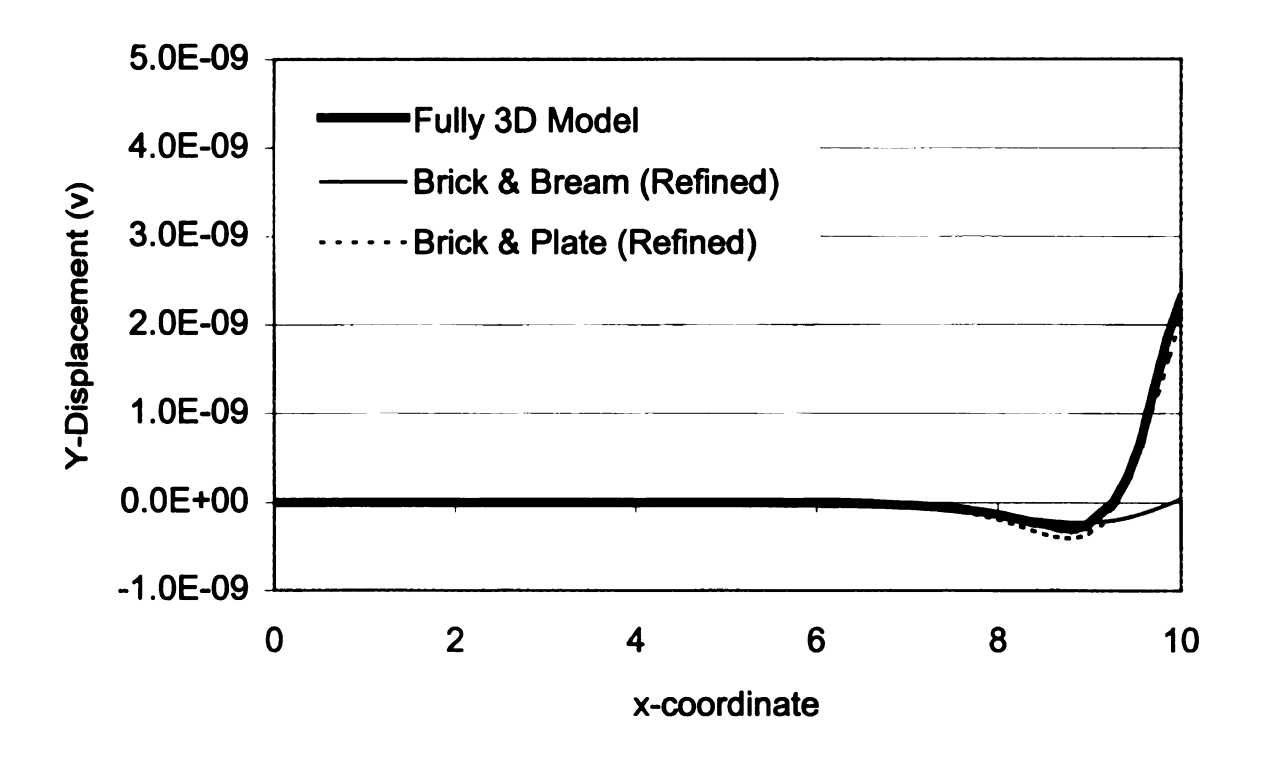


Figure 2.28 Normal displacement (v) along the tow centerline of the refined brick & beam and brick & plate models due to a torsional load.

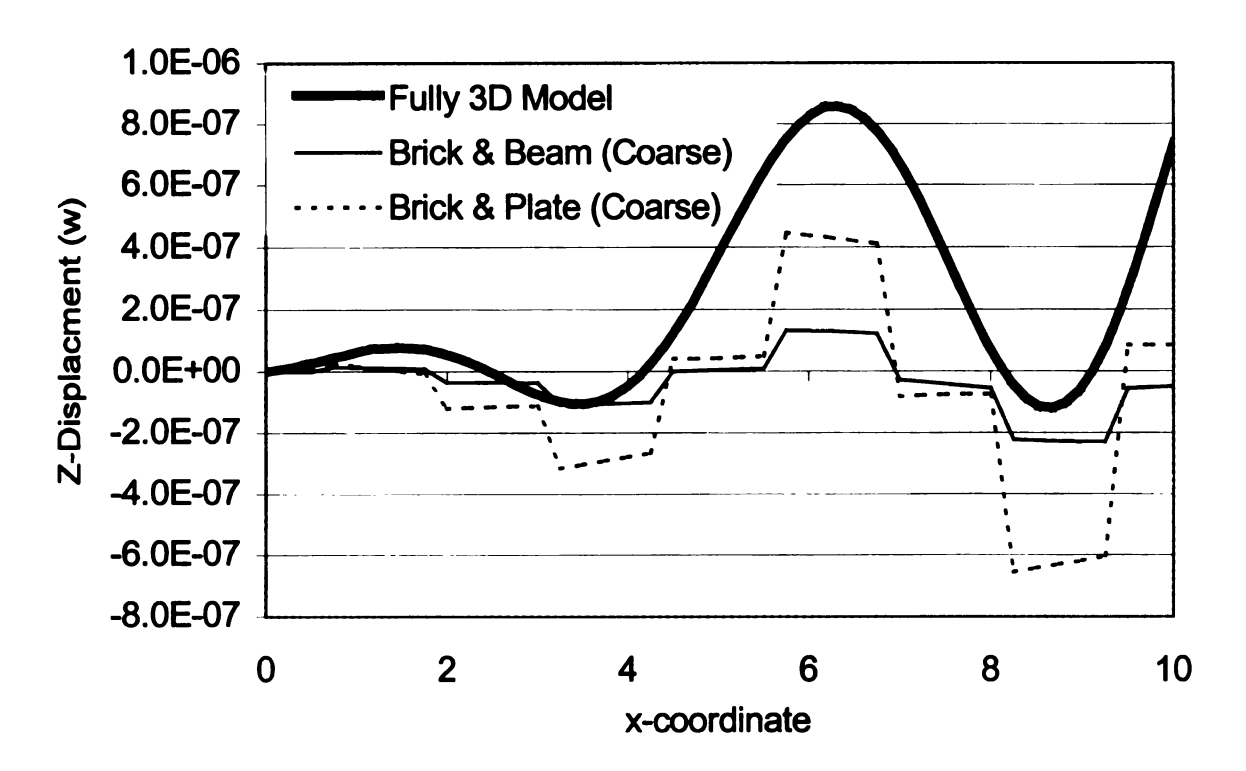


Figure 2.29 Transverse displacement (w) along the tow centerline of the coarse brick & beam and brick & plate models due to a torsional load.

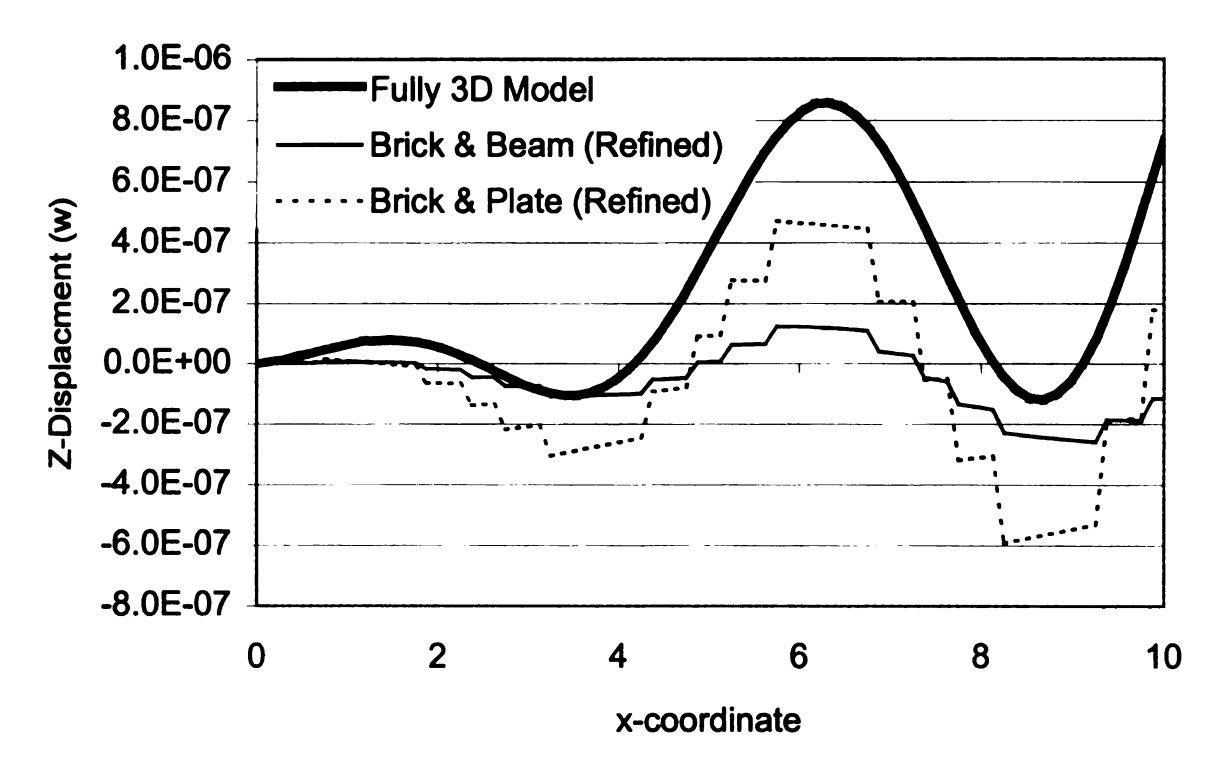


Figure 2.30 Transverse displacement (w) along the tow centerline of the refined brick & beam and brick & plate models due to a torsional load.

Chapter 3

The simplified discrete-tow model

3.1 Introduction

In most fiber-reinforced polymer-matrix composites, the fibers are much stiffer than the resin material. Therefore, the majority of the load in the structure is carried by the fibers while the resin serves to transfer load among the fibers. It is evident that the deformations and relative motions of fibers dictate the deformation of a fiber-reinforced composite structure.

3.2 The Simplified Discrete-Tow Model

Based on the above observations and experience with other modeling approaches, the present simplified discrete-tow model was conceived. The current model is constructed by representing the fiber tows using bar (or beam) elements and the resin using plane stress (or shell) elements. Repeating unit cells (RUC's) of plain weave and triaxial braid are shown in Figure 3.1a and 3.2a respectively. The RUC's of both weaves can be further broken down into repeating volume elements (RVE's), which can be seen in Figure 3.1b and 3.4. The two-dimensional discrete-tow models of the same unit cells are shown in Figure 3.4 and 3.7. As a result of the periodicity of the triaxial braid (Figure 3.5a), the triaxial braid model can be further simplified by modeling half of the RVE as shown in Figure 3.5b.

In the discrete-tow model, the true material properties of the resin and fiber tow cannot be assigned directly to the elements. This is a result of a beam

element's inability to represent the transverse stiffness, shear stiffness, and curvature of the tow. The resin in-plane and shear moduli must be modified to account for the transverse and shear stiffness of the tows. Also, the axial tow stiffness must be reduced to account for tow curvature. A general method has been derived that can be used to calculate the effective resin moduli for plain weave and triaxial braid materials. The effective resin properties are found through the use of a laminate analogy while the axial tow stiffness reduction is calculated using the theory of curved beams on elastic foundations in the same manner that Naik [22] used. It is important to note that the calculation of the effective resin properties for a plain weave is actually a sub-problem of the triaxial braid calculations. For this reason the effective moduli calculations will be derived for a triaxial braid starting with the geometrical definition of the triaxial braid.

3.2.1 GEOMETRY OF A TRIAXIAL BRAID

A half-model of the RVE of a triaxial braid is shown in Figure 3.5b. The geometry of this half-model RVE can be fully described through the use of the iterative procedure described by Naik et al. [23]. Using the same method as [23], it is only necessary to know d_0 , w, t, θ_{br} , V_f , p_d , n_0 , and n_{br} to describe the full geometry of the RVE of a triaxial braid. Where d_0 is the axial tow spacing, w is the width of the half-model of the RVE, t is the total thickness of the individual lamina, and θ_{br} is the braid angle. Additionally, V_f is the overall fiber volume fraction, p_d is the packing density of the fibers, while n_0 and n_{br} are the number of fiber filaments in the axial and braider directions.

In order to simplify the number of unknowns in the geometrical description of the triaxial RVE, Naik et al. [23] make several assumptions. The axial tows are assumed to be straight with no undulation (see Figure 3.2 b &c), while the braider tows are assumed to follow a sinusoidal path-line in the direction of the braid. It is also assumed that the axial and braider tow thicknesses, t_0 and t_{Br} respectively, must satisfy the relationship $t = t_0 + 2t_{Br}$. The assumption is also made that the cross sectional area of the axial and braider tows (A_0 and A_{Br} respectively) remains constant when sections are taken perpendicular to the tow path-line. The cross sectional area of the axial tow is idealized as a combination of straight and curved sections which correspond to the straight and undulating regions of the woven braider tows. The curved portion of the axial tow's cross section is assumed to follow a path that is parallel to the sinusoidal path of the braider yarn.

3.2.2 EFFECTIVE RESIN PROPERTIES OF A TRIAXIAL BRAID

Once the geometry of the RVE for the triaxial braid is fully described, it is then possible to calculate the effective resin properties needed to account for the transverse tow stiffness and shear stiffness. The RVE of a $[0/\pm \theta]$ triaxial braid is divided into two regions. The first region has a width equal to the width of the axial tow (w_0) as can be seen in Figure 3.7. This region is assumed to contain the entire volume of the axial tow (V_0) , along with a portion of the braider tows and of the resin material. The second region contains the remainder of the braider tows and resin volume that was not contained in the first region. Each region is then assumed to be an assemblage of lamina, with each ply

representing one of the region's components (tow or resin). This laminate analogy is represented graphically in Figure 3.6. From Figure 3.7 it can be seen that the materials within each region are treated as a parallel model using classical lamination theory (CLT) while the two regions are considered to be in series with each other.

The material stiffness matrix [Q] for each of the constituent (or ply) materials takes the following general form:

$$[Q] = \begin{bmatrix} \frac{E_{11}}{1 - v_{12}v_{21}} & \frac{v_{12}E_{11}}{1 - v_{12}v_{21}} & 0\\ \frac{v_{12}E_{11}}{1 - v_{12}v_{21}} & \frac{E_{22}}{1 - v_{12}v_{21}} & 0\\ 0 & 0 & G_{12} \end{bmatrix}$$
(1)

where E_{11} , E_{22} , v_{12} and G_{12} represent the material properties of the constituent (ply) material under consideration. Recall that the current model discretely represents the axial stiffness of each tow within a beam element. Because the axial tow stiffness is already accounted for explicitly in the model, it is necessary to set $E_{11}^t = 0$ in the tow plies used to calculate the effective resin properties.

This assumption also requires $v_{12}^t = 0$. The tow transverse and shear stiffness are not modified. The stiffness matrix of the tow plies can now be written as:

$$[\mathbf{Q}^t] = \begin{bmatrix} 0 & 0 & 0 \\ 0 & E_{22}^t & 0 \\ 0 & 0 & G_{12}^t \end{bmatrix}$$
 (2)

where the superscript, t, denotes properties of the axial or braider tows.

The orientation of the tows is taken into account by transforming the material stiffness matrices (Jones [24]):

$$\left[\overline{\mathbf{Q}}\right] = \left[\mathsf{T}\right]^{-1} \left[\mathbf{Q}\right] \left[\mathsf{T}\right]^{-\mathsf{T}} \tag{3}$$

where,

$$[\mathbf{T}] = \begin{bmatrix} \cos^2 \theta & \sin^2 \theta & -2\sin\theta\cos\theta \\ \sin^2 \theta & \cos^2 \theta & 2\sin\theta\cos\theta \\ -\sin\theta\cos\theta & \sin\theta\cos\theta & \cos^2 \theta - \sin^2 \theta \end{bmatrix}$$
(4)

and θ is the orientation angle of the ply (tow) under consideration. For a $[0/\pm 45]$ triaxial braid, θ is $\pm 45^{\circ}$ for the braider tow plies, 0° for the axial tow ply, and 0° for the resin ply. Using CLT, the effective stiffness properties for region one, $[\overline{Q}]_{(1)}$, are given by

$$[\overline{Q}]_{(1)} = V_{f0}^{(1)} [\overline{Q}_{Axial}]_0 + \frac{V_{fBr}^{(1)}}{2} ([\overline{Q}_{Br}]_{+\theta} + [\overline{Q}_{Br}]_{-\theta}) + V_{fm}^{(1)} [Q_m]$$
 (5)

where the tow volume fractions of the constituent materials are defined as

$$V_{f0}^{(1)} = \frac{V_0^{(1)}}{V_{tot}^{(1)}}$$

$$V_{fBr}^{(1)} = \frac{V_{Br}^{(1)}}{V_{tot}^{(1)}} \tag{6}$$

$$V_{fm}^{(1)} = 1 - V_{f0}^{(1)} - V_{fBr}^{(1)}$$

and the following definitions are used to calculate the respective volumes of the materials

$$V_0^{(1)} = A_0 I$$

$$V_{Br}^{(1)} = A_{Br} \frac{w_0}{\sin(\theta_{Br})}$$

$$V_{tot}^{(1)} = Iw_0 t$$
(7)

where *I* is the length of the RVE and *t* is the thickness. In a similar manner, the effective properties for region two can be calculated with

$$\left[\overline{\mathbf{Q}}\right]_{(2)} = \frac{V_{fBr}^{(2)}}{2} \left(\left[\overline{\mathbf{Q}}_{Br}\right]_{+\theta} + \left[\overline{\mathbf{Q}}_{Br}\right]_{-\theta}\right) + V_{fm}^{(2)} \left[\mathbf{Q}_{m}\right]$$
(8)

where the tow volume fractions of the constituent materials in the second region are defined as

$$V_{fBr}^{(2)} = \frac{V_{Br}^{(2)}}{V_{tot}^{(2)}} \qquad V_{fm}^{(2)} = 1 - V_{fBr}^{(2)}$$
 (9)

and the volumes of the respective materials in region two are

$$V_{Br}^{(2)} = A_{Br} \frac{w - w_0}{\sin(\theta_{Br})} \qquad V_{tot}^{(2)} = lt(w - w_0)$$
 (10)

The effective resin properties of regions 1 and 2 can now be combined in a series model to compute the overall effective properties. Using the relation $\left[\overline{S}\right]^{-1} = \left[\overline{Q}\right]$, the effective compliance matrices for each region are found and the effective material properties are found as:

$$E_{11}^{(1)} = \frac{1}{\overline{S}_{11}^{(1)}} \qquad \qquad E_{11}^{(2)} = \frac{1}{\overline{S}_{11}^{(2)}}$$

$$E_{22}^{(1)} = \frac{1}{\overline{S}_{22}^{(1)}} \qquad \qquad E_{22}^{(2)} = \frac{1}{\overline{S}_{22}^{(2)}}$$

$$v_{12}^{(1)} = -E_{11}^{(1)} \overline{S}_{12}^{(1)} \qquad \qquad v_{12}^{(2)} = -E_{11}^{(2)} \overline{S}_{12}^{(2)} \qquad (11)$$

$$v_{21}^{(1)} = -E_{22}^{(1)} \overline{S}_{21}^{(1)} \qquad v_{21}^{(2)} = -E_{22}^{(2)} \overline{S}_{21}^{(2)}$$

$$G_{12}^{(1)} = \frac{1}{\overline{S}_{66}^{(1)}} \qquad G_{12}^{(2)} = \frac{1}{\overline{S}_{66}^{(2)}}$$

Using the equations of mechanics of materials, the combined effective resin stiffness in the axial and transverse directions, E_{11}^r and E_{22}^r respectively, are given by

$$E_{11}^{r} = V_{f}^{(1)} E_{11}^{(1)} + V_{f}^{(2)} E_{11}^{(2)} \qquad \qquad E_{22}^{r} = \frac{E_{11}^{(1)} E_{11}^{(2)}}{V_{f}^{(1)} E_{11}^{(2)} + V_{f}^{(2)} E_{11}^{(1)}} \qquad (12)$$

where

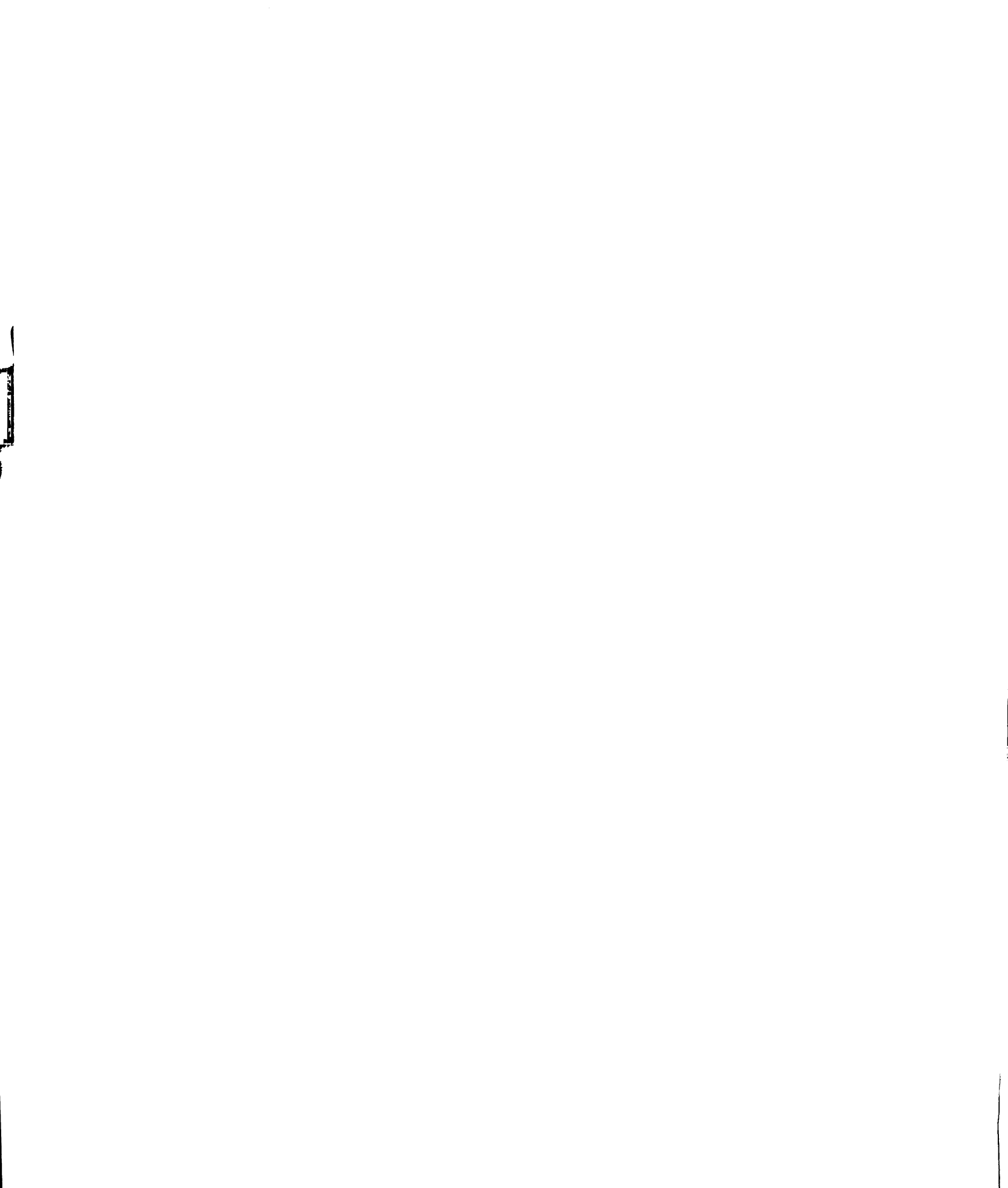
$$V_f^{(1)} = \frac{Vol_1}{Vol_{tot}} \qquad \qquad V_f^{(2)} = \frac{Vol_2}{Vol_{tot}}$$

In the same manner the combined effective Poisson's ratios, v_{12}^r and v_{21}^r , are found using

$$v_{12}^{r} = V_{12}^{(1)}v_{12}^{(1)} + V_{12}^{(2)}v_{12}^{(2)} \qquad v_{21}^{r} = \frac{E_{22}^{r}v_{12}^{r}}{E_{11}^{r}}$$
 (13)

Finally, the effective shear modulus, G_{12}^r , is given by

$$G_{12}^{r} = \frac{G_{12}^{(1)}G_{12}^{(2)}}{V_{f}^{(1)}G_{12}^{(2)} + V_{f}^{(2)}G_{12}^{(1)}}$$
(14)



3.2.3 EFFECTIVE RESIN PROPERTIES OF A PLAIN WEAVE

The effective resin properties of a plain weave are calculated in a manner very similar to the method previously discussed for the analysis of triaxial braids. Note that a plain weave can be completely represented by region two of a triaxial braid that only contains $\pm \theta$ braider tows. The effective stiffness matrix can then be defined by:

$$\left[\overline{\mathbf{Q}}\right] = \frac{V_{fBr}}{2} \left(\left[\overline{\mathbf{Q}}_{Br}\right]_{+\theta} + \left[\overline{\mathbf{Q}}_{Br}\right]_{-\theta}\right) + V_{fm} \left[\overline{\mathbf{Q}}_{m}\right]$$
 (15)

where the volume fractions of the constituent materials are defined as:

$$V_{fBr} = \frac{V_{Br}}{V_{tot}} \qquad V_{fm} = 1 - V_{fBr} \qquad (16)$$

and the volumes of the respective materials are:

$$V_{Br} = \frac{V_f}{\rho_d} V_{tot} \qquad V_{tot} = ltw \qquad (17)$$

3.2.4 TOW CURVATURE MODIFICATION

In the finite element representation of the simplified unit cell, the curved tows are modeled with straight beam elements. Consider both a curved and straight tow of the same axial length as pictured in Figure 3.7. The beam elements should be assigned a modulus such that the end shortening of the straight beam is the same as the end shortening of a curved tow when subjected to the same in-plane load. A stiffness reduction factor can be derived from the theory of curved beams on an elastic foundation [22]. This theory makes it

possible to include some of the three-dimensional tow curvature effects as well as the tow shape in a two-dimensional simplified model.

Figure 3.8a depicts the undulating portion of the fiber that is to be considered, while Figure 3.8b describes the load applied to the fiber tow. The fiber tow path-line is assumed to be sinusoidal. Taking the x-coordinate along the tow axis, the tow path-line is defined by the following equation

$$z_0 = A_0 \sin(\beta x)$$
, where $\beta = \frac{\pi}{L_{ub}}$ (18)

where L_{ub} is the length of the undulating portion of the fiber tow and A_0 is the amplitude of the sine wave. As shown in [20], the axial strain of the curved fiber is given by

$$\varepsilon_{x} = -\frac{1}{4} \left(\beta^{2} A_{1} (A_{1} + 2A_{0}) \left[1 + \cos(2\beta x) \right] + \varepsilon_{i-s}$$
 (19)

where

$$A_1 = \frac{-F\beta^2 A_0}{E_{11}^t I_V \beta^4 + F\beta^2 + k}$$
 (20)

$$a = 3 + \frac{t_{Br}}{A_0} \tag{21}$$

$$I_{y} = \frac{A_{ft}t_{Br}^2}{12} \tag{22}$$

$$k = \frac{4E_{zz}A_{ft}a}{t_{Br}^tA_0} \left(\frac{a}{\sqrt{a^2 - 1}} - 1\right)$$
 (23)

$$\varepsilon_{i-s} = \frac{F}{E_{11}^t A_{ft}} \tag{24}$$

 E_{zz} is the effective through thickness modulus of the woven composite, E_{11}^t is the axial modulus of the tow, and t_{Br} is the thickness of the undulating tow. The fiber tow cross-sectional area A_{ft} can be estimated from the following

$$A_{fl} = \frac{V_f}{\rho_d} \frac{Vol_{tot}}{L_T} \tag{25}$$

where V_f is the fiber volume fraction, p_d is the tow packing density, Vol_{tot} is the total volume of the RVE and L_T is the total length of the undulating fibers in the RVE. The axial component of displacement in the curved tow (u_c) is

$$u_{c} = \int_{0}^{a_{U}} \varepsilon_{X} dx + \frac{FL_{0}}{E_{11}^{t} A_{T}}$$
 (26)

where the total cross-sectional area A_T of the RVE can be calculated using A_T = lwt. The axial component of displacement in the straight tow (u_s) due to an applied load is given by

$$u_s = \frac{FL}{E_{11}^t A_T}, \quad L = L_{ub} + L_0$$
 (27)

The stiffness reduction factor (R.F.) necessary to model the effective curved tow deformation correctly using a straight beam finite element is taken to be the ratio of the displacements calculated above

$$R.F. = \frac{u_s}{u_c} \tag{28}$$

For many practical materials, R.F. takes a value above 0.9.

3.2.5 DETERMINING EFFECTIVE PROPERTIES

The effective properties of the RVEs for the weave geometries studies in this work were determined through the use of three sets of boundary conditions applied to a single RVE. For each boundary condition set a finite element analysis was performed. The results of the analysis can then be used to determine the effective properties of the various weave geometries under consideration. The three boundary condition sets and the simplifying stress-strain relations for each are summarized below

Boundary condition #1: $(\varepsilon_1 = 1, \varepsilon_2 = 0, \gamma_{12} = 0)$

$$\sigma_1 = \overline{Q}_{11} \varepsilon_1 \tag{29}$$

$$\sigma_2 = \overline{Q}_{12} \varepsilon_1 \tag{30}$$

Boundary Condition #2: $(\epsilon_1 = 0, \epsilon_2 = 1, \gamma_{12} = 0)$

$$\sigma_1 = \overline{Q}_{21} \varepsilon_2 \tag{31}$$

$$\sigma_2 = \overline{Q}_{21} \varepsilon_2 \tag{32}$$

Boundary Condition #3: $(\varepsilon_1 = 0, \varepsilon_2 = 0, \gamma_{12} = 1)$

$$\tau_2 = \overline{Q}_{66} \gamma_{12} \tag{33}$$

where the stresses σ_1 , σ_2 , and τ_{12} are found using

$$\sigma_1 = \frac{\sum F_1}{A_1}$$
 $\sigma_2 = \frac{\sum F_2}{A_2}$
 $\tau_{12} = \frac{\sum F_1}{A_2}$
(34)

Knowing both the state of stress and strain from the analysis and boundary conditions respectively, the effective stiffness matrix of the RVE can be calculated using Equations 29-33. After calculating the effective stiffness matrix, the effective compliance matrix can be found through

$$\left[\overline{S}\right] = \left[\overline{Q}\right]^{-1} \tag{35}$$

and the effective composite properties of the RVE can be determined using the following relations that are similar to those found in Equation 11.

$$E_{11} = \frac{1}{\overline{S}_{11}}$$

$$E_{22} = \frac{1}{\overline{S}_{22}}$$

$$v_{12} = -E_{11}\overline{S}_{12}$$

$$v_{21} = -E_{22}\overline{S}_{21}$$

$$G_{12} = \frac{1}{\overline{S}_{66}}$$
(36)

3.3 Numerical Results

3.3.1 ANALYSIS OF A PLAIN WEAVE

The first case considered is the prediction of the effective stiffness of two plain weave composites. As an example of the input used for the properties in the finite element analysis of this plain weave unit cell, the following effective resin properties were found to be $E_{11} = E_{22} = 7.27$ GPa, $v_{12} = -.258$, $G_{12} = 2.69$ GPa. These properties were then assigned to the shell elements in the model.

The tow stiffness reduction factor was found to be 0.968. Therefore, a value of 140.13 GPa was assigned to the axial stiffness of the beam elements.

Results from the current model are compared with results from Sankar and Marrey [13], Naik [25], and Foye [26]. The material and geometric properties are summarized in Table 3.1. The results for the two cases are presented in Table 3.2. It can be seen that the effective stiffness, E_{11} , and the shear modulus, G_{12} , predicted by the discrete-tow model agrees well with the other models. The Poisson's ratios predicted by the current model are lower than the other results presented in cases 1 and 2, however all of the results are small compared to unity.

3.3.2 EFFECT OF WAVINESS RATIO ON EFFECTIVE MATERIAL PROPERTIES

The ability of the simplified discrete-tow model to capture tow curvature effects makes it possible to investigate the effect of waviness ratio on the predicted effective properties. The waviness ratio, λ , is defined as

$$\lambda = \frac{L_{ub}}{L} = \frac{L_{ub}}{L_{ub} + L_0} \tag{37}$$

where L, L_0 , and L_{ub} are defined in Figure 3.9 for a plain weave. Three waviness ratios of 0.167, 0.25, and 0.5 were examined and compared to results presented by Raju and Wang [11], Whitcomb [15], and Aitharaju and Averill [12]. The waviness ratio for the three cases was determined by holding L_{ub} constant, while varying L_0 . The geometric and material data for the three cases is found in Table 3.3 and Table 3.4 respectively. The predictions of effective modulus, Poisson's

ratio, and shear modulus are shown graphically in Figures 3.12 through 3.14 and in tabular form in Table 3.5. The current predictions of the effective stiffness, E_{11} , (Figure 3.10) and shear modulus, G_{12} , (Figure 3.12) for the various waviness ratios agree well with those in the literature. Predicted Poisson's ratios are lower than the other models (Figure 3.11), however, all of the results are quite small compared to unity. All of the present results follow the expected trends as the waviness ratio is increased. The effective stiffness and the shear modulus both decrease with an increase in waviness ratio while Poisson's ratio increases.

3.3.3 ANALYSIS OF A TRIAXIAL BRAID

Four different triaxial braids were examined using the current model, and overall stiffness predictions were compared to the numerical and experimental results of Naik et al. [23]. The study investigates the effect of braid angle (θ_{Br}), relative tow sizes and axial tow content on the predicted effective properties. The material and geometrical data for each of the cases is summarized in Table 3.6 and Table 3.7. A comparison of the numerical results of the four cases can be found in Table 3.8. The present results, in general, compare very well with the numerical and experimental data found in Naik et al. [23].

3.4 Conclusions

A simplified discrete—tow model has been formulated and validated for predicting overall mechanical stiffness properties of plain weave and triaxial braid textile composite materials. In this model, the fiber tows and resin are discretely

represented using beam and shell finite elements, respectively, resulting in a simple, accurate and computationally efficient approach. Overall stiffness predictions using the current discrete-tow model agree very well with other analytical and experimental results found in the literature.

Table 3.1 Material properties for comparison of predicted stiffness

		Case 1 (Glass/Epoxy)	Case 2 (Graphite/Epoxy)
	Length (mm)	1.1879	3.9909
Unit Cell	Width (mm)	1.1879	3.9909
Dimensions	Height (mm)	0.228	0.2557
	E ₁₁ (GPa)	58.61	144.8
	E ₂₂ (GPa)	14.49	11.73
_	V ₁₂	0.25	0.230
Tow	G ₁₂ (GPa)	5.38	5.52
	Pd	0.7836	0.75
	V _f	0.26	0.64
	E (GPa)	3.45	3.45
Matrix	ν	0.37	0.35
	G (GPa)	1.26	1.28

Table 3.2 Comparison of results for a plain weave-

		E ₁₁ (GPa)	V12	G ₁₂ (GPa)
	Present Study	12.97	0.075	2.03
Case 1	Sankar & Marrey (1997): S.A.M	12.46	0.162	1.67
(Glass / Epoxy)	Sankar & Marrey (1995): F.E.A.	11.81	0.181	2.15
	Dasgupta et al (1990)	14.38	0.167	3.94
Case 2	Present Study	65.358	0.003	4.898
	Sankar & Marrey (1997): S.A.M	63.41	0.027	4.24
(Graphite / Fnoxy)	Sankar & Marrey (1995): F.E.A.	53.61	0.128	4.72
(Crapinte / Epoxy)	Naik (1994): TEXCAD	64.38	0.027	4.87
	Foye (1992): F.E.A.	63.78	0.031	4.82
	Foye (1992): Test	61.92	0.11	NA

Table 3.3 Geometric data for the three waviness ratios studied

λ	0.167	0.25	0.5
l/h	24	16	8
V _f	0.580	0.569	0.520
p_d	6	6	6

Table 3.4 Material properties for all waviness ratios studied

Tow	E ₁₁ (GPa)	134
	E ₂₂ (GPa)	10.2
1000	ν ₁₂ (GPa)	0.3
	G ₁₂ (GPa)	5.52
	E (GPa)	3.448
Matrix	v (GPa)	0.35
	G (GPa)	1.28

Table 3.5 Comparison of predicted effective properties for a plain weave composite.

	λ	0.167	0.25	0.5
	E ₁₁	68.8	67.1	60.2
Present Study	V ₁₂	0.001	0.001	0.003
	G ₁₂	5.38	5.30	4.95
	E ₁₁	67.7	65.1	56.2
Aitharaju & Averill (1999)	V12	0.043	0.044	0.044
	G ₁₂	5.36	5.29	5.08
	E ₁₁	66.7	63.8	54.4
Whitcomb (1991)	V ₁₂	0.037	0.034	0.026
	G ₁₂	5.30	5.19	4.80
	E ₁₁	68.4	66.2	57.1
Raju & Wang (1994)	V12	0.045	0.046	0.052
	G ₁₂	5.34	5.24	4.80
	E ₁₁	72.5	72.5	72.5
(0,90) _s	V12	0.043	0.043	0.043
	G ₁₂	5.52	5.52	5.52

Table 3.6 Geometric and braid data for triaxial weaves.

Case	Material	Axial Tow Spacing (mm)	Ply Thickness (mm)	Vf	Pd
1	[0 _{30k} /±70 _{6k}] 46%-axial	6.05	0.7075	0.55	0.75
2	[0 _{75k} /±70 _{15k}] 46%-axial	11.04	0.935	0.59	0.75
3	[0 _{36k} /±45 _{15k}] 46%-axial	5.52	0.94	0.58	0.75
4	[0 _{6k} /±45 _{15k}] 12%-axial	5.52	0.556	0.56	0.75

Table 3.7 Properties for the constituent materials of the triaxial weaves.

Material	E ₁₁ (GPa)	E ₂₂ (GPa)	V ₁₂	G ₁₂ (GPa)
AS4/1895 Yarn	144.8	11.73	0.23	5.52
1895 Matrix	3.45	3.45	0.35	1.28

Table 3.8 Comparison of effective properties for a triaxial weave with numerical and experimental methods.

		E _L (GPa)	E _T (GPa)	VLT	v_{TL}	G _{LT} (GPa)
[0 _{30k} /±70 _{6k}]	Present Study	54.18	46.77	0.12	0.10	9.39
	Naik	55.67	49.30	0.15	0.13	9.68
46%-axial	Naik Measured	60.25	47.50	0.20	0.09	11.65
	Naik Measured	59.15	43.60	na	na	na
	Present Study	58.67	51.13	0.11	0.10	10.18
$[0_{75k}/\pm70_{15k}]$	Naik	59.63	53.38	0.15	0.13	10.38
46%-axial	Naik Measured	62.46	48.12	0.16	0.05	11.03
	Nails Management	EQ 77	AE 77	The second second	WAS THE REAL PROPERTY.	GENERAL STATE
	Naik Measured	59.77	45.77	. na	na	na "i
	Present Study	61.89	19.84	0.61	na 0.20	17.54
[0 _{36k} /±45 _{15k}]						_
[0 _{36k} /±45 _{15k}] 46%-axial	Present Study	61.89 62.67	19.84	0.61	0.20	17.54
L COM TONG	Present Study Naik	61.89 62.67 65.63	19.84 20.78	0.61 0.65	0.20 0.21	17.54 18.04
L COM TONG	Present Study Naik Naik Measured	61.89 62.67 65.63	19.84 20.78 19.30	0.61 0.65 0.57	0.20 0.21 0.22	17.54 18.04 16.96
L COM TONG	Present Study Naik Naik Measured Naik Measured	61.89 62.67 65.63 61.70	19.84 20.78 19.30 19.23	0.61 0.65 0.57 na	0.20 0.21 0.22 na	17.54 18.04 16.96 na
46%-axial	Present Study Naik Naik Measured Naik Measured Present Study	61.89 62.67 65.63 61.70 27.35 27.92	19.84 20.78 19.30 19.23 19.45	0.61 0.65 0.57 na 0.72	0.20 0.21 0.22 na 0.51	17.54 18.04 16.96 na 25.83

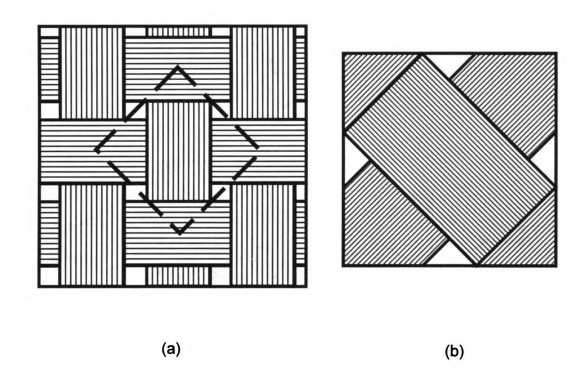


Figure 3.1. (a) Plain weave and (b) one possible repeating volume element of a plain weave.

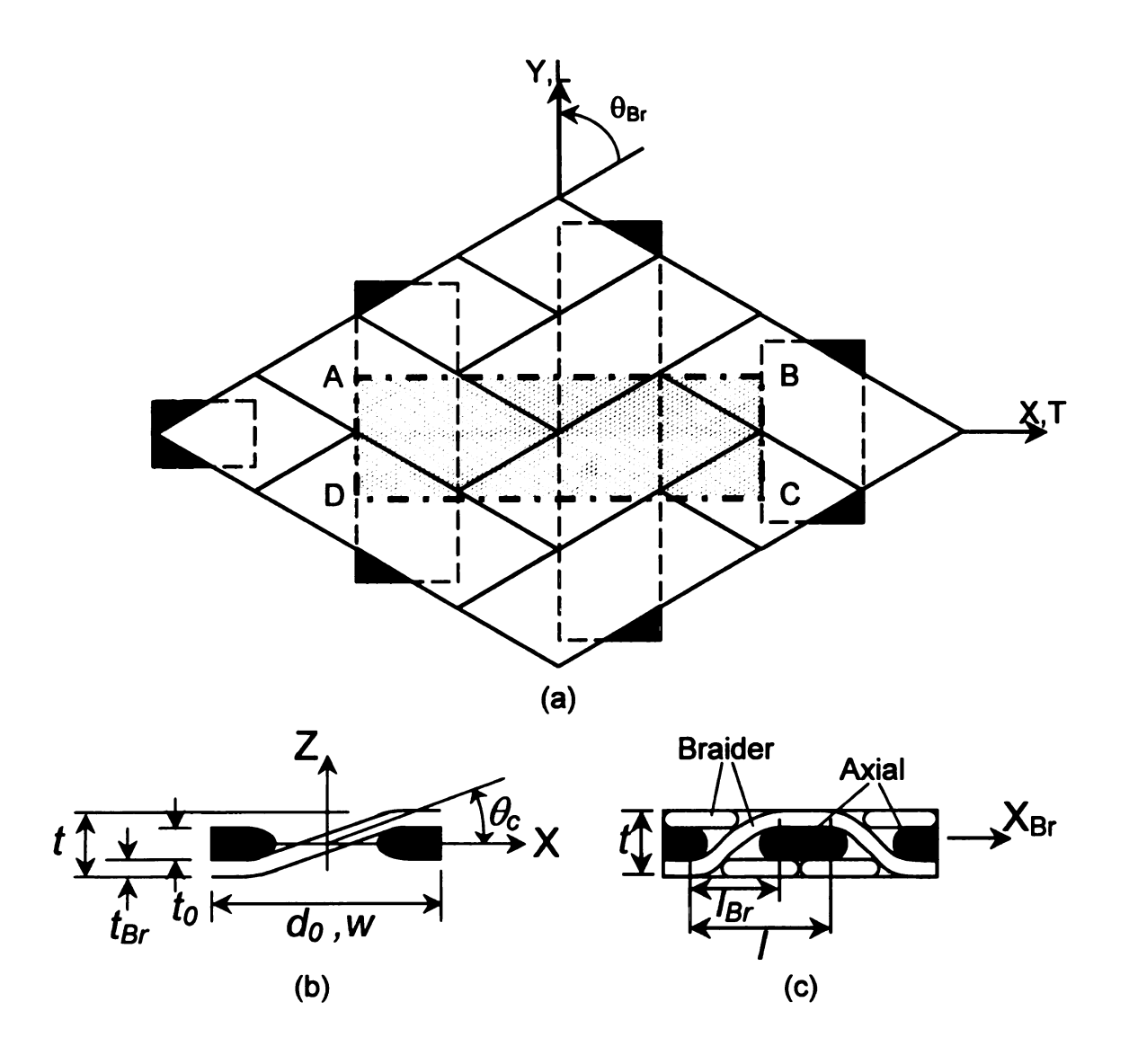


Figure 3.2 (a) Geometry of a triaxial braid (b) cross section of the triaxial braid made perpendicular to the axial tows (c) cross section of the triaxial braid made alone the direction of the braider tows.

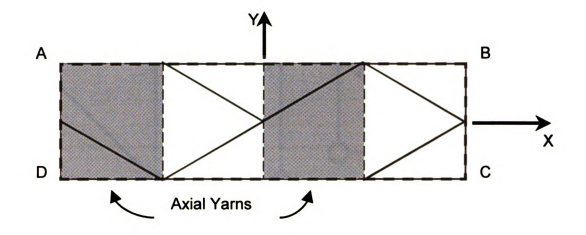


Figure 3.3 The area enclosed by A,B,C,D represents one possible RVE for a $[0/\pm 0]$ triaxial braided composite.

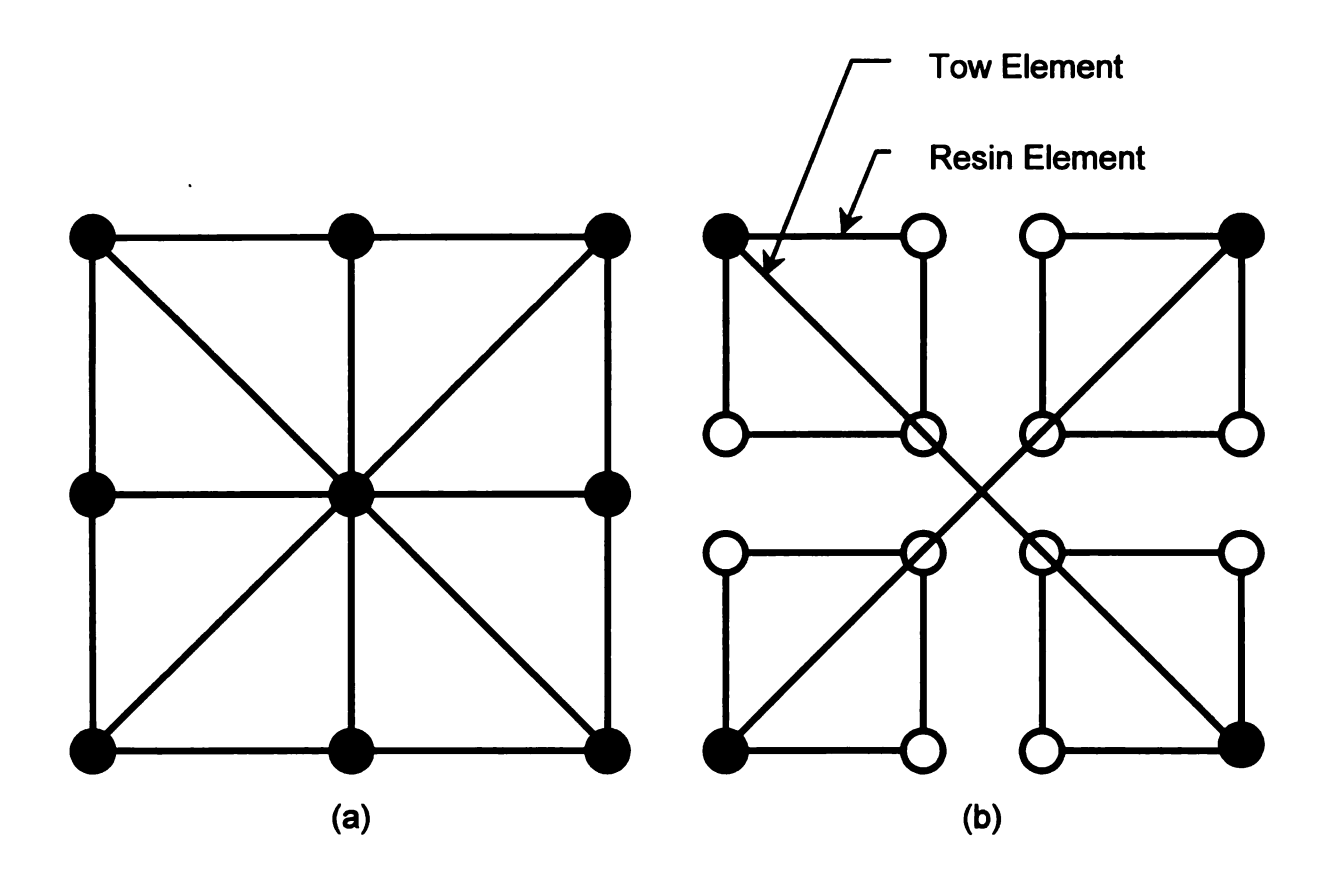
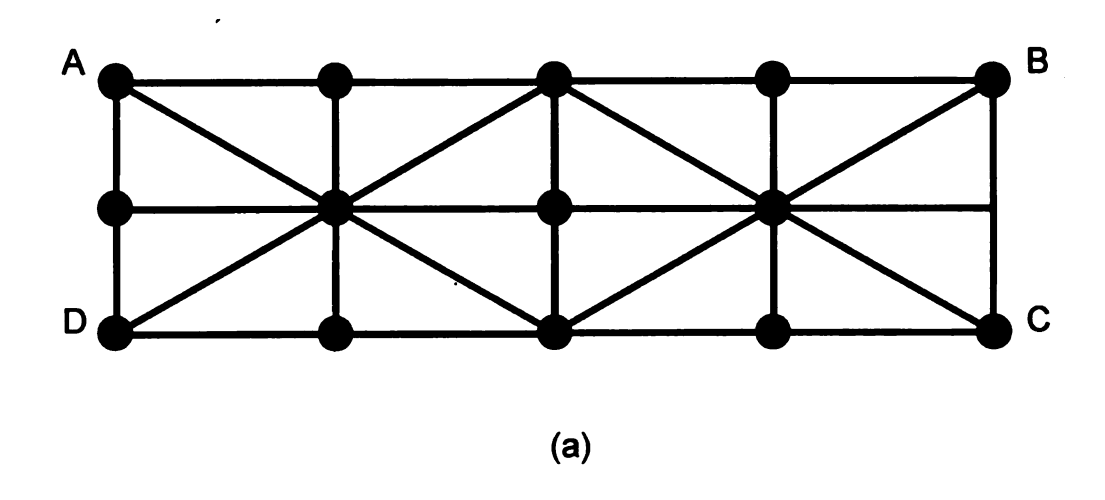


Figure 3.4 (a) Assembled finite element model of the unit cell and (b) exploded view of the finite element model for a plain weave material system.



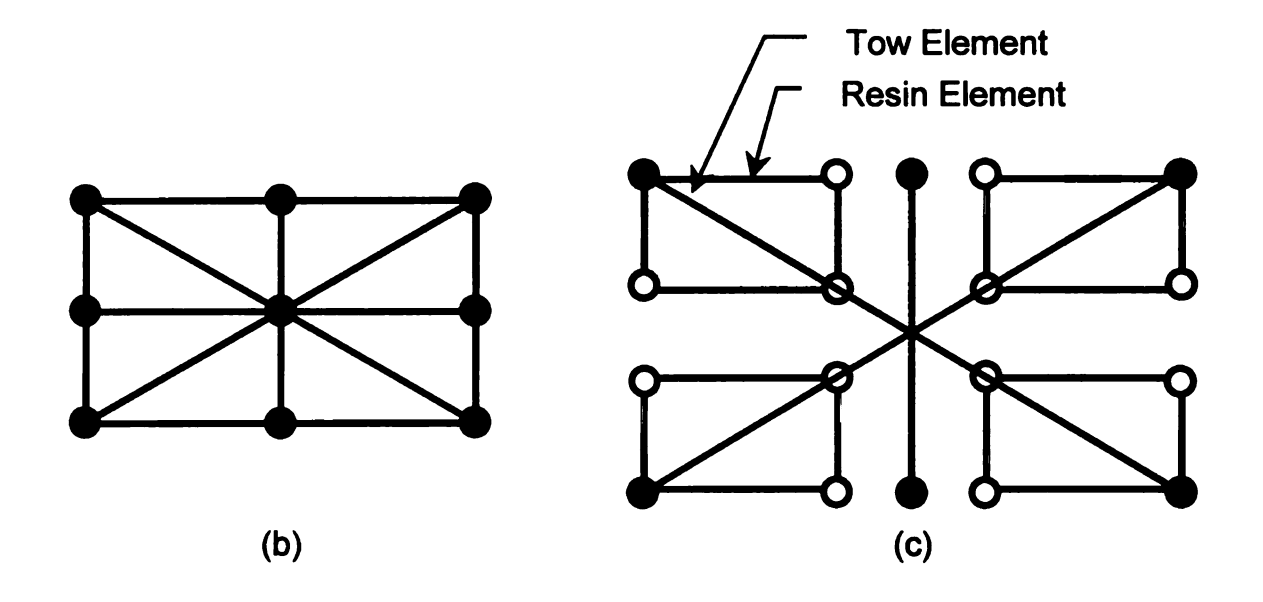


Figure 3.5 (a) Discretized representation of a RVE in a triaxial braid. (b)

Assembled and (c) exploded views of the finite element model for a triaxial braid.

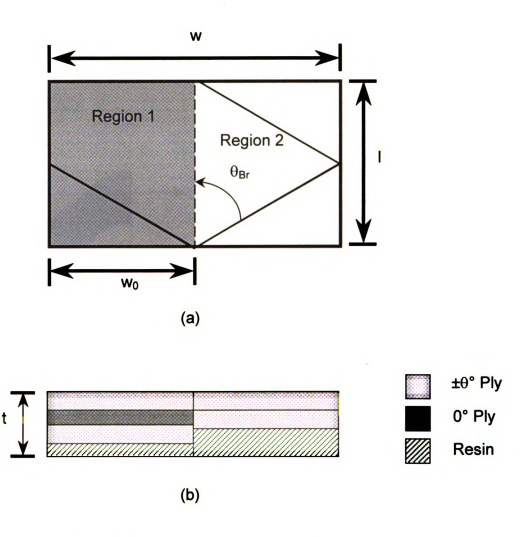


Figure 3.6 Division of the RVE of a triaxial braid into two regions for calculation of the effective properties (a) plan view (b) side view.

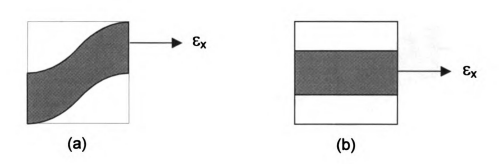


Figure 3.7 (a) Curved fiber tow. (b) Straight fiber tow.

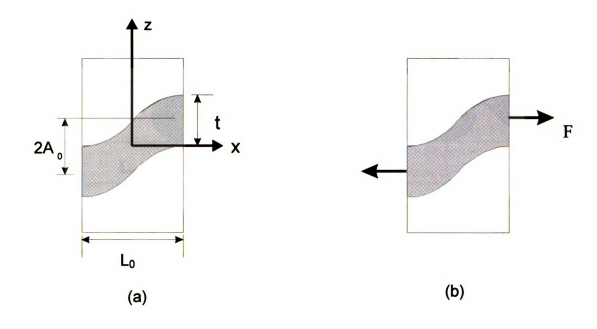


Figure 3.8 Curved beam on an elastic foundation (a) geometry of the undulating region and (b) applied load.

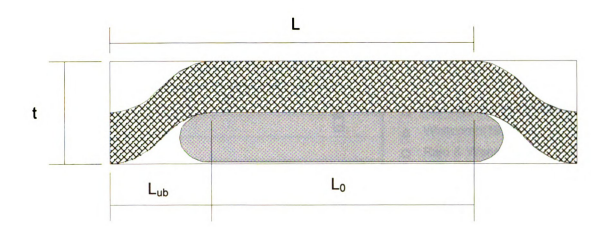


Figure 3.9 Geometry defining the waviness ratio ($\lambda = L_{ub} / L I$)

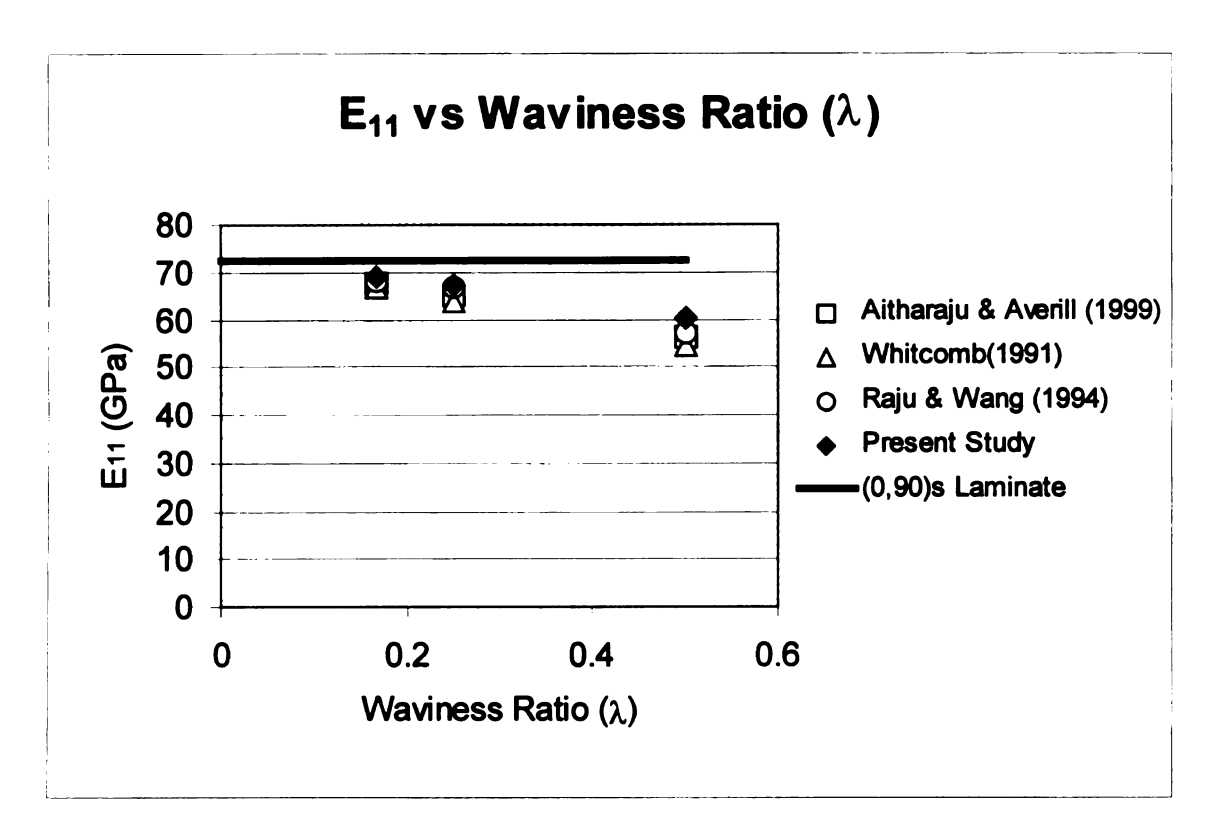


Figure 3.10 Plot of the effective stiffness E_{11} as the waviness ratio (λ) is increased.

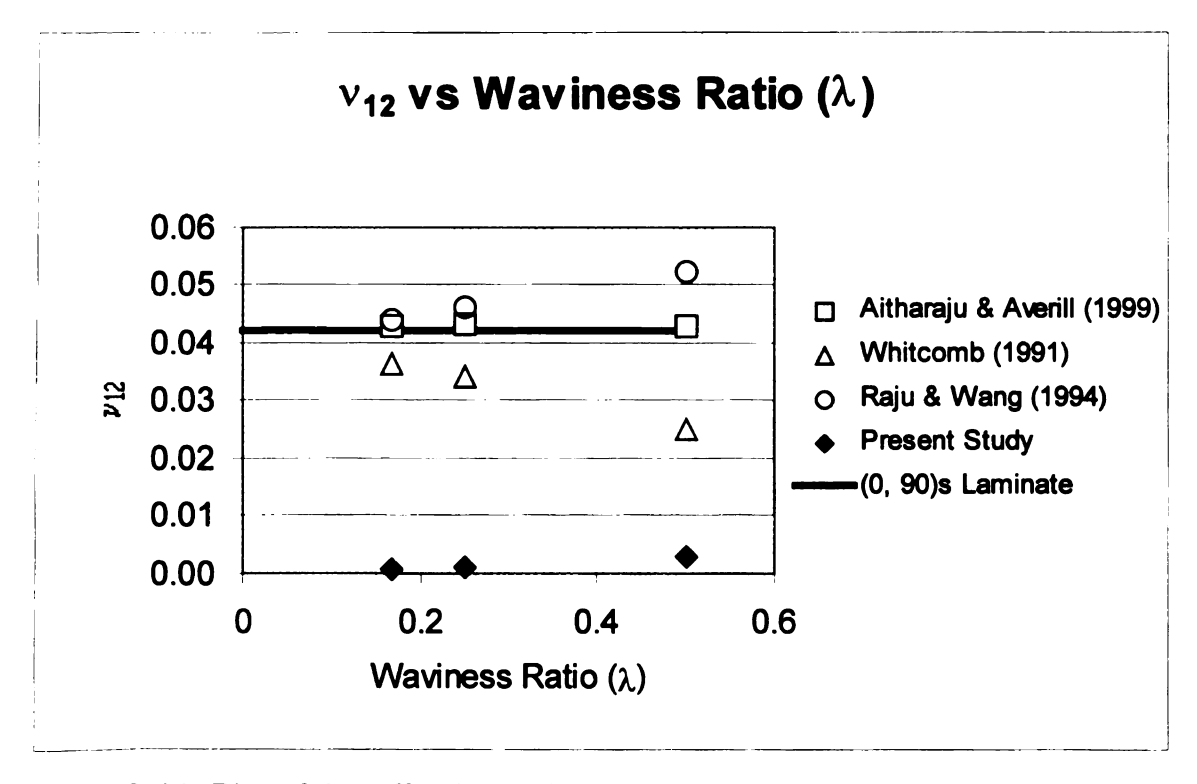


Figure 3.11 Plot of the effective Poisson's ratio v_{12} as the waviness ratio (λ) is increased.

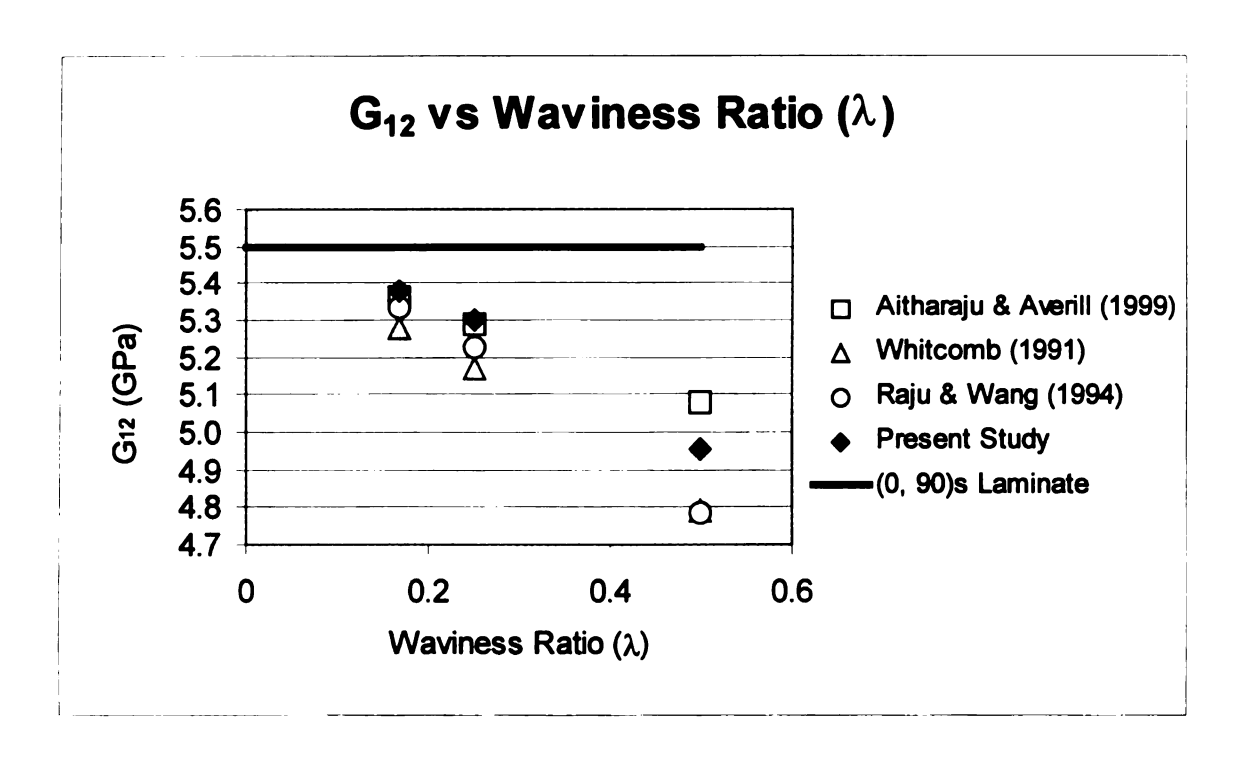


Figure 3.12 Plot of the effective shear modulus G_{12} as the waviness ratio (λ) is increased.

Chapter 4

Modeling progressive failure using the simplified discrete-tow model

4.1 Introduction

Using the simplified discrete-tow model presented in Chapter 3, it is possible to model progressive failure in woven composites. The simplified discrete-tow model discretely represents the fiber tows and resin independently as beam and shell finite elements respectively. The use of the discrete-tow model in progressive failure allows for the ability to better predict the behavior and physical orientation of the tows throughout the analysis in a manner that is more computationally efficient than a fully three-dimensional model.

In this chapter, the utility of the simplified discrete-tow model developed previously is expanded. Through the use of a stiffness reduction algorithm it is possible to model the progressive failure that occurs in both the beam and shell elements of the discrete-tow model to represent fiber and matrix damage respectively.

4.2 Progressive Failure Model

When using the finite element method to predict progressive failure it is necessary to accurately capture the energy release associated with the material failure throughout the analysis. In a nonlinear analysis, if errors are made early, they may propagate and result in erroneous results. The discrete-tow model has the advantage of representing the energy release associated with damage in the

matrix or fiber tows independently because the matrix and fiber tows are modeled discretely.

4.2.1 FINITE ELEMENT MESH

In order to effectively use the discrete tow model it is necessary to carefully consider the finite element mesh that will be used to model the woven composite structure. A finite element model of a single repeating volume element for a plain weave and triaxial braid were developed previously and are depicted in Figure 3.4 and 3.7. However, there are several competing mechanisms occurring within the model that must be discussed. First, due to the connectivity that exists between the shell and beam elements, singularities result due to the application of point loads from the beam elements. Knowing this it is desirable to have a finite element mesh that is coarse enough that the effects of these singularities are effectively averaged out of the volume of the element. Secondly, it is advantageous to use the discrete-tow model because of its ability to explicitly model the fiber tows and their deformations within the woven composite. Finally, if this model is used in a contact analysis, it is desirable to have smaller element sizes to better capture the contact behavior that occurs.

4.2.2 MODELLING PROGRESSIVE FAILURE

Material damage within the tows and resin was modeled through the use of stiffness reduction at each integration point within each element. Typically, in

a progressive failure analysis the integration point could be in one of three stages, undamaged ($\varepsilon < \varepsilon_{flr}$), damaged ($\varepsilon_{flr} < \varepsilon < \varepsilon^{*}$), and completely failed ($\varepsilon^{*} < \varepsilon$). The stress vs. strain plot as shown in Figure 4.2 demonstrates the three stages associated with progressive failure. However, for the purposes of this study, the tows and resin were assumed to transition nearly instantly from undamaged to completely failed ($\varepsilon_{flr} \approx \varepsilon^{*}$) as illustrated in Figure 4.3.

Another advantage to the discrete-tow model is that it allows for different failure criteria and values to be applied to the fiber tow and resin individually. In the case of this study the fiber tow failure was based upon the maximum principle strain failure criterion while the maximum principle stress failure criterion was used in the resin. The actual values used in the current analysis are summarized in Table 4.1. When a particular constituent material completely failed, its material properties were reduced by several orders of magnitude (essentially zero, but not exactly zero, to avoid numerical singularities in the analysis).

4.2.3 PROGRESSIVE FAILURE ALGORITHM

The progression of the failure in the finite element model is captured through the use of an incremental iterative procedure associated with a standard nonlinear analysis. This method of modeling progressive failure was first introduced by Dodds et al. [27] to model crack growth in concrete structures. In a nonlinear analysis the applied load or displacement is applied in small increments. For an implicit analysis, it may be necessary for the analysis to iterate several times before an equilibrium position is found. Once equilibrium

has been satisfied within an acceptable tolerance, the next increment of load or displacement is then applied. When a material point has failed, its stiffness is reduced by calculating a new secant modulus and the analysis must iterate in order to redistribute the load around the point of failure before the next increment is started. The current progressive failure algorithm was implemented via a user material subroutine in ABAQUS [28], a commercially available finite element package. The subroutine implementation is summarized graphically in Figure 4.1.

4.3 Numerical Results

In order to validate the implementation of the progressive failure algorithm, RVEs of both a plain weave and triaxial braid were constructed. Each RVE was then subjected to four geometrically nonlinear analyses. Two analyses were conducted without implementing the failure algorithm. The remaining two analyses were completed with the failure algorithm turned on. In both cases, with and without failure, one analysis was conducted using tensile loading while the other used compressive loading. The geometry of the plain weave and triaxial braid RVE's are summarized in Table 3.1 and Table 3.6, while the boundary conditions for each analysis can be found in Table 4.2 and illustrated graphically in

Figure 4.4.

Results of the analyses of the plain weave are found in Figures 4.5 through 4.12, while results for the triaxial weave can be seen in Figures 4.14

through 4.21. When examining the results from the materially linear analysis of the plain weave (Figures 4.5 through 4.8), the local and global behavior is nearly linear as would be expected from a sample as small as one RVE. When failure is included, and a geometrically nonlinear analysis is conducted of the plain weave (Figures 4.10 through 4.12), the resulting nonlinear trends clearly demonstrate that failure must be occurring within the constituent materials.

It is also important to note the significant behavioral differences between the plain weave and triaxial braid. Figure 4.9 and 4.12 illustrate how the majority of the initial load is carried by the resin. Upon failure of the resin the load is redistributed and carried by the tows until complete failure occurs. The load carrying behavior of a triaxial braid (Figure 4.17 and 4.21) differs from the plain weave due to the fact that the initial load carrying is accomplished by the axial tow. This, of course, is dependent upon the loading conditions, however, in this case the load was applied along the axis of the axial tow. Once the axial tow fails in the triaxial braid, the braider tows assume the role of carrying the load until complete failure occurs.

4.4 Conclusions

Using a standard nonlinear finite element analysis as a foundation, it is possible to add the ability to predict progressive failure in woven composites using the discrete-tow model. A progressive failure algorithm that represents failure in the form of material stiffness reduction was combined with the discrete-tow model to predict progressive failure of a plain weave and triaxial braid RVE.

Based upon the results of this study, it is quite reasonable to assume that this simplified methodology of modeling damage in woven composites could be extended to structures much larger than a single RVE.

Table 4.1 Failure criteria used in the resin and tow.

Case	Resin	Tow
Tensile Failure	S1 = 0.138 GPa	E1=0.02
Compressive Failure	S3 = 0.138 GPa	E3=0.02

Table 4.2 Applied boundary for the linear and failure cases studied.

Linear (without failure)			With Failure				
Tension Compression		Tension		Compression			
εχ	ε _y	εχ	ε _γ	εχ	ε _γ	εχ	ε _y
0.126	0	0.126	0	0.126	0	0.126	0

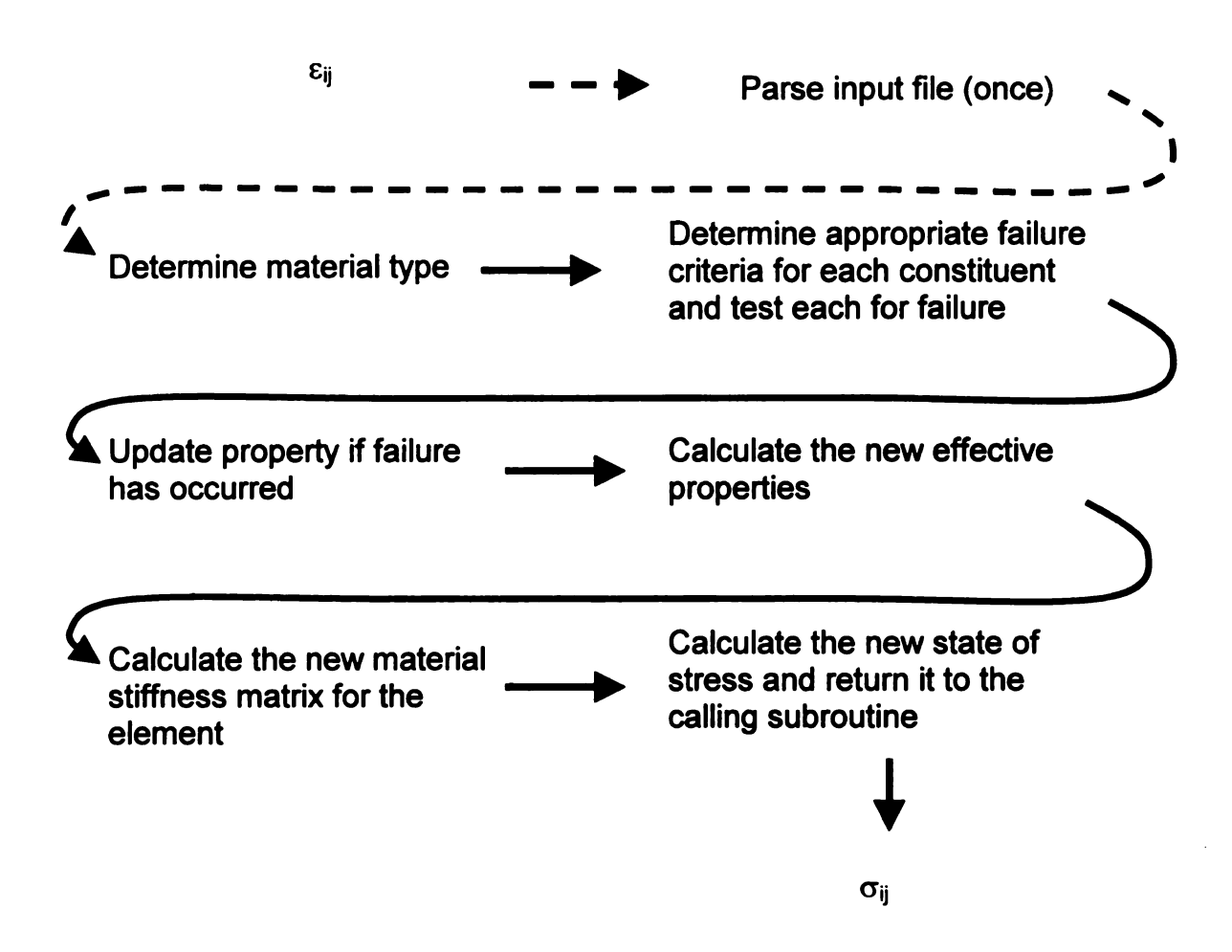


Figure 4.1 Implementation of the progressive failure algorithm.

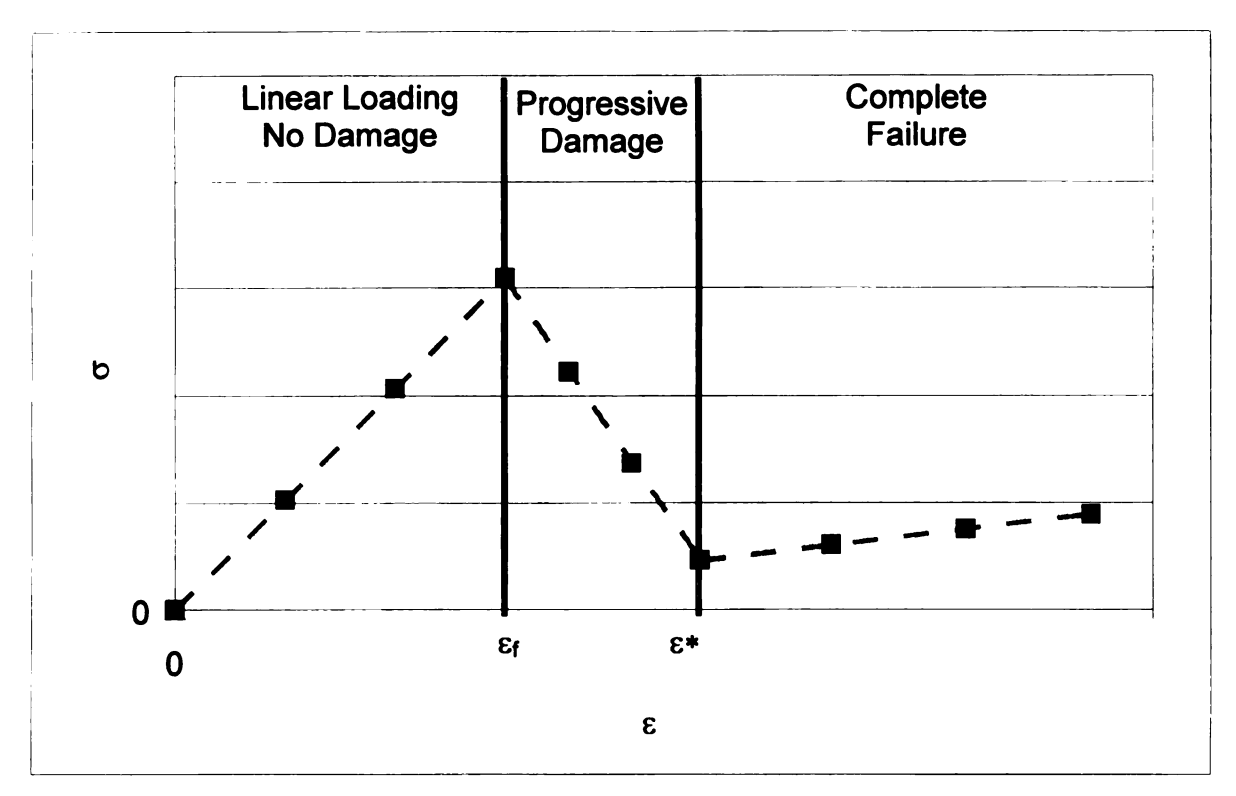


Figure 4.2 Stress strain curve illustrating progressive damage (not immediate).

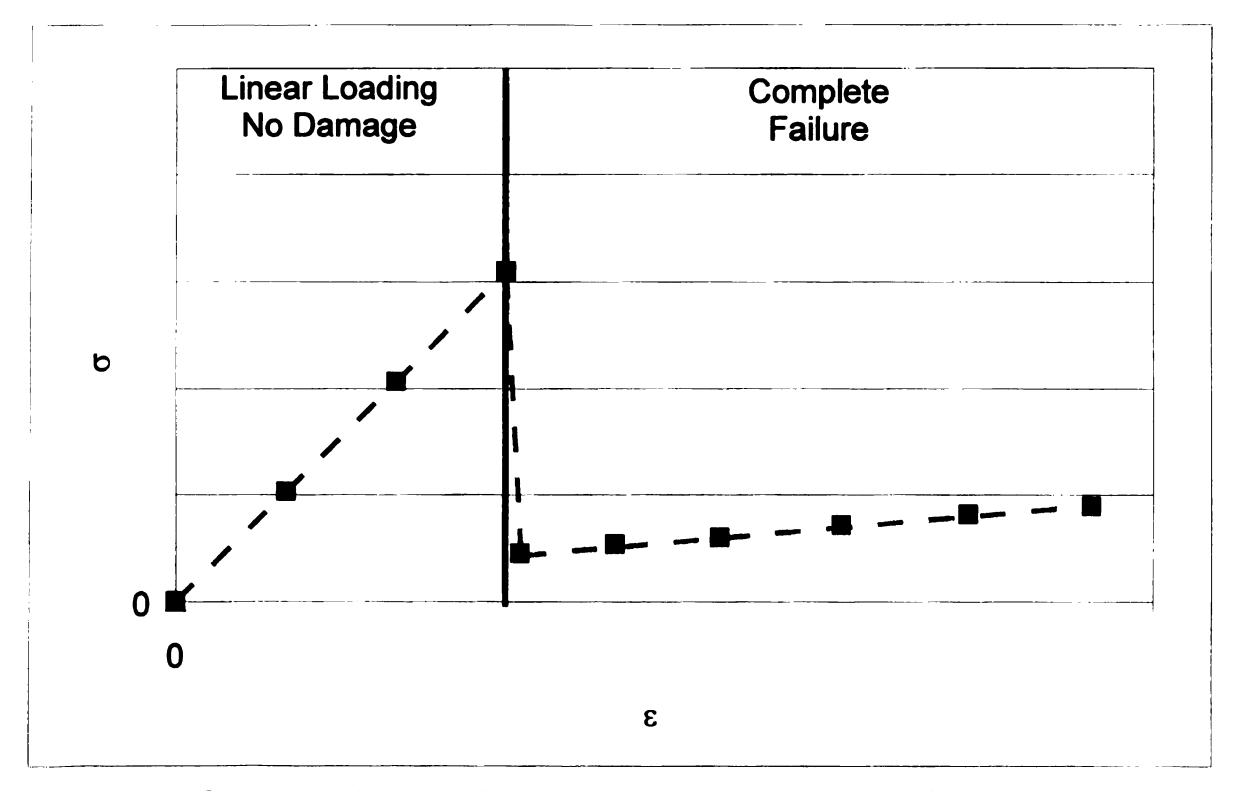
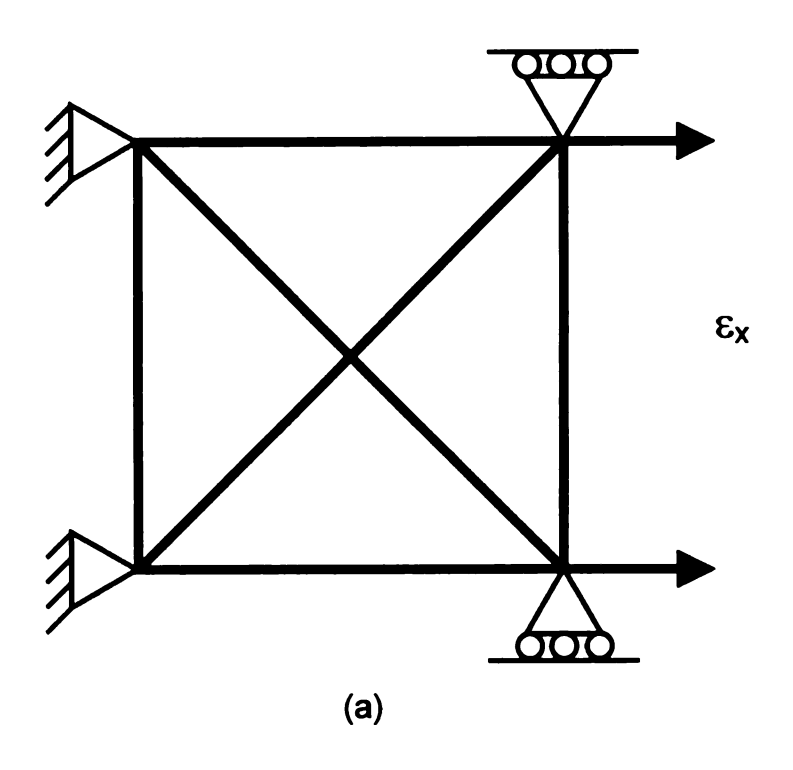


Figure 4.3 Stress strain curve illustrating immediate material failure.



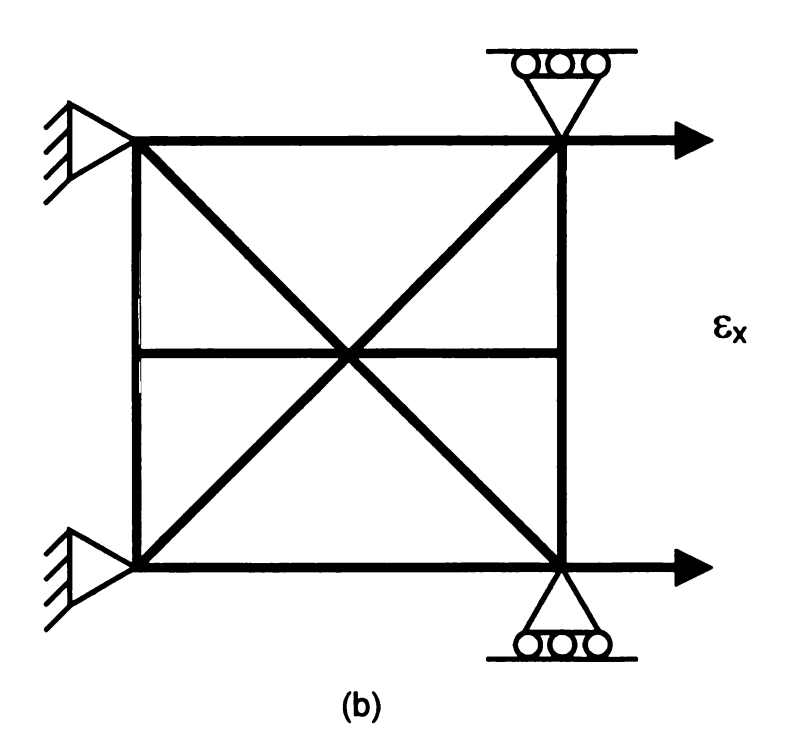


Figure 4.4 Illustration of applied boudary conditions to (a) a plain weave and (b) a triaxial braid.

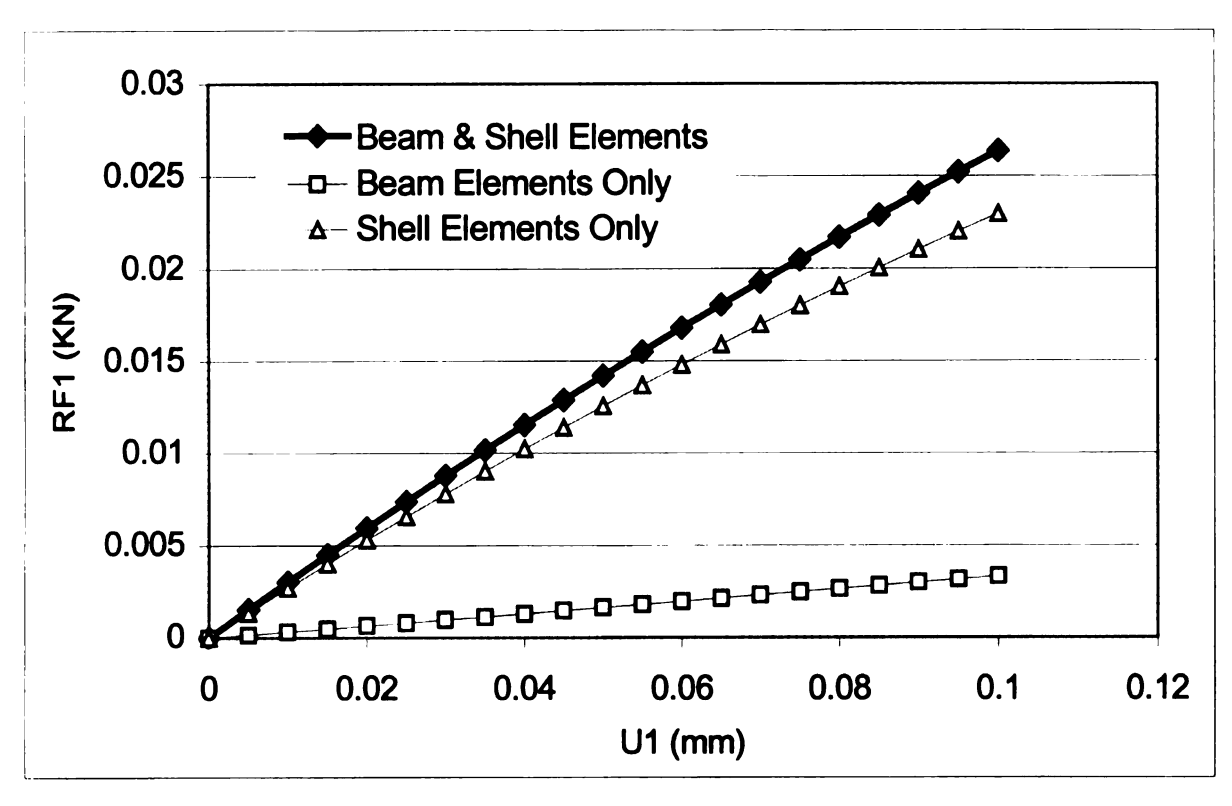


Figure 4.5 Force deflection curve for a plain weave under tensile loading (without failure).

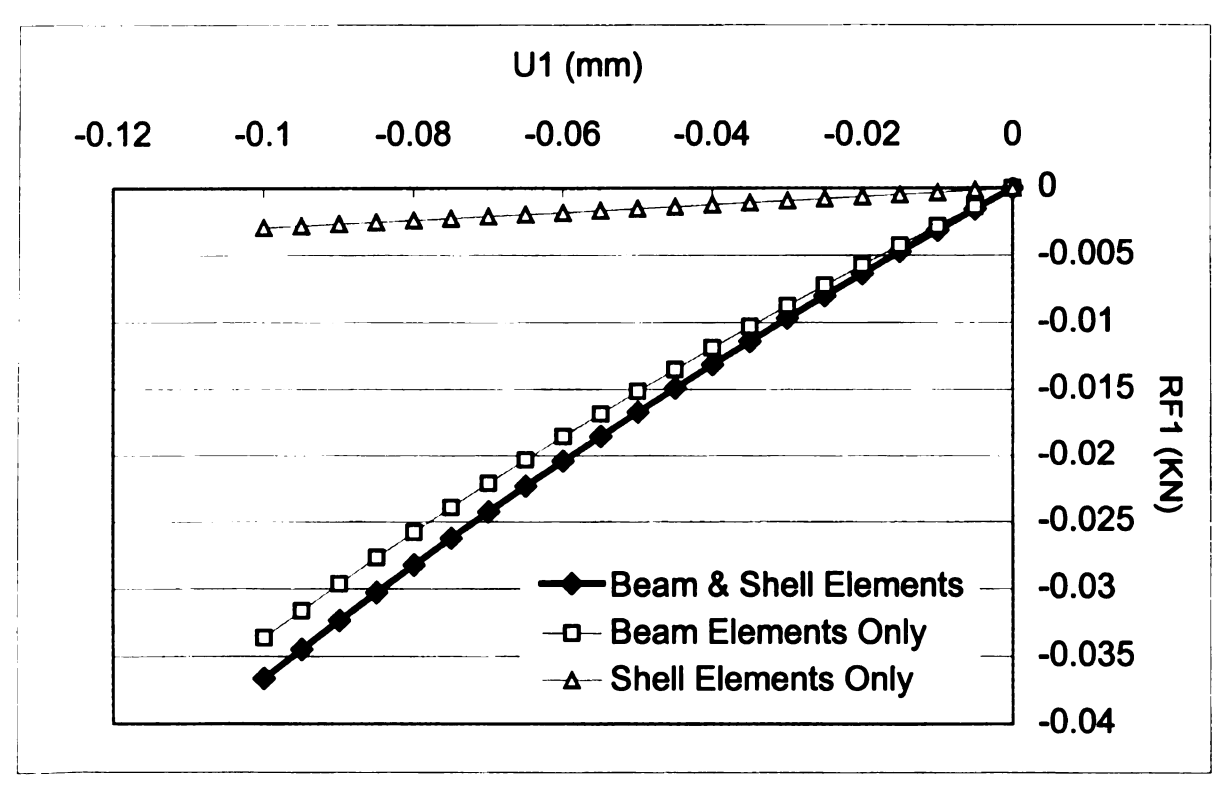


Figure 4.6 Force deflection curve for a plain weave under compressive loading (without failure).

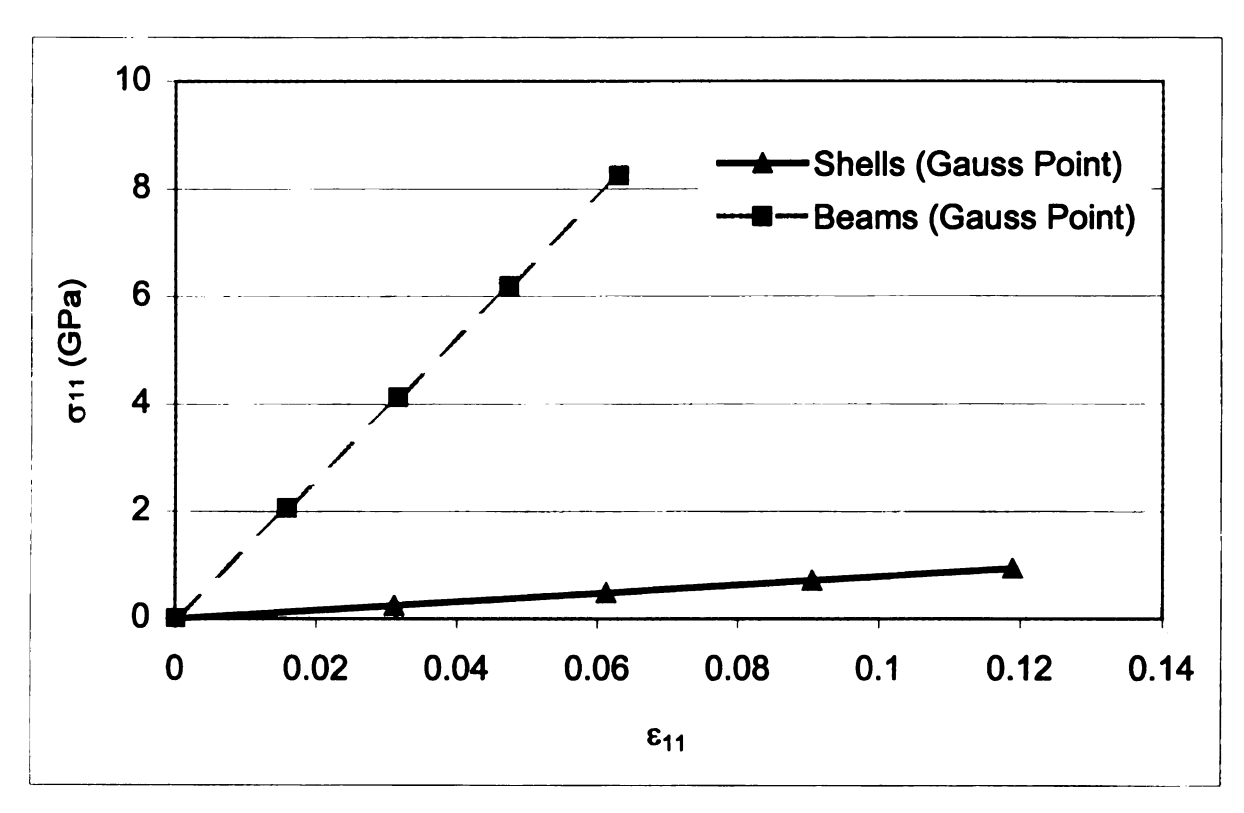


Figure 4.7 Linear validation of one RVE of a plain weave under a tensile load.

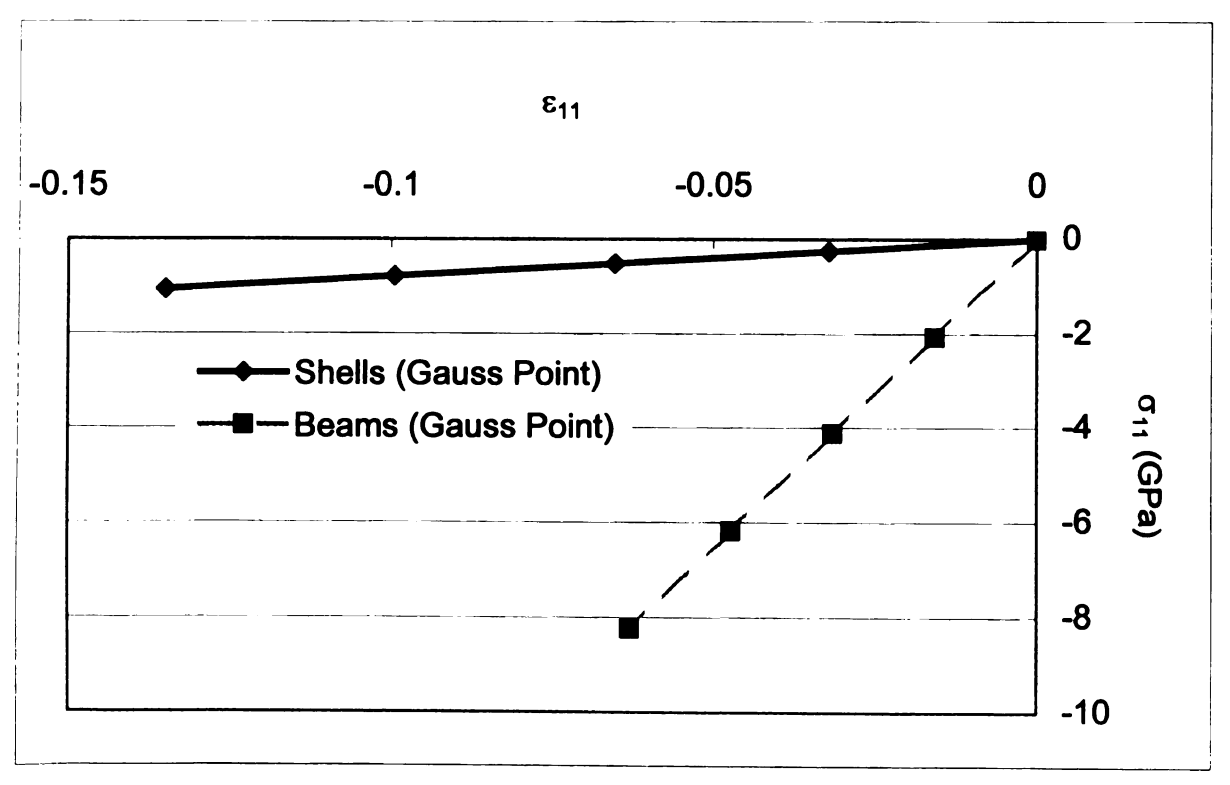


Figure 4.8 Linear validation of one RVE of a plain weave under a compressive load

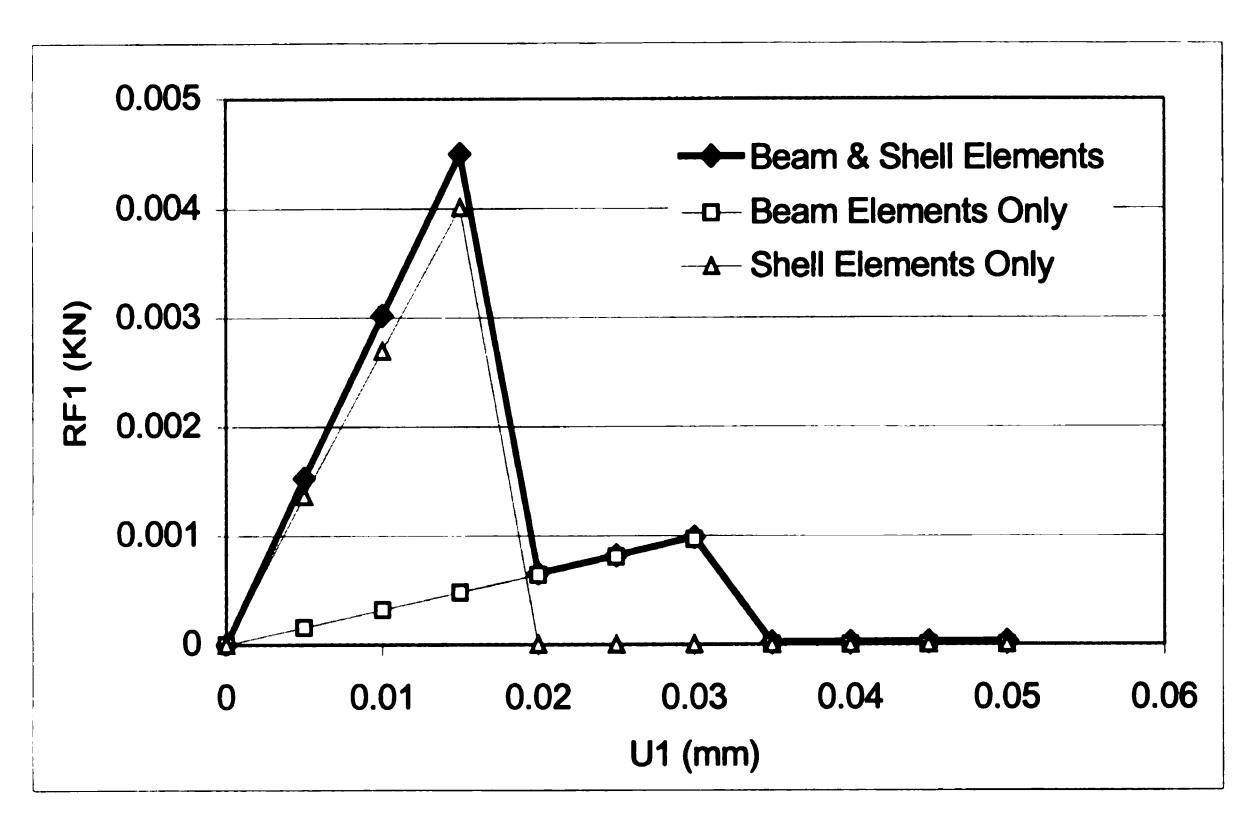


Figure 4.9 Force deflection curve for a plain weave under tensile loading (with failure).

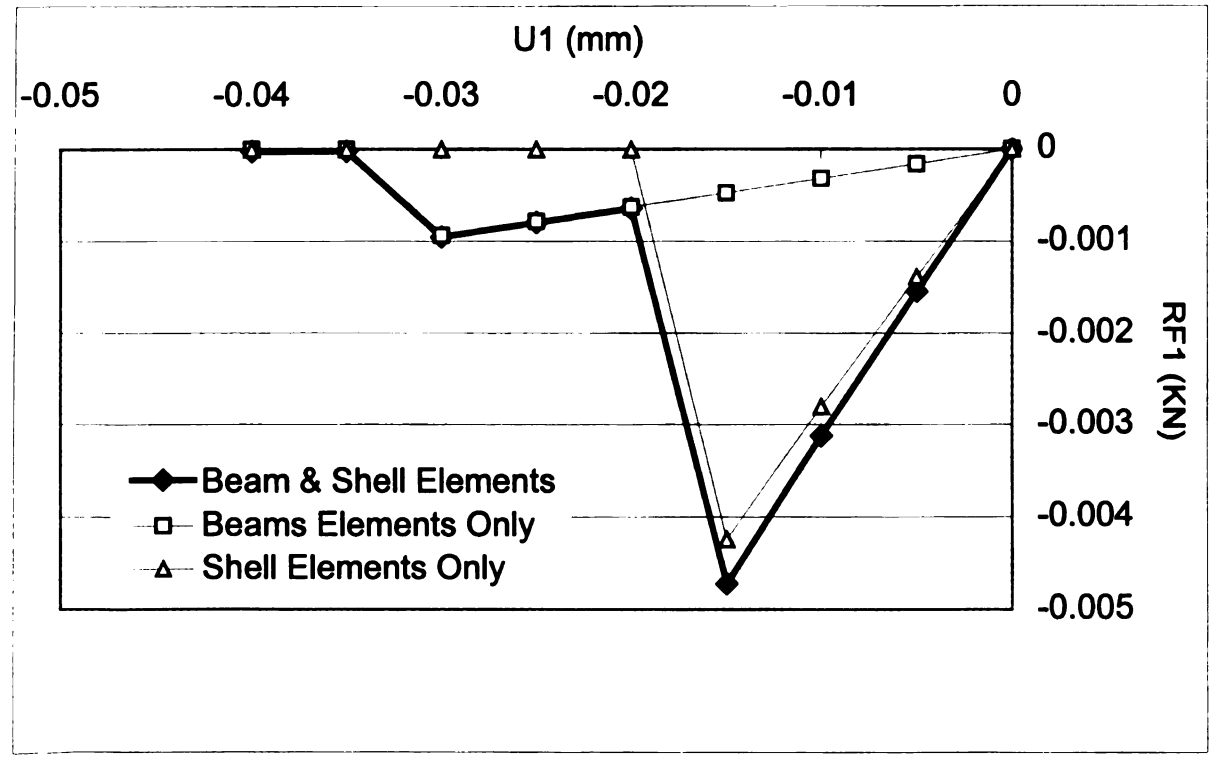


Figure 4.10 Force deflection curve for a plain weave under compressive loading (with failure).

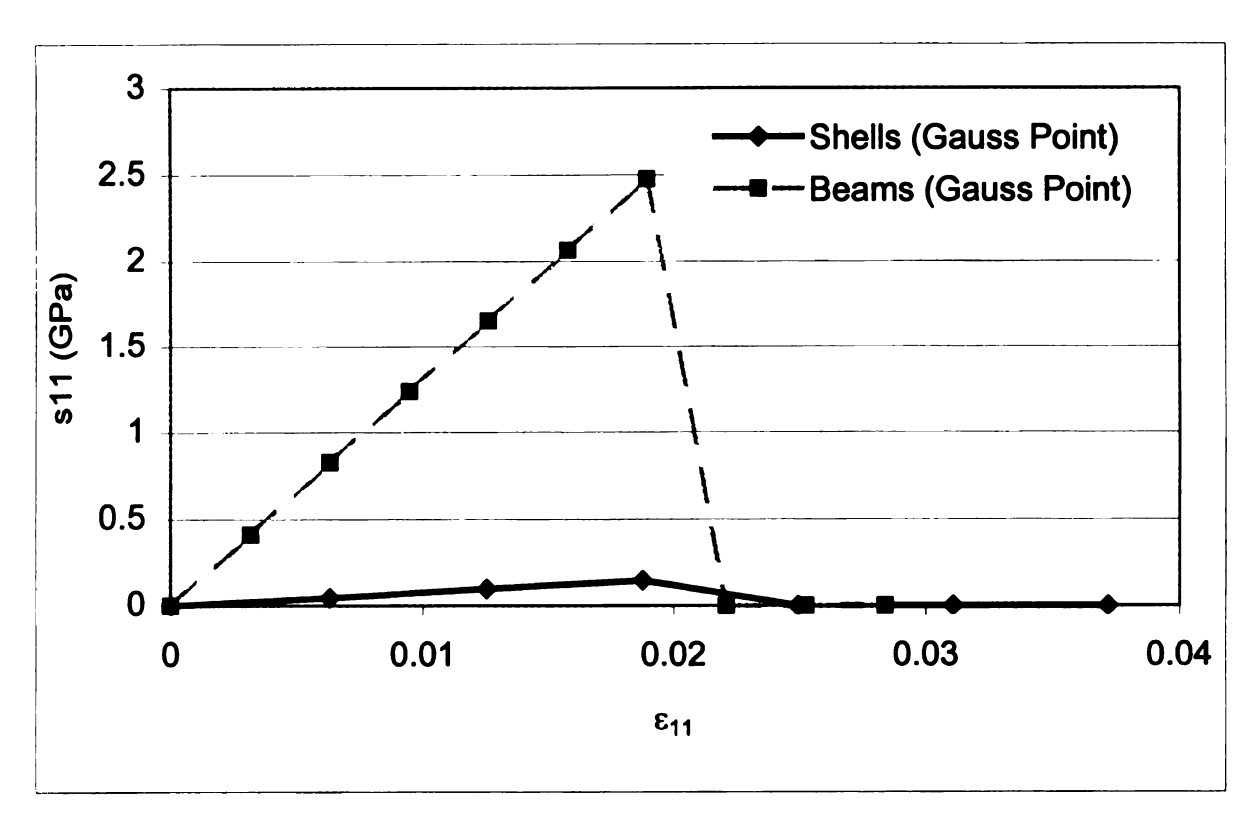


Figure 4.11 Failure validation of one RVE of a plain weave under a tensile load.

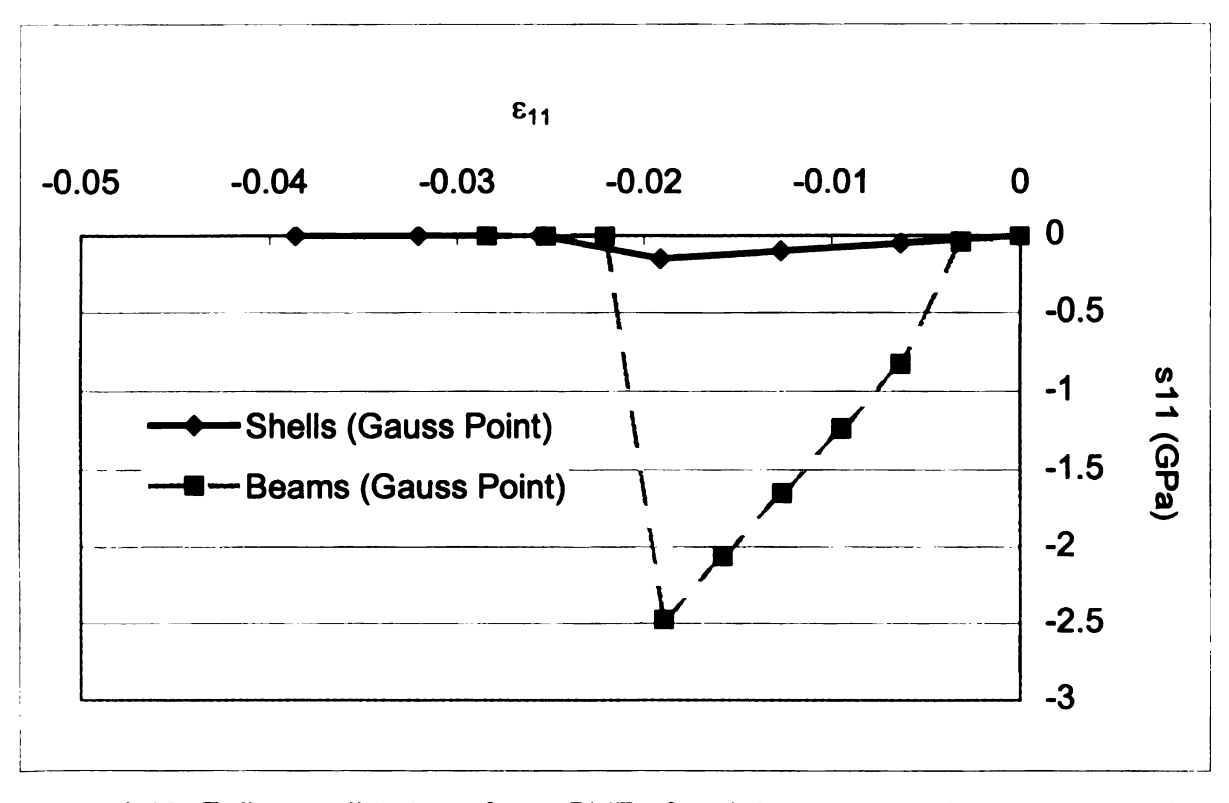


Figure 4.12 Failure validation of one RVE of a plain weave under a compressive load.

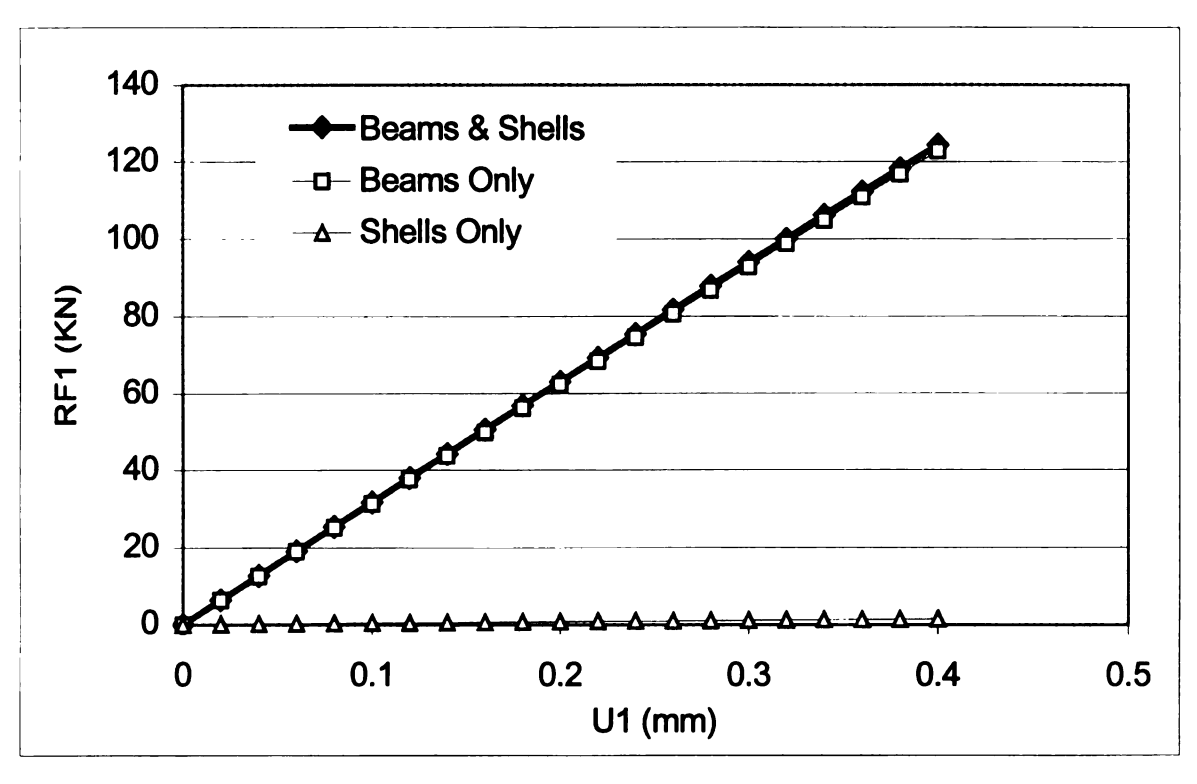


Figure 4.13 Force deflection curve for a triaxial weave under tensile loading (without failure).

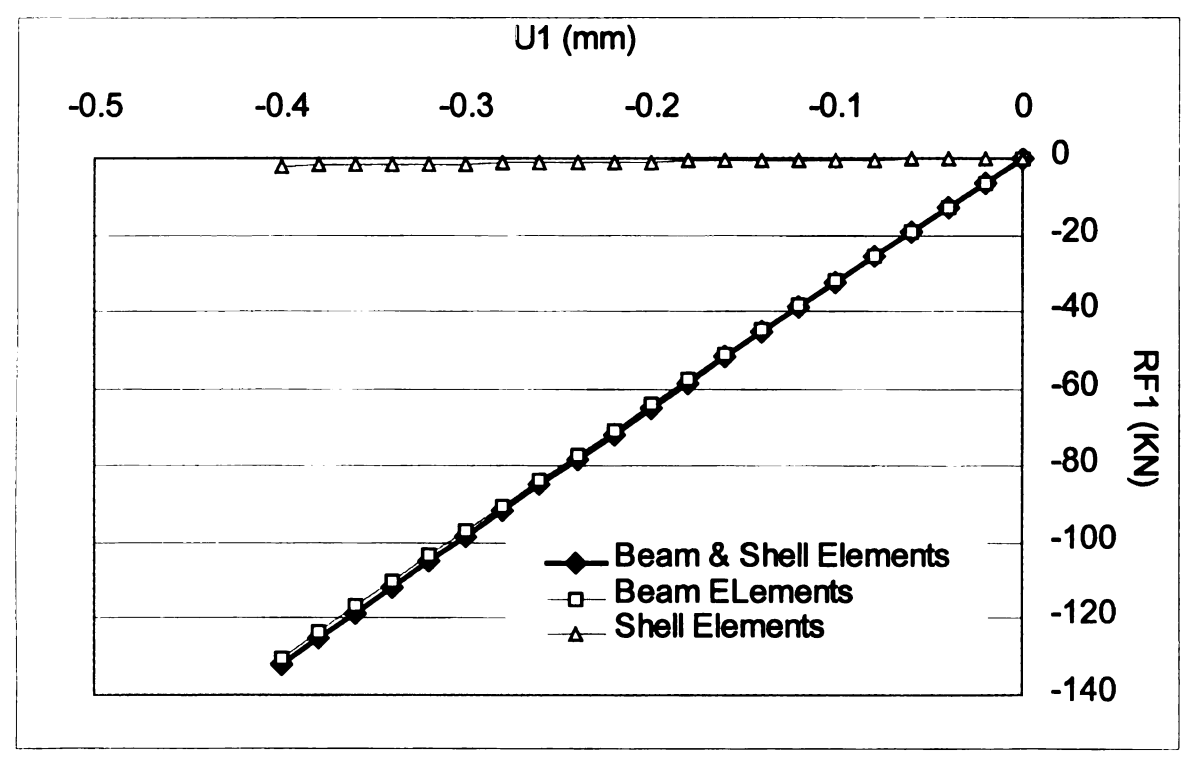


Figure 4.14 Force deflection curve for a triaxial weave under compressive loading (without failure).

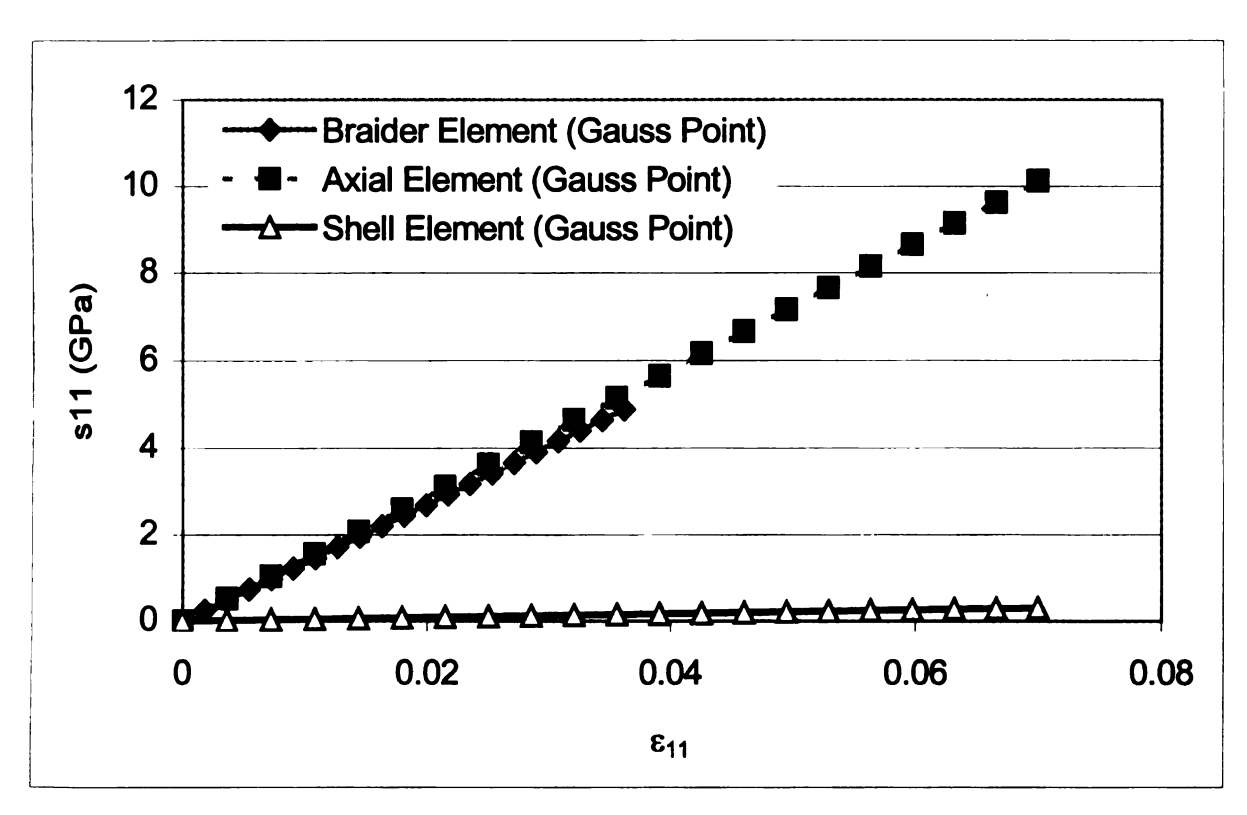


Figure 4.15 Linear validation of one RVE of a triaxial weave under a tensile load (without failure).

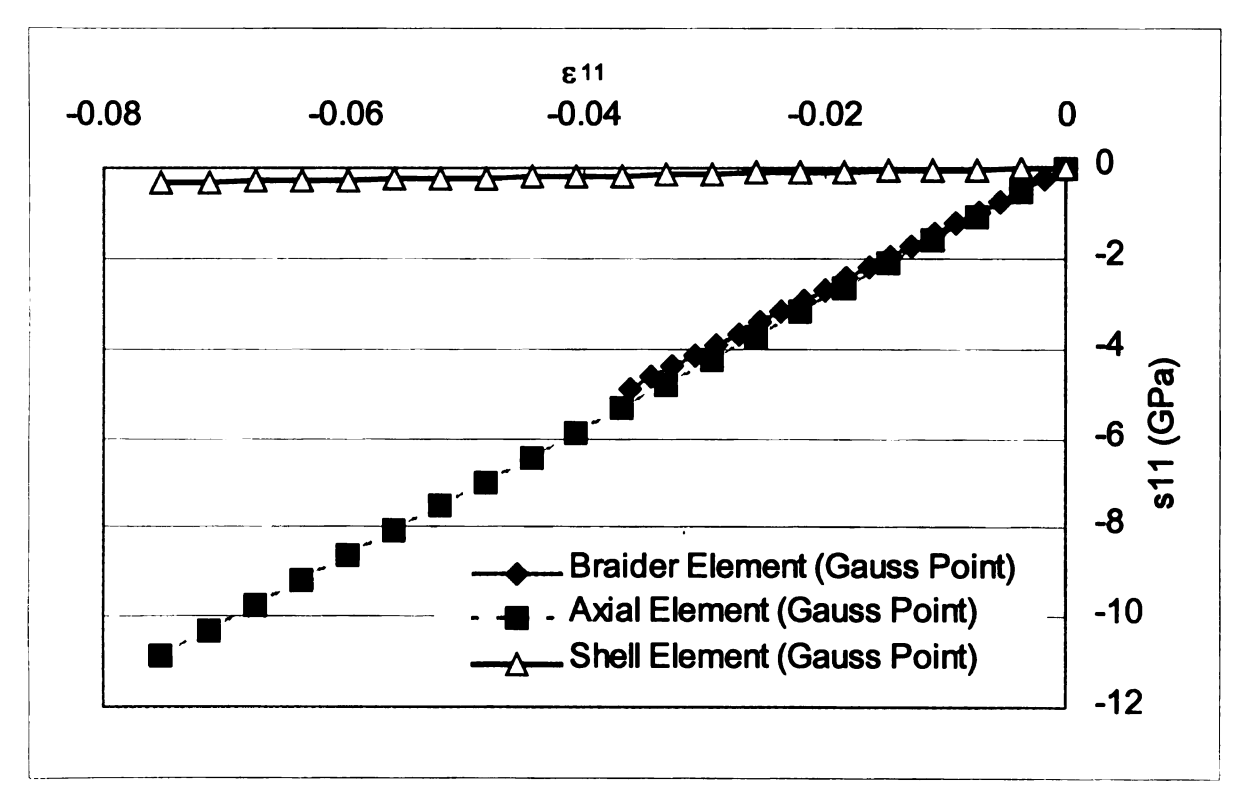


Figure 4.16 Linear validation of one RVE of a triaxial weave under a compressive load (without failure).

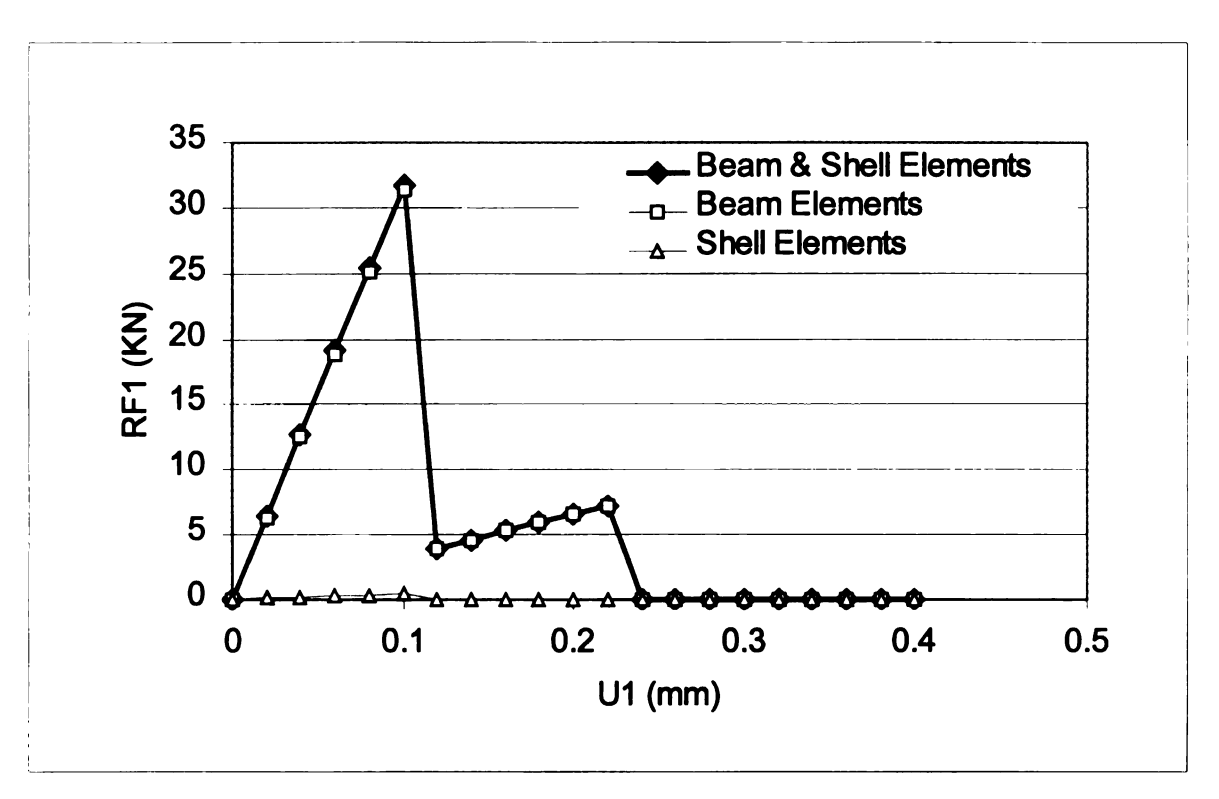


Figure 4.17 Force deflection curve for a triaxial weave under tensile loading (with failure).

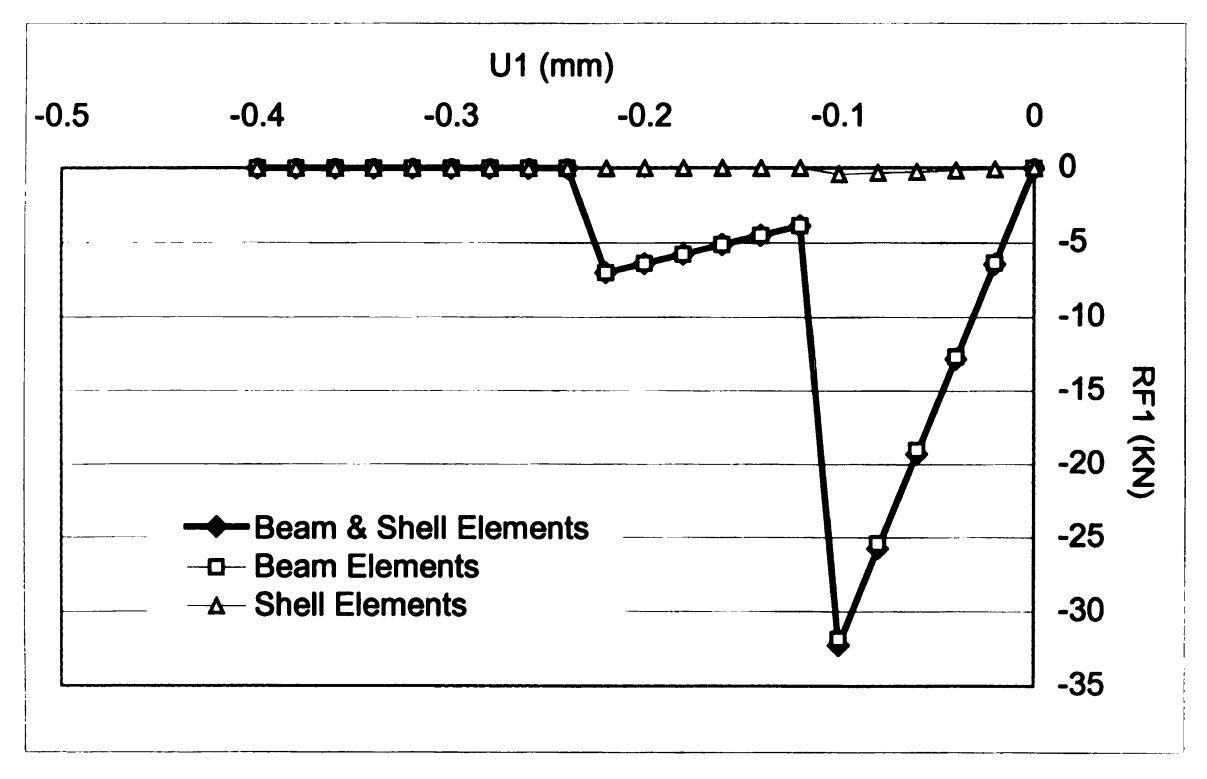


Figure 4.18 Force deflection curve for a triaxial weave under compressive loading (with failure).

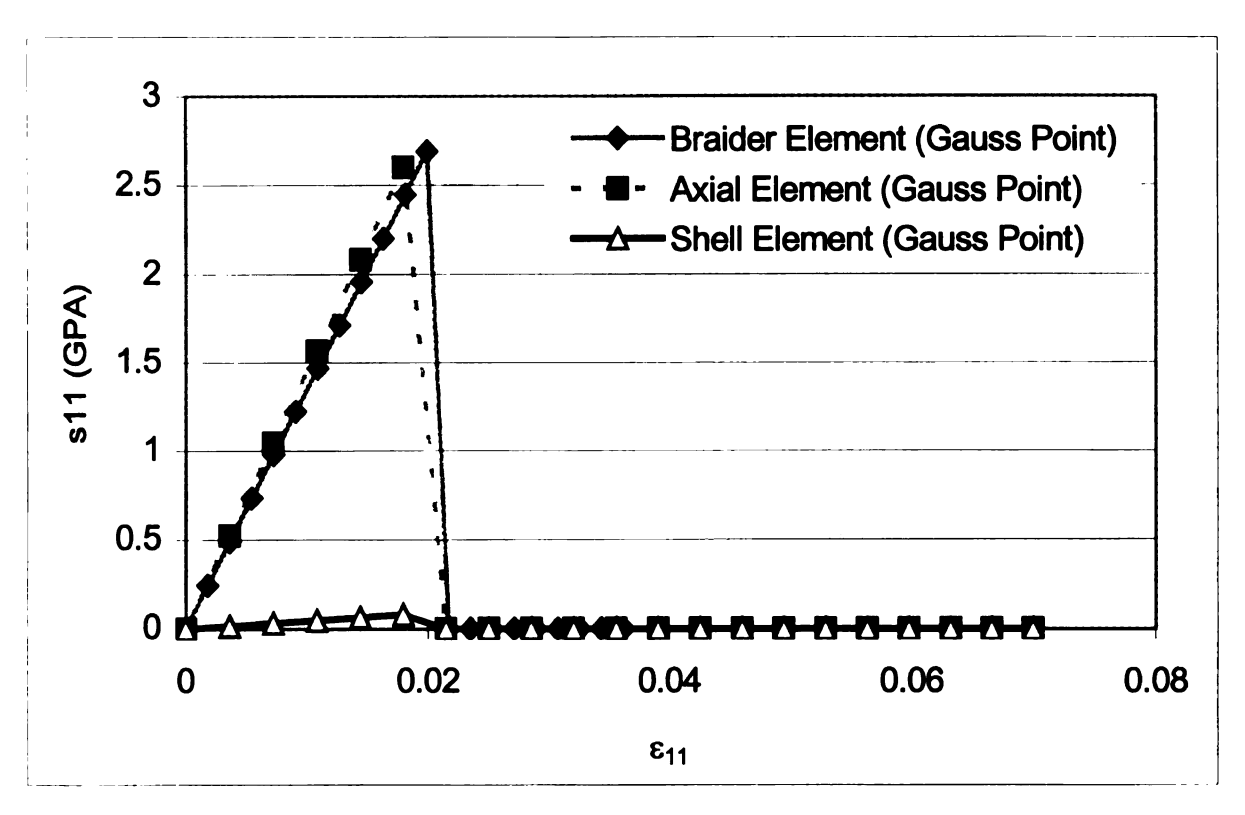


Figure 4.19 Failure validation of one RVE of a triaxial weave under a tensile load.

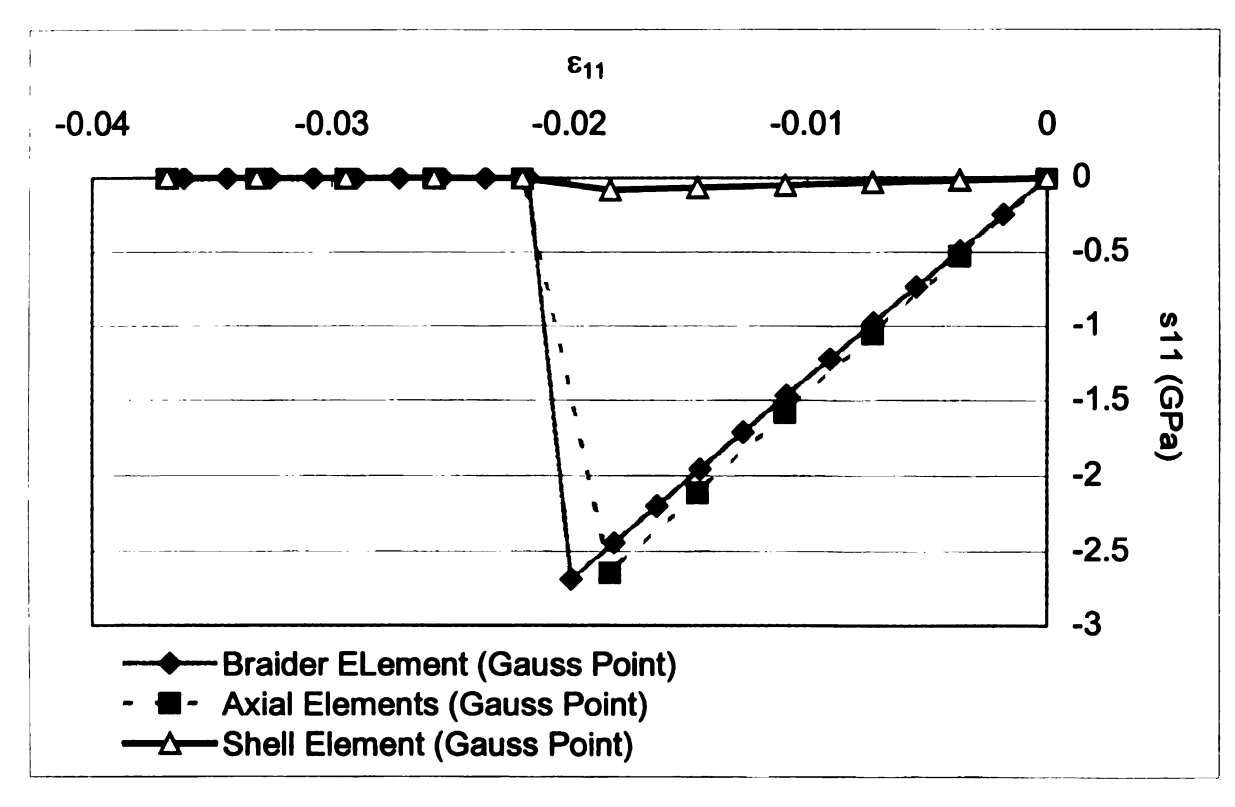


Figure 4.20 Failure validation of one RVE of a triaxial weave under a compressive load.

Chapter 5

Conclusions

5.1 Conclusions

A method for efficiently modeling two-dimensional woven composites was successfully developed. This simple discrete-tow model has the ability to accurately predict the stiffness of RVE's for plain weave and triaxial braids. The discrete-tow model also significantly decreases the number of degrees of freedom within a finite element model while greatly simplifying the model building process.

The utility of the discrete-tow model was also demonstrated by applying it to the problem of damage prediction within a woven composite. Although it is necessary to validate this process with experimental results, it does prove to be a promising tool for the analysis of woven composites.

5.2 Future Work

Although the discrete-tow model was shown to agree well with other stiffness prediction models and with experimental results, the model has yet o be applied to a large composite structure much larger than a single RVE. When the discrete-tow model is used to model larger sections several addition items must be addressed, including; variation of fiber volume fraction, tow cross-sectional variation, and tow crimp. Each of these alone is not a trivial matter and should be examined thoroughly.

Currently the application of the discrete-tow model to progressive failure needs to be validated with experimental results. In practice, the failure algorithm and subroutine derived from it perform correctly for single RVE models, however a detailed analysis should be conducted to gain confidence in its use for larger structures.

Bibliography

- 1. Cox, B.N. and Flanagan, G., "Handbook of Analytical Methods for Textile Composites," *Version 1.0, Rockwell Science Center Report*, January, 1996.
- 2. Tan, P., Tong, L. and Steven, G.P., "Modeling for Predicting the Mechanical Properties of Textile Composites A Review," *Composites Part A*, Vol. 28A, 1997, pp. 903-92
- 3. Ishikawa, T. and Chou, T.-W., "Elastic Behavior of Woven Hybrid Composites," *Journal of Composite Materials*, Vol. 16, January 1982, pp. 2-19.
- 4. Ishikawa, T. and Chou, T.-W., "One-Dimensional Micromechanical Analysis of Woven Fabric Composites," *AIAA Journal*, Vol. 21, NO. 12, 1983, pp. 1714-1721.
- 5. Ishikawa, T. and Chou, T.-W., "Stiffness and Strength Behaviour of Woven Fabric Composites," *Journal Materials Science*, Vol. 17, 1982, pp. 3211-3220.
- 6. Pastore, C.M. and Gowayed, Y.A., "A Self-Consistent Fabric Geometry Model: Modification and Application of a Fabric Geometry Model to Predict the Elastic Properties of Textile Composites," *Journal of Composites Technology & Research*, JCTRER, Vol. 16, No. 1, January 1994, pp. 32-36.
- 7. Ko, F.K., Pastore, C.M., Lei, C. and Whyte, D.W., "A Fabric Geometry Model for 3-D Braid Reinforced FP/Al-Li Composites," Proceedings, International SAMPE Metals Conference: Competitive Advances in Metals/Metal Processing, Cherry Hill, NJ, Aug. 1987.
- 8. Ma, C.-L., Yang, J.-M., and Chou, T.-W., "Elastic Stiffness of Three Dimensional Braided Textile Structural Composites," *Composite Materials: Testing and Design (Seventh Conference), ASTM STP 893*, J.M. Whitney, Ed., American Society for Testing and Materials, Philadelphia, 1986, pp. 404-421.
- 9. Yang, J.M., Ma, C.-L, and Chou, T.W., "Fiber Inclination Model of Three Dimensional Structural Composites," *Journal of Composite Materials*, Vol. 20, September 1986, pp. 472-484.
- 10. Naik, N.K. and Ganesh, V.K., "Prediction of elastic Properties of Plain Weave Fabric Composites," *Composites Science and Technology*, Vol. 45, 1992, pp. 135-152.
- 11. Raju, I. S. and Wang, J. T., "Classical Laminate Theory Models for Woven Fabric Composites," *Journal of Composites Technology and Research*, JCTRER, Vol. 16, No. 4, October 1994, pp. 289-303.
- 12. Aitharaju, V. R. and Averill, R. C., "Three Dimensional Properties of Woven-Fabric Composites" *Composites Science and Technology*, Vol. 59, pp. 1901-1911, 1999.

- 13. Sankar, B.V. and Marrey, R. V., "Analytical Method for Micromechanics of Textile Composites," *Composites Science and Technology*, Vol. 57, 1997, pp. 703-713.
- 14. Dasgupta, A., S. Bhandarkar, M. Pecht and D. Barkar, "Thermo-elastic Properties of Woven Fabric Composites Using Homogenization Techniques," *Proceedings of the American Society for Composites, Fifth Technical Conference*, Technomic Publishing Co., 1990, pp. 1001-1010.
- 15. Whitcomb, J. D., "Three Dimensional Stress Analysis of Plain Weave Composites, " *Composite Materials: Fatigue and Fracture (Third Volume)*, ASTM STP 1110, T.K. O'Brien, Ed., American Society for Testing and Materials, Philadelphia, 1991, pp. 417-438.
- 16. Whitcomb, J.D., Woo, K. and Gundapaneni, S., "Macro Finite Element Analysis of Textile Composites," *Journal of Composite Materials*, Vol. 28, No 7, 1994, pp. 607-617.
- 17. Woo, K. and Whitcomb, J.D., "Global/Local Finite Element Analysis for Textile Composites," *Journal of Composite Materials*, Vol. 28, No. 14, 1994, pp. 1305-1320.
- 18. Marrey, R.V. and Sankar, B.V., "A Micromechanical Model for Textile Composite Plates," *Journal of Composite Materials*, Vol. 31, No. 12, 1997, pp.1187-1213.
- 19. Blackketter, D.M., Walrath, D.E. and Hansen, A.C., "Modeling Damage in a Plain Weave Fabric-Reinforced Composite Material.", *Journal of Composites Technology & Research*, Vol. 15, No. 2, Summer 1993, pp. 136-142.
- 20. Xu, J., Cox, B.N., McGlockton, M.A., and Carter, W.C., "A Binary Model of Textile Composites-II. The Elastic Regime," Acta Metallurgica et Materiallia, Vol. 43, No. 9, 1995, pp. 3511-3524.
- 21. Lei, C., Cai, Y.J., and Ko, F., "Finite Element Analysis of 3-D Braided Composites," *Advances in Engineering Software*, Vol 14, No. 3, 1992, pp. 187-194.
- 22. Naik, Rajiv A., "Failure Analysis of Woven and Braided Fabric Reinforced Composites," *Journal of Composite Materials*, Vol. 29, No. 17, 1995, pp. 2334-2363.
- 23. Naik, Rajiv A., Ifju, Peter G., and Masters, John E., "Effect of Fiber Architecture Parameters on Deformation Fields and Elastic Moduli of 2-D Braided Composites," Journal of Composite Materials, Vol. 28, No. 7, 1994, pp. 656 681.
- 24. Jones, Robert M., *Mechanics of Composite Materials, Second Edition*, Taylor & Francis, Philadelphia, PA, 1999.
- 25. Naik, Rajiv A., "Analysis of Woven and Braided Fabric Reinforced Composites," *Composite Materials: Testing and Design (Twelfth Volume), ASTM STP 1274*, R.B. Deo and C.R. Saff, Eds., American Society for Testing and Material, 1996, pp. 239-263.

- 26. Foye, R.L., "Approximating the Stress Field within the Unit Cell of a Fabric Reinforced Composite using Replacement Elements," NASA CR-191422, National Aeronautics and Space Administration, Washington DC, 1993.
- 27. Dodds, R. H., Lopez, L. A., and Pecknold, D. A., "Numerical and Software Requirements on General Nonlinear Finite Element Analysis," *Report No. UILU-ENG-78-2020*, Civil Engineering Studies, University of Illinois at Urbana-Champaign, Sept. 1978.
- 28. "ABAQUS users manual, version 5.7," Hibbit, Karlsson & Sorenson, Inc. 1996.

